MUSCULOSKELETAL ULTRASOUND SCANNING OF SOME CANINE LIMB JOINTS: A COMPARISON OF SCANNING TECHNIQUES

A thesis submitted to the Faculty of Veterinary Medicine,

University of Glasgow,

for the Degree of Master of Veterinary Medicine

by

KATERINA MARINOU, BVMS

Division of Veterinary Anatomy,

Department of Veterinary Preclinical Studies,

Glasgow University Veterinary School,

April 2001,

LIST OF CONTENTS

SUMMARY

In the past diagnostic ultrasound was a relatively under utilised technique in the particular field of musculoskeletal imaging. This can be mainly attributed to the low frequency transducers available at that time which were inadequate for imaging of superficial structures because of their limited resolution. The presence of bones in the joint regions also inhibited the imaging of small and physically slight structures due to the limited access through small acoustic windows and non through transmission of sound waves at bony surfaces. More recent developments in transducer technology have managed to overcome many of the problems by the construction of ultra high frequency probes with conveniently sized footprints.

Their increased resolution has produced considerably better image quality, which has led to the detection of many anatomical structures, that had not been readily visible in the past. In addition the advanced postprocessing software of the new generation of ultrasound scanners has resulted in the ability to produce panoramic images over considerable lengths of the body surface displaying the topography of many of the underlying structures leading to the development of the extended field of view imaging modality. Reconstructed three dimensional presentations of various organs or body areas on screen constitutes a very recent capability that has the potential of detecting abnormalities and placing them in their anatomical context.

The aim of this study has been to present what has been accomplished to date with ultrasound in the small animal musculoskeletal field using conventional ultrasonographic technology. Using the regions of the shoulder, stifle and tarsal joint of live dogs, the aim was to investigate the potential of using very high frequency transducers, extended field of view imaging and three dimensional

technology with a view of identifying the anatomical structures involved and also conduct repeated individual measurements with the use of specific anatomical landmarks to see if an increase in consistency of results could be achieved. Normal adult Greyhound cadavers were initially used with a colour marker echocontrast agent to verify that structures imaged were indeed the real anatomical structures, but subsequent studies were on live normal Greyhounds and some clinical cases with lameness problems. The results of the project proved that the quality of images obtained with the use of a 16 and a 22 MHz transducers were superior to the ones acquired by conventional scanning so that identification of previously difficult structures was successfully carried out on screen. Furthermore, the extended field of view modality was a contributor to solving problems of topography and repeated identification of landmarks, whereas three dimensional imaging revealed in some areas the component structures in multiplanar detail.

The conducting of repeated individual measurements of some anatomical structures with conventional ultrasound has proved that there was poor consistency, so that it would be difficult to estimate differences in size that could lead to diagnosis of various physiological or pathologic conditions. The use of the ultra high frequency transducers did not contribute to the accuracy, because the problems concerning the anglulation of the transducer and the narrow acoustic window of the joint remained. Measurements obtained with the use of the extended field of view modality when calling up images of specific parts of the structure proved to be more accurate and could offer a future potential for the monitoring of pathologic and healing processes. Three dimensional imaging appears as an exciting and most promising technique that could offer accuracy to measurements but needs to be further investigated.

ACKNOWLEDGEMENTS

I would like to express my gratitude to my Supervisor and Head of the Division of Veterinary Anatomy, Professor J.S. Boyd for allowing me to carry out this project and his scientific and moral support throughout all this period.

I am most indebted to the Supervisor of the Ultrasound Unit Mr Calum Paterson for his assistance with image processings and computer facilities and his moral support. My special thanks to the Lecturer Miss Alison Dickie for her help and advice for the case reports and the completion of this thesis.

I am indebted to Professor S. Love and Dr K. MacEachern of the Weipers Centre for Equine Welfare for allowing me to use the Elegra scanner and to Ramsay MacIvor of Dynamic Imaging for the use of the Diasus scanner.

Many thanks to Leona Cromarty for her invaluable help during the practical sessions of this project and her encouragement and endless sense of humour.

I am grateful to Alan May for his expertise in the Department of Photography.

I would like to thank Alan Reid and all staff technicians of the Division of Veterinary Anatomy, including David Newham (who helped during the cadaver preparations), Alan Purvis, Barbara Lambie, Pat Wilson and Frances Waterson.

My acknowledgements to my Greek friend Stavros Katsikis for his invaluable help with the statistical analysis of my results.

I would also like to thank my Greek friend Rania Konstantatou for the love and support that she has shown during my presence in Glasgow.

I am indebted to the Lecturer of the University of Thessaly Veterinary School, Karditsa, Greece, Dr Georgios Amiridis for the opportunity and information that he offered me in order to deal with this particular field of knowledge.

Finally I would like to express my sincere gratitude and love to my parents Andreas and Maria Marinou as well as my sister Ilia Marinou for their continuous love and guidance, without which this project would have never been accomplished.

DEDICATION

To my parents Andreas and Maria Marinou.

To the memory of my Greek friend Katerina Abatzi.

May her soul rest in eternal peace.

DECLARATION

I hereby declare that the work presented in this thesis was done solely by the author in the Division of Veterinary Anatomy.

Katerina Marinou

Katerina Marinou

LIST OF FIGURES

Page

LIST OF TABLES

CHAPTER 1.

INTRODUCTION AND REVIEW OF LITERATURE

1. INTRODUCTION AND REVIEW OF LITERATURE

1.1. General Introduction

The first attempt to use ultrasonography in animals was described in 1956 in Colorado, United States of America (Temple et al., 1956). In the beginning of the 1960's Holmes and Howry (1963) were able to image abdominal organs of dogs and cats. By 1966 it was possible to detect pregnancy in ewes (Lindahl, 1966). As time passed, it began to be used as an aid for detection of abdominal disease in veterinary practice. Koch (Koch and Rubin, 1969) and Rubin (Rubin and Koch, 1968) first published research on the ultrasonography of the canine eye. It was documented that in the early 1970's Helper (1970) and Lamm (1970) managed to image beating hearts in canine fetuses.

In the 1980's abdominal ultrasound began to be established as a method for diagnosing various abnormalities (Poulsen Nautrup, 2000). For example Dr Norman Rantanen and his colleagues at Washington State University began using ultrasound to detect abnormalities in different organs of horses (Rantanen, 1981; Rantanen et al., 1982). Cartee (Cartee, 1981, Cartee et al., 1980) and Nyland with their colleagues (Nyland and Bernard, 1982, Nyland et al., 1981) dealt with the ultrasonographic appearance of abdominal disease in dogs and cats.

A literature review illustrated that despite the fact that a considerable amount of research has been carried out as far as the examination of equine tendon or joints is concerned (Craychee, 1995), ultrasonographic techniques for detecting abnormalities of the musculoskeletal system in dogs have not been used widely in the past. This has been mainly attributed to the fact that the imaging of small non-bony structures which are close to bones is difficult due to the lack of an optimal scanning angle (Engelke et al., 2000).

Critics of the techniques concerning human diagnostic imaging declared that ultrasound's reliability depends on the sonographer's experience and, consequently, this facility is not able to help visualise some structures in areas like the shoulder, although it can be used for assessing injuries to the mm. supraspinatus, infraspinatus, subscapularis and teres minor and defining pathologic conditions of the articular labrum of this joint (Sandriek, 2000). Magnetic Resonance Imaging constitutes a considerably higher quality diagnostic means for such pathological conditions (Erickson, 1997), which can provide additional information for conditions like muscle atrophy, which is important for orthopaedic surgeons to organise treatment (Sandriek, 2000).

In small animals, some research has been published concerning examination of bones, joints, muscles, ligaments, tendons and the area of the brachial plexus, where different abnormal conditions were scanned (Kramer et al., 1997, Kramer et al., 1999, Long and Nyland, 1999, Reed et al., 1995).

More recent developments in transducer design in order to allow scanning with much higher frequences, as well as innovative developments in signal processing and image reconstruction have renewed the interest in small animal musculoskeletal diagnostic ultrasound.

Ultrasound extended field of view imaging technology has been able to use high resolution real - time imaging capability to produce large field of view images with excellent image quality (Weng et al., 1997). It has been able to overcome the pitfalls and take advantage of the innovations of both real-time and static B-mode scanners (Weng et al., 1997). During the last few years the use of three dimensional ultrasonographic techniques has begun to be explored in clinical medicine (Campani et al., 1998), as since 1994 appropriate software became available and three dimensional images were able to be reconstructed (Campani et al., 1998).

1. 2. Scientific Review

1. 2. 1. Joints

1.2.1.1. Normal ultrasonographic anatomy:

Ultrasound examination of canine joints has proved to be quite difficult, with problems of coupling of the transducer to the body surface, due to the narrow acoustic windows provided because of joint size and shape. However, with the appropriate joint manipulation both the synovial and the articular surfaces have proved to be easily observed, the former being presented as a hypoechoic structure with hyperechoic foci and the latter, in the shoulder joint for instance, with a convex reflective surface that produces acoustic shadowing (Kramer et al., 1997).

The ultrasonographic appearance of hyaline cartilage has been observed as a hypoechoic line between the more echogenic bones and joint tissue. In cases where hyaline cartilage is covered by fluid, a hyperechoic line may be imaged due to the acoustic impedance between cartilage and fluid (Erickson, 1997). Calcifications of cartilage which can normally be found in its deeper layers (Dyce et al., 1987) appear as a hyperechoic line (Erickson, 1997). Fibrous cartilage usually appears hyperechoic compared to hyaline cartilage (Engelke et al., 2000), due to its percentage of coarse type I collagen fibres versus the latter which contains type II collagen fibres, constituting 40% of its dry weight and having a relatively high content of water (Junqueira et al., 1995).

1.2.1.2. Joint pathology:

Pathologic conditions, such as joint effusion (Kramer et al., 1997), especially in cases of bacterial arthritis (Pedersen et al., 2000), defects of the hyaline cartilage due to degenerative causes (Kramer et al., 1997), especially in the case of osteochondritis dissecans on the humeral head or the femoral condyles (Engelke et al., 2000) or cystic lesions have been detected (Beggs, 1998). Joint effusion is easily distinguishable owing to the anechoic or hypoechoic areas present in the joint cavity, whereas haematogenous or purulent effusions usually contain cell structures, that produce hyperechoic reflections (Engelke et al., 2000). Synovial cysts have also proved to be easily observable and they usually appear anechoic, but they may present with internal echoes, since gelatinous or villous content might exist (Beggs, 1998).

Ultrasonographic means have proved to be effective in the diagnosis of synovitis in both large and smaller joints located at various depths within the body. The distinction between a simple effusion and synovial hypertrophy can be made easily, whilst determination of the cause of a synovial swelling is possible, for instance between tenosynovitis or peritendinous oedema (Wakefield, 1998).

Ultrasound-guided aspiration of synovial fluid can help the clinician reach an accurate diagnosis of several diseases. Ultrasound can also facilitate the practical aspect of therapeutic injection of drugs (Long and Nyland, 1999). This constitutes a significant aid for the clinician, since the needle can be visualised during the procedure and the distribution of any injection performed may be constantly monitored (O'Connor, 1998).

Extensive research has shown that ultrasonographically guided needle biopsy in humans may be efficiently used both for monitoring and evaluating the progress of solid and cystic benign and malignant tumours of joint soft tissues. It has been estimated that this procedure is regarded as a risk minimising diagnostic technique in order to assess soft-tissue tumours from a cytological or histologic point of view (Konermann et al., 2000). Moreover it is more effective in limbs as high frequency probes offering better axial resolution can be used (Rubens et al., 1997).

Nevertheless, it has been reported that limitations exist in detecting intraosseous tumours by this method, since most of the sound waves are reflected by the bony structures and, consequently, penetration is very limited (Konermann et al., 2000). There still exist some reservations concerning the use of ultrasound, because there have been reported some unsuccessful attempts to detect and, consequently, intervene in soft tissue lesions using only ultrasonographic means (Rubens et al., 1997).

(A) Shoulder joint:

1.2.1.3. Normal ultrasonographic anatomy:

A thorough study has been conducted recently into the ultrasonographic evaluation of the shoulder joint. The normal anatomical features, including muscles lying around the joint (Long and Nyland, 1999), tendons, bursas and, even, layers of subcutaneous fat (Forrester, 1998) have been scanned and an accurate presentation in B-mode sagittal and transverse images has been achieved (Long and Nyland, 1999). High frequency transducers are capable of distinguishing between different shoulder structures, but the interpretation of the image display depends on the sonographer's skill and experience (Forrester, 1998).

The shoulder joint capsule can be seen deep to the tendons of the mm. supraspinatus, infraspinatus and teres minor, although normally does not appear to have identifiable characteristics (Long and Nyland, 1999). However, approaching the shoulder joint cranially is difficult due to the limited transducer application, caused by the protruding greater tubercle. Moreover, an acoustic window cannot be found when trying to image the joint caudally and medially, because of the limited space and the close fibromuscular connection between the scapula and the thoracic wall respectively (Gassner, 2000). The hyaline cartilage has been visualised as a thin anechoic line between the humerus and the joint capsule, which cannot be detected easily in cases of fluid effusion (Long and Nyland, 1999).

1.2.1.4. Pathology:

It has been demonstrated that there is a possibility of recognising abnormal amounts of synovial fluid, distension of the bursa of the tendon of origin of the m. biceps brachii, calcification of tendons and loss of normal fibre pattern of muscles. It has been illustrated that ultrasonography can be of significant value in identifying causes of forelimb lameness due to soft tissue injury (Long and Nyland, 1999).

In cases of bicipital tenosynovitis considerable deviation from the normal ultrasonographic appearance may be seen. A loss of imaging of the hyaline cartilage (sclerosis of the intertubercular groove) in combination with excessive fluid and loss of the normal tendon echotexture are indicative of this pathologic situation (Long and Nyland, 1999).

It has been reported that ultrasonographic means are able to detect osteochondritis dissecans even at its early stages. The caudal irregularities of the humeral head are distinct and, with progression of the disease, infractions of the contour of the humeral head take place. Detached cartilage may be viewed as a hyperechoic, free objects moving within the joint space, while in cases of calcification distal acoustic shadowing is evident. As the disease evolves, reactive thickening and joint effusion may be visualised (Gassner, 2000).

Even very small amounts of fluid may be visualised in the subacromial or subdeltoid bursa. Occasionally, the m. deltoideus may present with internal septations, the anechoic parts of which may mimic a thickened bursa. This may be avoided if the structures under suspicion are followed laterally, so that the real bursa can be visualised underneath the m. deltoideus and end up at the proximal humerus (Zanetti and Hodler, 2000).

(B) Stifle joint:

1.2.1.5. Normal ultrasonographic anatomy:

The ultrasonographic anatomy of the canine stifle has also been published (Reed et al., 1995). Both long and short axis ultrasonographic images have been recorded concerning most anatomical structures of the stifle. Fascia (although a distinction is not always evident), the patellar ligament (Kramer et al., 1999), the infrapatellar fat (Engelke, 2000, Kramer et al., 1999), the medial and lateral menisci, bony surfaces, normal cartilage, as well as the cranial cruciate ligament have been readily observed (Kramer et al., 1999).

A well designed study has shown that medial and lateral menisci can be seen as homogeneous, hyperechoic and triangular-shaped tissues in live dogs (Reed et al., 1995). The use of a stand-off pad improves the imaging of these structures (Kramer et al., 1999). The same image has been obtained in human cadavers, where intra-articular imaging has proved that the menisci can be visualised in their entirety together with other intra-articular structures, such as the cruciate ligaments, that cannot be seen easily otherwise and the hyaline cartilage, which covers the articular surface (McDonnell et al., 1992). It has been shown that the latter produces a well defined hypoechoic line at the level of the boundaries between bone and cartilage or cartilage and soft tissues (Reed et al., 1995).

The infrapatellar fat has been viewed as a hyper reflective structure and with indistinct margins. There usually exists some fluid between the patella and the fat which ranges from hypoechoic to anechoic, whereas, in cases of chronic diseases it turns out to be more hyperechoic and inhomogeneous (Kramer et al., 1999).

1.2.1.6. Pathology:

A carefully designed study concerning the human stifle joint has demonstrated that in cases of arthritis the cartilage may be affected as well. Arthritis is suspected in cases of narrowing of the cartilage in combination with synovial thickening and effusion (Aisen et al., 1984). A defect of the stifle cartilage occurring in cases of osteochondritis dissecans in dogs has been reported and it has been observed on the lateral condyle of the femur, in the form of detached hyper reflective structures of various sizes, whilst the surface of the underlying bone appears to have irregular margins (Kramer et al., 1999).

Meniscal cysts have been observed successfully by ultrasonographic means. They have been imaged as small in size, multilocular and with internal echoes. Their detection helps in the diagnosis of partial or full ruptures of the menisci (Beggs, 1998), which, although they are considered to be difficult to demonstrate ultrasonographically (Kramer et al., 1999), can be visualised by this way, because these cysts are considered to contain joint fluid, that has changed position due to a meniscal tear (Beggs, 1998). It should be noted however that this diagnostic method must be evaluated carefully since misdiagnosis is frequent (Engelke, 2000).

Stifle joint effusion can be easily assessed (Kramer et al., 1999). Dilation of the suprapatellar recess is evident (Beggs, 1998) and medial displacement of the infrapatellar fat body is easily recognised. Cartilage abnormalities due to osteochondrosis dissecans can also be diagnosed (Kramer et al., 1999).

Tumours protruding into the stifle joint are easily detectable. They do not usually present with the same echogenicity in all their parts, varying from anechoic to very hyperechoic. It has been illustrated that tumours in the distal femur have been detected ultrasonographically in dogs and have proved to be hypoechoic with indistinct margins. Lipomas can also be easily identified as such because of their hypoechoic appearance with irregular dots or streaks (Kramer et al., 1999).

(C) Tarsal joint

1.2.1.7. Normal ultrasonographic anatomy:

The normal anatomy of the tarsal joint has been investigated in humans. The anterolateral (dorsolateral) pouch of the tarsal joint capsule has been detected ultrasonographically in humans, but its boundaries have not been determined with accuracy, since the lateral collateral ligament, which constitutes one of them, has not been imaged successfully (Friedrich et al., 1993).

1.2.1.8. Pathology:

It has been reported in humans that small amounts of fluid can be found normally in the tarsal joint, as well as in the tendon sheaths. But, even when fluid increases in asymptomatic patients, it cannot be considered as an abnormal situation as it appeared to vary in amount in healthy volunteers (Nazarian et al., 1995). However blood effusions due to injuries have been observed due to the convex shape that the joint cavity acquires (Friedrich et al., 1993).

It is important to mention that pathologic situations of most anatomical structures of the tarsal joint are prone to misinterpretation if an accurate ultrasonographic technique is not applied properly. Both longitudinal and transverse scannings "in orthogonal planes" are essential in order to evaluate any kind of deviation from normal characteristics (Waitches et al., 1998).

1. 2. 2. Ligaments

Experimental studies carried out some years ago showed that it was difficult to scan ligaments due to their close position to the bone surface (Kramer et al., 1997). There is evidence however suggesting that it is possible to image them with a certain degree of accuracy, although the use of large amounts of acoustic coupling gel or a stand-off pad are required in order to optimize the imaging of superficial structures (Reed et al., 1995).

Ligaments in the horse seem to be slightiy more echogenic compared to tendons with a more homogeneous appearance and a coarser fibre pattern on a long axis view (Craychee, 1995).

1. 2. 2. 1. Pateliar ligament:

It is possible to identify the pateilar ligament in live dogs, appearing as a homogeneous hypoechoic to moderately echoic structure, containing parallel longitudinal echogenic collagen fibres and having an oval shape when imaged in a transverse plane (Reed et al., 1995). It seems, though, to be of lower echogenicity when compared to that of the superficial fat lying dorsally (Fornage et al., 1984). Both the superficial and deep fascia are able to be visualised cranial to the patellar ligament (Reed et al., 1995).

Pathology of the patellar ligament usually includes traumatic injuries (ruptures in most cases) followed by haemorrhages, which appear as hypoechoic structures. However, in cases of partial ruptures the amount of fluid is less and does not produce any acoustic enhancement (Fornage et al., 1984). If the patellar ligament has been pulled off the patella, small hyperechoic pieces creating acoustic shadowing may be seen, corresponding to patellar fragments. In cases of partial ruptures mentioned above a fragment of the tibial tuberosity may be observed (Kramer et al., 1999).

Patellar tendinitis can be identified by ultrasonographic means as well as calcifications, which are indicative of a chronic pathological condition (Fornage et al., 1984). It has been proved that patellar sonographic lesions may be observed even in cases of asymptomatic human patients and are related to a greater risk of a later incidence of patellar rupture (Cook et al., 2000).

The processes of healing and consolidation of the patellar ligament after rupture has taken place can be documented. During the early days of the injury the ligament looks thicker and appears with varying echogenicity, while its two parts can be distinguished. The ligament thickness decreases during the next six weeks, since the fibres obtain a more normal orientation, which results in a normal echoic appearance. However some inhomogeneous regions may be detected for months (Kramer et al., 1999).

1. 2. 2. 2. Cranial cruciate ligament:

The cranial cruciate ligament has been imaged ultrasonographically with the dog's leg in full flexion, in order to obtain a better acoustic window. It has been illustrated that the cranial cruciate ligament appears echogenic, but due to the anisotropy artifact it may be imaged as more hypoechoic in comparison with the patellar ligament mentioned above, as well as with the surrounding fat (Reed et al., 1995). The use of a stand-off pad in large and very large breeds of dogs is not recommended due to the creation of reverberation artifacts which can be misleading in the diagnosis of pathologic situations of this ligament (Kramer et al., 1999).

1. 2. 2. 3. Caudal cruciate ligament:

The imaging of the caudal cruciate ligament has presented several difficulties (Reed et al., 1995). The caudal cruciate ligament has been scanned successfully only in large breed dogs that have undergone maximal extension of the stifle joint and appears as a hypoechoic round structure. This suggests a difficulty in visualizing intra-articular structures of the stifle joint, because the acoustic window provided is very narrow (Kramer et al., 1999).

1. 2. 2. 4. Collateral ligaments of the stifle joint:

The collateral ligaments can be imaged by placing the transducer on the medial or lateral side of the stifle joint but, usually, it is not possible to differentiate between them and the adjacent subcutaneous tissue (Engelke, 2000) due to their close proximity to the underlying bones and their narrow width. The use of a stand-off pad has not contributed in that goal. In cases of injuries, though, haematomas have been detected by ultrasonographic means (Kramer et al., 1999).

The medial collateral ligament, that extends between the medial epicondyle of the femur and the medial border of the tibia (Evans, 1993) has appeared in human ultrasonograms as a thin and relatively homogeneous hypoechoic band, whereas, it has been imaged as thickened with areas of different echogenicities when injured (Lee et al., 1996).

1. 2. 3. Muscles

1. 2. 3. 1. Normal ultrasonographic anatomy:

Real-time ultrasound has proved to be valuable for the assessment of the muscular system in dogs (Kramer et al., 1997, Siems et al., 1998, Farrow, 1996). There is a potential of viewing the normal appearance of muscle structures, in particular the musculotendinous junction, but also the normal fibre pattern and the differing echogenicities among the various parts of a muscle and its surrounding tissues, such as the connective tissue fascia or subcutaneous tissue (Craychee, 1995). The muscle fibres are imaged like a group of parallel orientated hypoechoic "lines" surrounded by the hyperechoic perimysium (or intermuscular septum). Meanwhile, the whole muscle is surrounded by the epimysium, which is hyperechoic as well. Muscles, especially those in contraction, tend to be more hypoechoic than subcutaneous fat or tendons (Winter, 1998).

Certain muscles appear to have a characteristic sonographic image. For instance, the m. biceps brachii has, according to Engelke and Gassner (2000), "a typical fish-bone pattern", whilst the m. infraspinatus appears "with a one-sided, dorsal muscle fibre appearance".

1. 2. 3. 2. Masses:

Ultrasound is considered to be of great value in confirming and diagnosing an existing mass, in as much as it could be a normal muscle asymmetry or subcutaneous fat (Beggs, 1998). Sonographic classification of muscle masses can be made according to the compressibility of the mass, various differing mobile echoes within a single structure or the degree of septation and vascular supply. It is extremely useful for planning the next steps to be taken by the clinician (Engelke and Gassner, 2000).

1. 2. 3. 3. Abscesses:

Muscle abscesses have proved to be simple to examine (Kramer et al., 1997). Their ultrasonographic appearance varies from a totally anechoic mass to an indistinct structure with varying echogenicity (Beggs, 1998). It is possible to evaluate both the age and the position of an abscess (Kramer et al., 1997), by including the presence of air, cellular debris (Craychee, 1995) or even calcification (Engelke and Gassner, 2000). Abscesses of the mm. semimembranosus and semitendinosus have been reported in horses (Craychee, 1995). Diffuse inflammatory processes, by contrast, can be detected with great difficulty (Kramer et al., 1997). Pathologic conditions with similar ultrasonic appearance, such as muscle lymphoma or pyomyositis, are more characteristic (Beggs, 1998), but muscle atrophy is not easily detectable (Kramer et al., 1997).

1. 2. 3. 4. Oedema:

Muscle oedema has been reported to produce a certain sonographic appearance in equine subcutaneous tissue, which is attributed to the distribution of fluid in adipose tissue. The presence of lymphoedema has also been documented (Craychee, 1995).

1. 2. 3. 5. Foreign bodies:

It has been shown from previous research that foreign bodies can be imaged only when their size is larger than 2-3 mm (Kramer et al., 1997). Ultrasonography, however, tends to be more effective than radiographic techniques, since more materials can be viewed by B-mode echo display systems including wood, pencil graphite and plastic. Its value is of great importance, especially in preventing complications like osteomyelitis or other infections or even in loss of a limb. Furthermore, ultrasonography is able to determine the depth of foreign bodies from the skin surface (Shah et al., 1992) and facilitate their surgical removal (Fornage and Schernberg, 1986).

1. 2. 3. 6. Hyperextension:

Resultant fibrosis of the m. semitendinosus after hyperextension has been reported to have been evaluated ultrasonographically in horses as an accompanying important lesion in such cases (Craychee, 1995).

1. 2. 3. 7. Ruptures:

According to Farrow, "a complete separation is called a rupture, unless it occurs at the origin or insertion of the muscle, in which case it is called an avulsion". Ruptures, as in the case of the part of the m. gracilis inserting onto the tuber calcanei in racing dogs, especially Greyhounds, may occur (Hermanson and Evans, 1993). Farrow implies that "contemporary classification schemes describe muscle tears as being mild, moderate or severe in degree" (Farrow, 1996). However, most of the studies carried out concerned cattle, sheep, horses and of course humans. Two dimensional, real-time ultrasonography can facilitate the estimation of such cases and, furthermore, can be used for avulsions (at the origin or insertion of muscles) (Farrow, 1996). This is significant, because such conditions are able to cause serious problems with the animal's movement (Vaughan, 1979).

1. 2. 3. 8. Muscle contractures:

Contractures of the mm. infraspinatus, supraspinatus, gracilis, semimembranosus and quadriceps femoris have been reported in dogs causing subsequent lameness, while producing a characteristic sonographic image. The m. infraspinatus especially appears with a fibrous induration imaged at the acromion level, but, in general, the scanning of a contracted muscle in a longitudinal plane reveals inhomogeneous echogenic muscle lesions (Engelke and Gassner, 2000).

1. 2. 3. 9. Haemorrhage:

It has been pointed out that haemorrhage into muscles can be relatively easily observed, especially after severe traumas or sequential to bleeding disorders. Differing degrees of echogenicity can be estimated according to the stage of organisation of haematomas and the frequency of the transducer. Subsequent muscle enlargement can be imaged and various patterns of echogenicity are distinguishable in cases of chronic or recurrent injuries. Haemorrhage of the mm. semimembranosus and semitendinosus has also been reported in horses (Craychee, 1995).

1. 2. 3. 10 Muscle healing:

Extensive research has shown that the whole process of muscle healing, after a traumatic or post-operative rupture may be documented (Kramer et al., 1997, Siems et al., 1998). The different echogenicities associated with scar formation and reconstruction of muscle tissue, including organisation of haematomas, have been explored (Kramer et al., 1997, Siems et al., 1998, Farrow, 1996). This is of particular interest because true muscle regeneration requires almost ideal conditions in order to occur properly and, as a result, mostly includes connective tissue creation (Vaughan, 1969).

1. 2. 3. 11 Tumours:

Ultrasound can be generally accurate in determining muscle tumours, especially when they have a respectable size (Farrow, 1996). Their inter- or intra- muscular position can also be determined (Gerwing and Kramer, 1995). Furthermore, a distinction between benign and malignant characteristics can be recognised ultrasonographically (Craychee, 1995), although the distinction between cystic and solid masses could be misleading, since a benign tumour, for example, may appear with a solid and indistinct echotexture. In those cases a fine needle aspiration can be performed successfully despite the high risk prevalence (Beggs, 1998).

1. 2. 4. Tendons

The normal sonographic anatomy of tendons has been observed (Farrow, 1996, Kramer et al., 1997). Ultrasonography is considered to be a more accurate diagnostic method than Magnetic Resonance Imaging in several situations and, especially, in assessing areas of differing texture within an injured tendon and even slight abnormalities (Waitches et al., 1998).

1. 2. 4. 1. Normal ultrasonographic anatomy:

Using repetitive long axis and transverse scans, it has been shown that tendons are highly echogenic structures owing to the high levels of collagen that they contain (Craychee, 1995). The numerous hyperechoic lines are due to the strong acoustic interfaces between collagen bundles and endotendineus septa within a tendon. It has been well documented in human medicine that tendons deriving from a single muscle appear with a homogeneous echogenicity, whereas, tendons which are formed from the insertions of more than one muscle (i.e. the common calcaneal tendon or the tendon of the m. quadriceps femoris) usually have a different echotexture, resulting from the various heads of the muscles participating in their formation. A final common trunk can also be seen in their distal part (Martinoli et al., 1999).

It has been shown that tendons lying close to each other can be distinguished ultrasonographically by a hypoechoic interface resulting from the imaging of their tendon sheaths. Meanwhile, sesamoid bones which lie inside tendinous structures (Martinoli et al., 1999), e.g. fabellae in the medial and lateral head of the m. gastrocnemius, as well as in the tendon of the m. popliteus (Evans, 1993), can be visualised. Furthermore, the musculotendinous junctions have been able to be distinguished. More specifically, the tendon attachments to muscles are more gradual compared to those concerning bones, which are more prominent and include a narrow hypoechoic zone corresponding to fibrocartilage (Martinoli et al., 1999).

Tendons are usually surrounded by a paratenon or a synovial sheath, the latter being constituted by two layers, an internal visceral and an external parietal layer connected between each other with a mesotendon, that provides adequate blood supply. It has been shown in human orthopaedics that ultrasonographic means are able to distinguish those two layers as hypoechoic lines separated by an anechoic surface, which represents a slight amount of fluid existing within the mesotendon space (Martinoli et al., 1999).

The tendon of the m. biceps brachii has been detected by using a 10 MHz probe as a homogeneous hyperechoic structure (Long and Nyland, 1999) lying in the intertubercular groove of the humerus (Hermanson and Evans, 1993), which in the musculotendinous junction is converted to a hypoechoic structure corresponding to the muscle fibres. The bursa of the tendon of the m. biceps brachii has also been visualised by researchers in its distal part as a fluid-filled pouch, with a small amount of anechoic fluid being also detected at the level of origin of the tendon of the m. biceps brachii on the supraglenoid tubercle (Long and Nyland, 1999); in a transverse view this offers the more characteristic image of the tendon of the m. biceps brachii appearing as a round or oval structure surrounded by the joint capsule sac (Engeike and Gassner, 2000).

The tendon of the m. supraspinatus has been imaged as a short tendon with a broad insertion, lying almost underneath the patient's skin (Long and Nyland, 1999). The tendon of the m. infraspinatus has also been seen as a long homogeneous structure inserting at the lateral aspect of the distal part of the greater tubercle (Long and Nyland, 1999; Hermanson and Evans, 1993).

The tendon of the m. extensor digitorum longus has been detected in the canine stifle joint by means of a stand-off pad. Its exact location has been determined, as well as the soft tissues surrounding it (Kramer et al., 1999).

The common calcaneal tendon can be easily imaged, owing to its length, although a stand-off pad is almost always necessary. A hypoechoic area may be seen just proximal to the calcaneal tuberosity, since all the tendon fibres, that constitute the insertions of various muscles, do not insert with the same angle (Gassner and Engelke, 2000) but they do this in a curved path (Bertolotto et al., 1995). This necessitates the change of the angle in order to achieve an optimal view (Gassner and Engelke, 2000).

The subcutaneous and calcaneal bursae cannot be imaged, unless they become oedematous. Moreover, fat surrounding both the tendon and the adjacent bones appears hypoechoic and with indistinct margins. The bone surfaces of the tibia, the calcaneus and the talus are viewed as highly reflective structures causing acoustic shadowing (Gassner and Engelke, 2000)

1. 2. 4. 2. Ruptures:

Tendon ruptures differ from strains in that the latter term usually refers to microscopic tissue damage, which is not able to be detected clinically, radiologically or surgically (Jozsa and Kannus, 1997). Both partial or complete rupture of a tendon may occur (Kramer et al., 1997) as a result of a trauma or a weight overload (Martinoli et al., 1999) and have been reported for the common calcanean tendon in beagles and spaniels, especially those which are permanently kept in cages (Jozsa and Kannus, 1997). In either case, an accurate sonographic view has been obtained in dogs (Kramer et al., 1997), whereas in humans intracapsular ruptures of the tendon of origin of the m. biceps brachii and discontinuity of the common calcaneal tendon fibres in partial ruptures have been most frequently reported to be detected by scanning (Jozsa and Kannus, 1997).

It has been proved that degenerative or minor traumatic conditions already pre-exist in most cases of tendon ruptures, which offers an explanation to spontaneous ruptures of apparently unknown origin. Metabolic changes due to underlying systemic diseases, such as systemic lupus erythematosus, are considered to be responsible for tendon ruptures without previous traumatic incidence. Patients with a previous history of endotendinous steroid injections have proven to be prone to ruptures as well. It has been illustrated that scanning techniques are able to identify tissue changes resulting from degenerative causes, and in combination with the possibility of differentiation between partial and complete tears, can provide the clinician with extremely useful information with regard to treatment (Martinoli et al., 1999).

It is documented that to diagnose a full rupture it may not be necessary to evaluate it ultrasonographically, because the clinical appearance is characteristic (Waitches et al., 1998). In cases of complete rupture an ultrasonogram can reveal a full disruption of tendon fibres (Martinoli et al., 1999) with the two parts of the tendon hyperechoic and in some cases thickened as the case of rupture of the tendon of origin of the m. biceps brachii (Gassner and Engeike, 2000) and a subsequent development of a hypoechoic haematoma or even granulomatous tissue. The absence or presence of these characteristics are indicative of the time passed since the rupture occured (Martinoli et al., 1999).

In the case of a complete rupture of the tendon of origin of the m. biceps brachii the intertubercular groove is empty, but, in the mean time, the paratenon, the synovial sheath and, sometimes, even granulomatous tissue may mimic the presence of a real tendon structure (Gassner and Engeike, 2000).

Partial ruptures, conversely, are more common and difficult to diagnose, which necessitates the need for ultrasonographic evaluation (Waitches et al., 1998). They are characterised by the disappearance of the classic fibrillar pattern in the ruptured part and the preservation of it in the intact part of the tendon (Martinoli et al., 1999). The common calcaneal tendon has been reported to be thickened in that specific area, whereas a hypoechoic surrounding area appears when effusion in the tendon sheath exists. Tendon fragments are imaged, according to the authors, as "club-like and shaggy" (Gassner and Engelke, 2000).

When the tendon sheath is ruptured as well, the amount of fluid usually found in cases of simple rupture appears to increase and a larger haematoma is produced, which is ultrasonographically detectable with irregular and indistinct margins. The two parts of the tendon must be defined carefully, because they might be found at various distances from the injury site (Martinoli et al., 1999).

1. 2. 4. 3. Avulsions:

Chronic tendon avulsions can be diagnosed by means of ultrasound scanning and other diagnostic methods (Jozsa and Kannus, 1997), while sonographic assessment of avulsion of the tendon of the m. gastrocnemius has been reported (Farrow, 1996). Cases of avulsions of the tendon of the m. biceps brachii are characterised by hypoechoic areas due to oedema or haemorrhage. Tendon displacement is very often evident, whilst bone fractures are very frequently visualised within the tendon. Haematomas may be imaged under the periosteum in the fracture area. The sonographic image of a fractured bone with differences between the echotexture of the cortex and the spongiosa is detected (Gassner and Engelke, 2000).

1. 2. 4. 4. Tendinitis:

Tendinitis has been reported being imaged with a varying appearance. In cases of equine acute tendinitis the sonographic characteristics constitute an image of decreased echogenicity (Craychee, 1995). The tendon is enlarged and looks inhomogeneous with focal hypoechoic regions (Martinoli et al., 1999), while its sheath contains more fluid than normal. Conversely, chronic tendinitis appears with a thickening, inhomogeneity and decreased echogenicity of the affected tendon (Craychee, 1995), as well as loss of specular echoes. Such lesions can be detected ultrasonographically also in older patients (tendinosis), but it has not been clarified whether they are a result of age or a forthcoming rupture (Martinoli et al., 1999). In either case, it has been proved that ultrasound is highly reliable in detecting sequel conditions (e.g. calcifications parallel to the tendon fibres - Engelke and Gassner, 2000), even minor ones (Craychee, 1995) or ruptures of the subacromial bursa (Martinoli et al., 1999).

1. 2. 4. 5. Calcifications:

Calcifications of the tendon of the m. supraspinatus have been well documented in dogs. Various focal hyperechoic regions representing calcification, creating acoustic shadows in the far field can be imaged, indicating the presence of calcified tissue. Acoustically mixed lesions have been reported to be seen in cases of trauma of the m. supraspinatus (Long and Nyland, 1999). When calcifications are imaged in an acute phase they are usually accompanied by oedema, whereas when they appear inside the tendon they may have either a focal or a diffuse appearance and sometimes do not cause an acoustic shadow (Engelke and Gassner, 2000).

Calcifications of the tendons of the mm. supraspinatus, infraspinatus, subscapularis and teres minor have been reported in humans despite the difficulty sometimes encountered in their location. They usually form hyperechoic foci that are more easily detectable by ultrasonographic means rather than fluoroscopy (Farin et al., 1995).

1. 2. 4. 6. Tenosynovitis:

Modern equipment has made it possible to image even slight abnormalities to the paratenon and the synovial sheaths (Martinoli et al., 1999). As far as the former structure is concerned, peritendinous fluid in combination with thickening of the tendon and peritendinous structures and formation of fibrous tissue are the main ultrasonographic findings encountered. Synovial inflammation is characterised by thickening of the synovial sheath and production of excessive amounts of fluid. Imaging with high resolution transducers has shown that fluid echogenicity can vary from totally anechoic to hyperechoic and with a flocculent appearance. In hypertrophic synovitis hypoechoic villous protrusions can be detected among the fluid effusion, whereas in cases of calcifying tendinitis the bones involved appear with bony irregularities (Martinoli et al., 1999).

1. 2. 4. 7. Intertubercular groove osteophytes:

They are usually produced as sequels of degenerative lesions, calcifications or calculi embedded in the intertubercular groove. In short axis views the groove seems to lose its round pattern, while the edges of the groove fall into it and produce acoustic shadowing. Acute lesions are followed by the presence of fluid. The humeral surface becomes more irregular and different degrees of echogenicity are encountered (Engelke and Gassner, 2000).

1. 2. 4. 8. Dislocation:

Dislocation usually takes place in tendons that are surrounded by synovial sheaths and constitutes the sequel of injury, which is usually confirmed by the detection of peritendinous effusion (Martinoli et al., 1999). Dislocation of the tendon of the m. flexor digitorum superficialis has been reported, being assessed sonographically in dogs, especially for confirmation of diagnosis made by palpation of the affected region (Farrow, 1996).

Dislocation of the tendon of the m. biceps brachii can be easily identified in dogs (Kramer et al., 1997). A flattened intertubercular groove and a defective transverse ligament are considered as the most important predisposing factors (Josza and Kannus, 1997). It usually happens medially in humans and the transverse ligament tends to remain intact. However, it is reported that the ligament is torn in some cases and the tendon of the m. biceps brachii is displaced superficial to the tendon of the m. subscapularis, which can lead to a safe ultrasound diagnosis, since the intertubercular groove is found to be empty and the tendon is in a medial position (Martinoli et al., 1999), usually at the groove edge or on the lesser tubercle (Engelke and Gassner, 2000). Ultrasound techniques on the other hand can offer the potential for misinterpretation in cases of synovial debris remaining in the groove (Martinoli et al., 1999). Entrapment of joint mice in the sheath of the tendon of the m. biceps brachii has been imaged in dogs as well (Kramer et al., 1995).

1. 2. 4. 9. Oedema:

Peritendinous oedema can be evaluated readily by ultrasonographic means, since oedematous fluid lends itself well as a fluid-soft tissue interface, helping in normal displaying of the tendon, but allowing the paratendon to be imaged separately from the skin. Peritendinous oedema and in a similar way, peritendinous haemorrhage of the tendon of the m. flexor digitorum superficialis has been recorded in horses (Main, 1995).

1. 2. 4. 10. Tendon healing

Real-time ultrasound can be extremely useful in the estimation of tendon healing. Repetitive scans can allow a successful monitoring of the healing process and the time required to obtain full tendon reconstruction (Kramer et al., 1997), or, conversely, deterioration of a lesion (Craychee, 1995). Generalised tendon thickening, scars and granulomatous tissue can easily be imaged with ultrasound, especially in the case of the common calcaneal tendon. Such processes are extremely helpful in cases of older common calcaneal tendon tears which cannot be easily diagnosed clinically due to the time interval between the accident and the possible diagnosis (Jozsa and Kannus, 1997). Therapeutic results of anti - inflammatory drugs and exercise protocols can be assessed with ultrasound (Craychee, 1995).

1. 2. 4. 11. Postoperative evaluation of various tendons:

Wound healing after surgical repair can be accurately estimated by means of ultrasonographic procedures. It has been shown in human postoperative scans that the tendons of the mm. supraspinatus, infraspinatus, subscapularis and teres minor usually appear hyperechogenic and thinner compared to their contralateral tendons (Martinoli et al., 1999). The acromion is imaged as a less smooth and homogeneous surface, whereas, the echogenicity of the tendon of the m. supraspinatus is abnormal in relation to the contralateral one (Mack et al., 1988). In addition, postoperative imaging of the common calcaneal tendon has revealed that the tendon appears enlarged and without the classical fibrillar echotexture (Martinoli et al., 1999).

Suture remnants are often easily distinguishable (Craychee, 1995), even after extremely long periods of time (e.g. years). The latter are visualised as bright specular reflections producing a comet tail artifact or an acoustic shadow (Martinoli et al., 1999).

Tendon reconstruction can be monitored with ultrasound (Craychee, 1995). A degree of normal fibre echotexture of the common calcanean tendon may be seen six weeks after the operation (Engelke and Gassner, 2000). It has been reported, though, that " the normal longitudinal oriented echostructure cannot be detected during the first 6 months after rupture" and it is doubtful whether a full histological recovery may be obtained in the following years (Rupp et al., 1995).

1. 2. 4. 12. Tumours:

It has been illustrated that primary tendon tumours, although rare in general, usually occur around tendon sheaths. They tend to be anechoic, but sometimes expand within the tendon substance and render it prone to spontaneous rupture (Martinoli et al., 1999). Extremely hyperechoic areas corresponding to calcifications have been reported in tumours of the tendon of the m. biceps brachii (Engelke and Gassner, 2000). Ultrasound is capable of determining the exact location of a tendon tumour effectively (Martinoli et al., 1999).

1. 2. 4. 13. Limitations:

It is important to comment on the limitations of ultrasonography in the diagnosis of specific pathologic conditions, such as tendon microtears. A decreased echogenic appearance is not always able to indicate whether a minor tendon disruption or another lesion (e.g. tendon oedema) is present, which indicates the necessity of a concurrent clinical evaluation in order to decide upon the healing progress and further prognosis (Craychee, 1995).

1. 2. 5. Errors in Measurements

It is well known that conventional ultrasound is widely used in order to evaluate the size of or the changes to an organ during a disease process (Riccabona et al., 1995). In recent times, three dimensional ultrasound has been investigated as to its potential in clinical use for this purpose, by questioning that its measurements are reliable and valid (Farrell et al., 2000).

Reliability refers to the ability of a trial to present the same results in the same subject of study repeatedly, which is best known as intra-rater reliability. When the same results are produced by different observers, who follow the same procedure, then the term "inter-rater reliability" can be used. Furthermore, validity of a test refers to the degree of success where the taken measurement coincides with the true or definitive result produced with a widely recognised reference test (Farrell et al., 2000).

The reliability and validity has to be taken into account, because errors in distance measurements usually occur. These are observed in all ultrasound images and are dependent on the nonzero size of the image pixels, the specific image-acquisition process utilised and are different for each image processing system (Goldstein, 2000).

Image pixelation errors can occur when the operator selects two image pixels on the screen in order to take a distance measurement. Taking into account that the echoes are displayed on the screen in the form of discrete square pixels and their amplitude is expressed by various degrees of gray colour, it can be easily deduced that the smallest unit of length that is able to be measured is the pixel width, which is displayed with a uniform shade of gray. Errors can also be made in cases of wrong caliper orientation by the operator himself or herself (Goldstein, 2000).

It has been reported that if the operator takes many measurements from a frozen image and averages these results, then this may lead to higher accuracy. But even better results can be achieved if an individual ultrasound image is taken for each distance measurement, because in this case they will be independent of pixel size (Goldstein, 2000).
Ultrasound-specific errors may also occur, since some anatomical features (in this case mentioned as targets) are not placed in the imaging plane properly (Goldstein, 2000). According to the same author, "they are due to target misregistration and edge shifting".

When the acoustic velocity between adjecent tissues is not 1540 m/sec, or when the sound beam does not travel in a straight line (usually because of reflection, refraction or reverberation artifacts) then the target will not appear on the screen in the right way but, in most cases, errors due to the above are minimal (Goldstein, 2000).

Nonzero lateral beam width (which implies worse lateral resolution) may hinder the imaging of the real edge of some structures, by shifting its position towards a region with weaker echoes. According to Goldstein, "the image gray scale is proportional to the logarithm of the echo amplitude, so the low amplitude image tail edge extends further from the true edge than its high amplitude peak" and "there are more digital gray levels at low echo amplitudes". These constitute the two main factors for edge shifting ultrasound-specific distance measurement errors.

Distance measurements taken with the use of 2D ultrasound are considered to have an overall accuracy within 2% of the actual length, whereas the same percentage for volume measurements with 3D ultrasound devices lies between 5 and 20% for regular shaped organs (Farrell et al., 2000). The latter kind of measurements turns out to be extremely inaccurate in cases of irregularly shaped or too large to be imaged in a limited field of view structures (Riccabona et al., 1995). But, in general, 3D ultrasound is considered to be of equally high reliability with 2D ultrasound as far as distance measurements are concerned and of superior validity for volume measurements (Farrell et al., 2000).

The use of a measurement protocol has been suggested in order to minimize ultrasound-specific errors. The use of the same transducer for the same distance measurement and the selection of a standardised frequency range can be useful. Moreover, the placement of the organ to be observed in the centre of the image plane, or in a parallel or, at least, standardised angle to the pixel lines is expected to improve the measurement's precision. The adjustment of image magnification into at least one half of the image field of view is expected to contribute to the higher accuracy of measurements. Finally, the proper adjustment of gain for the display of a uniform gray scale image at the point where the measurement is about to be taken can be helpful (Goldstein, 2000).

CHAPTER 2.

PHYSICAL PRINCIPLES

2. PHYSICAL PRINCIPLES

2.1. Physical properties of ultrasound

The transducers used in diagnostic ultrasound contain one or more crystals with piezoelectric properties. It has been quoted in several books in the literature that the term "piezo" derives from the Greek word meaning pressure. However, it should be spelt as "pieso", which corresponds to the actual meaning of pressure in Greek (piesi), rather than "piezo", which stands for the Greek verb meaning press. In either case, it represents the ability of these crystals to produce an electric current when deformed by returning echoes and, conversely, to undergo mechanical transformation, in case of a transmission of an electric current (Ginther, 1995).

Diagnostic ultrasound is based on the pulse-echo principle. This can be explained by means of the following example:

The pulse corresponds to a shouting "Hello" of a man standing on one side of a canyon towards the other. That pulse travels at the speed of sound (340 m/sec) and hits at the opposite side of the canyon. It then turns back to the man who emitted the sound at the same speed and, consequently, he hears the echo (Bartrum and Crow, 1977).

If the man mentioned above had a stopwatch, he would be able to calculate the distance to the other side of the canyon, if he measured the time required for the echo to come back to him. He could then work out the distance using the following equation: $d = v \times t/2$,

where v is the speed of sound and t the time that has passed between the emission of the sound and the return of the echo to the man (Bartrum and Crow, 1977).

Ultrasound uses approximately the same model: A short pulse leaves the transducer and travels through the body tissues at a specific speed, until it encounters a reflective surface. The pulse returns back to the transducer and the scanner calculates the time that has passed and is able to find out the distance that has been covered by the echo pulse. The co-ordinate for the reflective surface is then displayed on the screen in the form of a dot and its position is indicative of the distance the ultrasound pulse and the returning echo has travelled (Bartrum and Crow, 1977) (Fig. 2.1.).

Some useful terms commonly used in diagnostic ultrasonographic imaging are described below:

Amplitude refers to the loudness of the sound waves (Ginther, 1995) and is the peak pressure or height of the wave compared to the resting value (Meire and Farrant, 1995).

Frequency represents the number of vibrations or oscillations of the sound source per second (Meire and Farrant, 1995).

Wavelength is the distance the wave travels during a single cycle. The wavelength is calculated by dividing the velocity by the frequency (Poulsen Nautrup, 2000).

Velocity refers to the speed of the wave and depends on the physical characteristics of the medium in which ultrasound travels, such as elasticity and density (Ginther, 1995). Sound velocity is constant in similar body tissues (1540

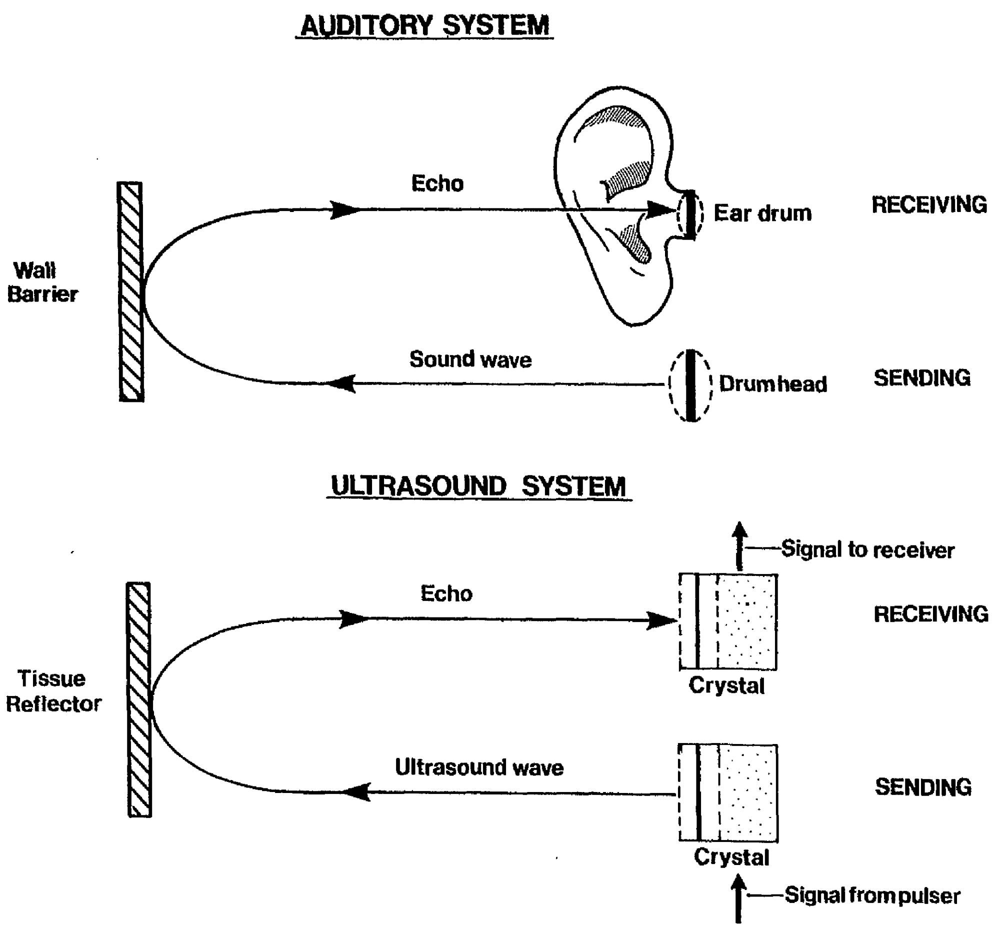

Fig. 2.1. Comparison of the reception of echoes from audible sound and diagnostic ultrasound.

m/sec in soft tissues) (Nyland et al., 1995), yet is different when a sound beam encounters lung tissue (600 m/sec due to the air in the tissue) or bone (4080 m/sec) (Ginther, 1995). Sound velocity has a relationship with frequency and wavelength, which is shown in the equation:

Velocity (m/sec) = Frequency (cycles/sec) x Wavelength (m)

(Nyland et al., 1995).

Intensity is indicative of the ultrasound volume that reaches the transducer and consists of the peak pressure or height of a wave (Poulsen Nautrup, 2000).

Sound waves are a series of repeating pressure waves, that can be represented as sine wave forms. A single wave moves along the horizontal axis representing the time, starting at zero, reaching a peak, returning back to zero and continuing to a negative value before reaching zero again. A continuous wave consists of subsequent single sine waves (Bartrum and Crow, 1977).

2.2. Interaction of ultrasound with tissues

Ultrasound beams are attenuated as they pass through the different body tissues (Nyland et al., 1995). This appears to have a negative effect on the image produced during scanning, especially when gain and time-gain compensations are not applied (Nyland et al., 1995, O'Brien, 1998). Attenuation is a result of sound beam absorption, reflection and refraction or scattering (Nyland et al., 1995, Ginther, 1995).

Absorption:

Absorption refers to the conversion of sound to heat (Nyland et al., 1995). It results in the reduction of beam strength (Farrow, 1996). The phenomenon can be used in therapeutic ultrasound as the basis for ultrasound diathermy.

Intensities used in diagnostic ultrasound are not thought to cause significant thermal effects (Ginther, 1995) (Fig. 2.2.).

Reflection:

Reflection occurs when a sound beam encounters a tissue interface at a right angle, resulting in a returning of it towards the transducer (Ginther, 1995) (Fig. 2.2.). Different kinds of tissue produce different degrees of reflection (known as acoustic impedance) of the sound beam (Nyland et al., 1995), which expresses the interaction of the transmission of the sound beam between two tissues with different molecule connection and elementary substance inertia. The acoustic impedance (Z) is calculated by multiplying the tissue density (p) with the propagation velocity (c): $Z = p \times c$ (Poulsen Nautrup, 2000). Acoustic impedance results in an impairment of image quality of the structures lying underneath (Nyland et al., 1995).

If there are only minor differences in the acoustic quality of neighbouring tissues, it is possible to image structures at considerable depth, but with bone and gas, which have a very high and low acoustic impedance, respectively, there is an inability to image structures deep to these types of tissues or areas. The latter badly affects B-mode images, which makes diagnosis very difficult to almost impossible (Nyland et al., 1995).

Refraction:

When sound beams fall onto an interface in a direction other than a perpendicular one, the reflected echoes will not return to the transducer in a direct way. The sounds that are not reflected will continue their route to the next medium with an altered direction. The phenomenon mentioned above is referred to as refraction of the sound beam (Poulsen Nautrup, 2000).

Scattering:

Scattering occurs when the ultrasound beam encounters interfaces that are irregular, smaller than the ultrasound beam (Ginther, 1995) and lie at various angles. This may hinder interpretation, since there are echoes missed by the crystal, which leads to a lesser image quality as far as the normal anatomy is concerned (Nyland et al., 1995) and thus potential confusion by considering normal structures as pathologic findings. At the other extreme, scattering can prove to be useful in helping the clinician to differentiate between various organs due to alternative tissues that might constitute their components. These tissues are able to produce a characteristic scattering pattern for each organ. In conclusion, scattering has to do with diffusely reflected sound waves due to small uneven interfaces (Poulsen Nautrup, 2000) (Fig. 2.2.) in contrast to refraction, where sound beams encounter large interfaces at an angle other than a right one.

Resolution:

Resolution of ultrasound systems refers to the ability of the machine used to distinguish details between two reflectors located close to each other. It is usually defined as axial and lateral, according to the reflectors' position in relation to the ultrasound beam axis (Ginther, 1995).

Axial resolution is related to the frequency of the transducer (Ginther, 1995). There is an indirectly proportional relationship between the frequency of the ultrasound and the wavelength of the sound waves. The higher the frequency the shorter the wavelengths produced and, consequently, the better the resolution (Nyland et al., 1995). This is extremely useful for the detection of tissues lying close to each other in the axial plane (Ginther, 1995), as they are not included in the same wavelength. With a longer wavelength they would appear on the screen as a single structure.

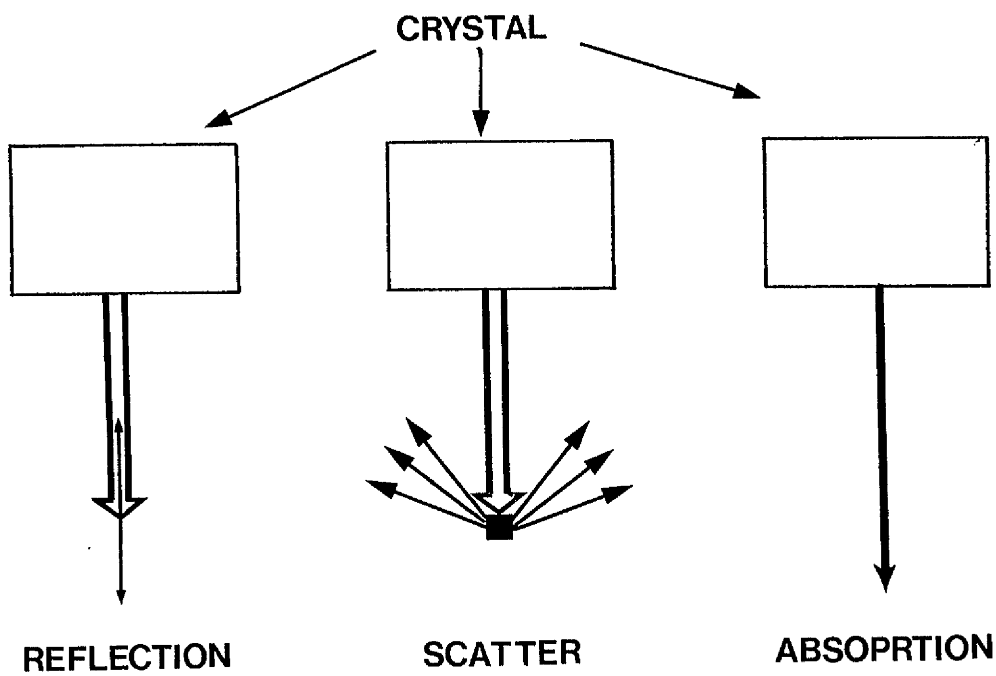

Fig. 2.2. Conditions of ultrasound beam attenuation

Using high frequencies, however, causes a limitation to imaging at increasing depths, due to the fact that the ultrasound beams are absorbed much more rapidly in this case.

In the opposite plane, Nyland et al. define lateral resolution as "the ability to resolve adjacent points perpendicular to the axis of the sound-beam". It refers, consequently, to the diameter of the ultrasound beam, which varies with the transducer frequency, as well as the distance from the transducer (Nyland et al., 1995). Lateral resolution can be useful in detecting slight differences in tissue structures of the same level, as far as the beam is focused on the region of interest for optimal results (Fig. 2.3.).

<u>Beam focusing:</u>

The ultrasound beam usually has the shape of the piezoelectric crystal (Meire and Farrant, 1995). The part of the beam which is located nearer to the transducer is called the near field (Ginther, 1995) or Fresnel zone (Meire and Farrant, 1995), whereas its distal part is called the far field (Ginther, 1995) or Fraunhofer zone (Meire and Farrant, 1995). The near field usually has the same width as the sound beam, resulting in optimal lateral resolution. The sound beam normally tends to diverge from its straight orientation when emitted by a piezoelectric crystal (Ginther, 1995) (Fig. 2.4.).

The location of the transition between the two zones is represented by the equation: $d = r^2 / L$

where d is the length of the near field, r is the transducer radius and L is the ultrasonic wavelength (Hankaga, 1995). If the transducer size is increased, the boundary between the near and far fields will be further from the transducer (Bartrum and Crow, 1977). This appears to have an impact on the lateral resolution, which may be overlapped by focusing the ultrasound beam at the desired depth (Ginther, 1995).

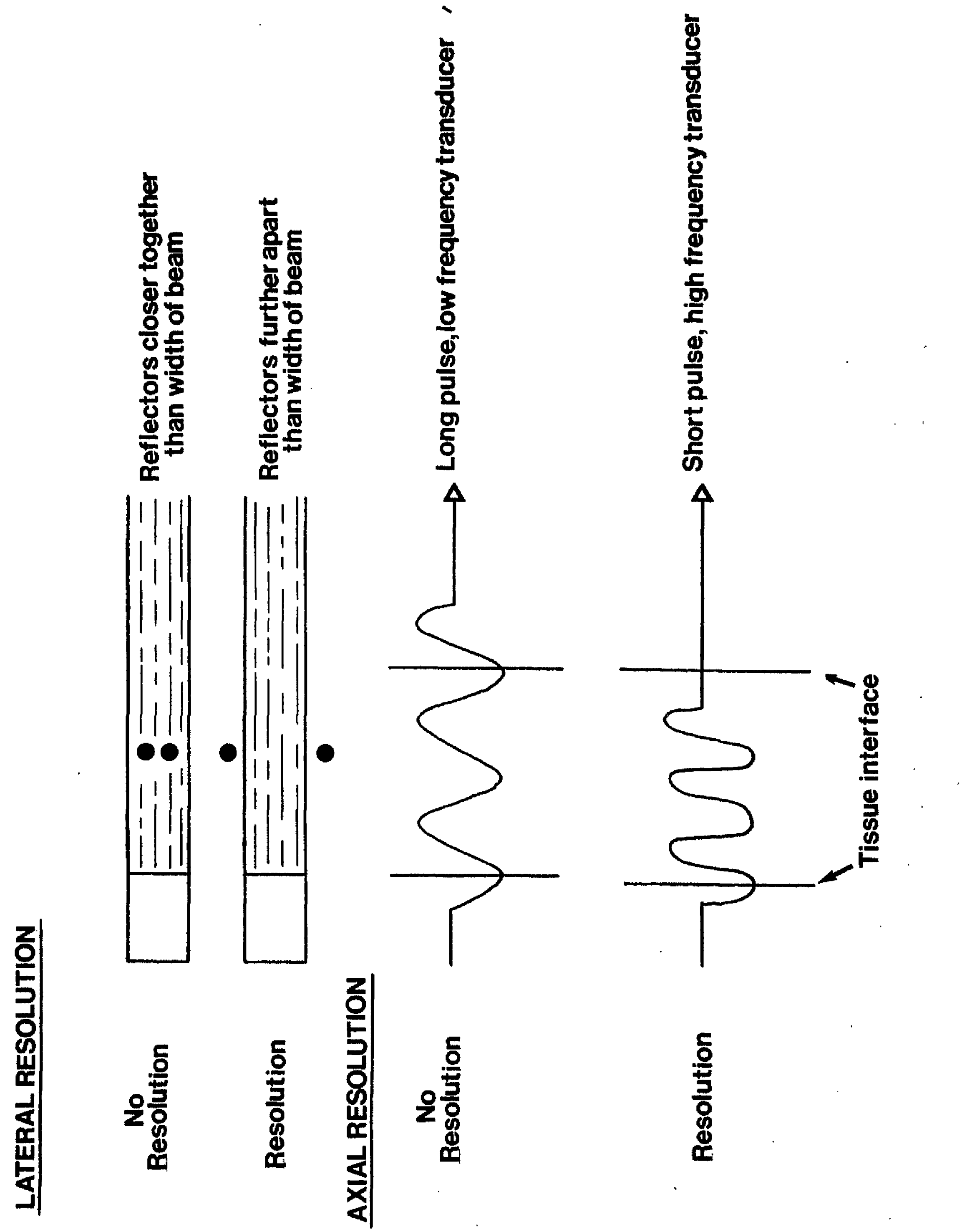

Fig. 2.3. Axial and lateral resolution.

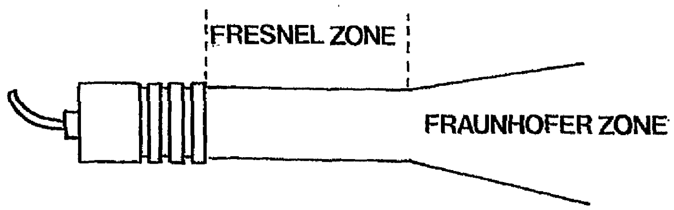

Fig. 2.4. The two sections of a sound beam from a non focused transducer.

Beam focusing refers to the narrowing of the distance between the constituents of a beam profile, which increases lateral resolution at a certain depth. Focusing falls broadly into two major categories, known as fixed and dynamic focusing (Ginther, 1995).

Fixed focusing occurs mainly in cases of mechanical sector transducers, which are able to focus the beam according to their physical shape. There can be an improvement, as far as the results in focusing of the ultrasound beam are concerned, if concave or convex lenses of appropriate material are used in front of the transducer. By these ways the ultrasound beam is focused at a certain depth, which cannot be altered by the ultrasonographer, necessitating switching between two or even more different probes for differing depths (Meire and Farrant, 1995).

Dynamic focusing, on the other hand, refers to the varying focal distances that can be achieved electronically (Ginther, 1995), by delaying the firing of certain elements, that can be altered according to the desired depth that the ultrasonographer wishes to focus at (Meire and Farrant, 1995). Dynamic focusing may occur either automatically or after the operator's intervention, but it results in providing ultrasonic imaging with a slower frame rate, which might be of great importance in cases of imaging moving structures (Ginther, 1995).

2.3. Ultrasound image artifacts

Artifacts produced in ultrasound diagnostic procedures usually occur due to the phenomena mentioned in the previous section. Their presence is very important for the sonographer, since with prior knowledge he or she can either reach a diagnosis more easily (e.g. cystic calculi by means of detection of acoustic shadowing) or misinterpret artifactual images for abnormal tissue (Penninck 1995, Kirberger, 1995).

Acoustic shadowing:

One of the most common artifacts and one that can cause major interference in musculoskeletal ultrasonography is acoustic shadowing. There is no transmission of sound through some tissues due to the total reflection of the ultrasound beam and a degree of absorption of the sound by the reflecting structure (Ginther, 1995). The field deep to the reflective surface seems anechoic on the screen, since no image can be displayed, although some reverberation echoes could appear in that particular area. Distinct shadowing, however, can only be distinguished in cases where the highly reflective tissue is similar or greater in size than the width of the ultrasound beam (Kirberger, 1995) and is located near the focal zone of the transducer (Penninck, 1995).

This artifact is observed, in cases where the ultrasound beam encounters gas, mineral elements, usually calculi or bones or even fluid-filled structures. When there is a significant difference in acoustic impedance at the interface between two tissues of different echogenicities, as in the case of soft tissues and bowel gas, most of the ultrasound beam is reflected (Ginther, 1995) and reverberation artifacts may occur at the same time (Penninck, 1995). When ultrasound waves meet bone or other calcified structures, the acoustic shadow is distinct and clear and can help in the identification of these structures but also impedes imaging at longer distances.

Edge-shadowing:

An acoustic shadow may be seen distal to fluid-filled structures (for example the gallbladder) due to the different acoustic velocity between the rounded structure and the surrounding tissues, resulting in refraction and reflection of the ultrasound waves at their margins. The reflecting beam does not return to the transducer since the reflecting surface is not perpendicular to the beam (Kirberger, 1995), while the refracted one is addressed to another part of the screen. Moreover, changes appear to occur in the diameter of the ultrasound beam owing to the focusing action and the difference in velocity when passing through fluid (Penninck, 1995).

Reverberation echo:

This kind of artifact refers to the presence of reflective signals coming back at the transducer, which leads to the apparent imaging of a single structure repeatedly at longer distances and with decreased intensity (Goddard, 1995). It usually happens in areas where the beam may encounter a strong interface between two tissues of large acoustic impedance mismatch. Once the signal has been reflected back to the transducer the signal processor assumes that it has travelled once and then for the same time again through the body tissues in a greater depth misinterpreting, consequently, the signal as originating from a point twice as deep as the original soft tissue-air interface. For that reason the signals appear equidistant (Ginther, 1995). The amplitude of the repetitive echoes is weaker (Kirberger, 1995) and, consequently, each image in sequence diminishes in intensity (Ginther, 1995).

Another distinguishing feature of reverberation artifacts constitutes their parallel orientation to the reflective interface, especially when they originate from highly reflective tissues, such as gas or bone. In this case, reverberation artifacts may appear in the acoustic shadow created, or in the non echogenic fluid in cases of fluid - filled structures (Ginther, 1995).

Reverberation artifacts occur frequently even when bones are placed further than the displayed depth (Ginther, 1995). Consequently, in cases where bones are quite close to the region of the body being scanned, (ie. joints) this kind of artifact constitutes a limitation to the imaging of such structures.

Reverberation artifacts may also be observed in cases of inadequate contact of the probe with the patient's skin, of trapped air between the probe and the contact surface or of lack of contact with the entire transducer footprint. They lead to a decrease of the image quality displayed on the screen (Poulsen Nautrup, 2000).

<u>Comet tail artifact:</u>

A characteristic example of the reverberation artifact is the comet tail artifact; it is produced by small, highly reflective interfaces such as metal objects or gas bubbles (Penninck, 1995). The greater the attenuation and the broader and more perpendicular the interface, the more intense the comet tail artifact (Kirberger, 1995). Its homogeneous streak is due to reverberation echoes coming from both the reflections between the transducer and the metallic object and the reverberations being produced from the object itself. Comet tail artifacts usually diminish in intensity on the image produced by real-time ultrasound (Farrow, 1996). Bones tend to produce comet tail artifacts, which make visualisation of adjacent soft tissues difficult.

<u>Mirror-image artifact:</u>

Mirror-image artifacts are produced by rounded, strongly reflective interfaces such as the diaphragm-lung interface (Kirberger, 1995). Sound reflected from this structure does not return directly to the transducer, but it is reflected by another interface and then turns back. The processor assumes that sound can only travel in a straight line and, thus, contributes to the interpretation of time delay by displaying the echo signals as if originating beyond the original interface (Penninck, 1995). Mirror-image artifacts should, therefore, always be considered in cases of detecting an abnormal finding behind a strongly reflective and absorptive interface.

Acoustic enhancement:

This is an artifact concerning an increase in amplitude due to intervening tissues of low echo reflection (Kirberger, 1995). The ultrasound is not absorbed to the same degree when travelling through a fluid-filled structure as it would be travelling through tissues located at the same depth, but not beneath the cystic structure (Ginther, 1995). This may be observed when imaging synovial sheaths especially in cases when they are extensively fluid-filled (Main, 1995). It is helpful in distinguishing cystic structures from solid, hypoechoic masses, e.g., tumours, abscesses or granulomas; it can also be observed, however, in areas of hyperechoic masses of low attenuation and, thus, constitutes a diagnostic inconvenience for the clinician (Penninck, 1995), especially when using high frequency transducers (Ginther, 1995).

Specular reflections:

They appear in cases where an ultrasound beam impinges at right angles to a structure that is smooth, regular-shaped, fluid-filled and wider than the beam's width. A portion of the beam is reflected back to the transducer, whereas the rest goes through the interface. If the beam strikes a second smooth interface, then another portion of it will be reflected. The interfaces displayed on the screen seem hyperechoic. Underneath the deeper interface, the artifact of distant (acoustic) enhancement is created (Ginther, 1995), because there is minimal loss of energy as the ultrasound beam passes through fluid-filled structures (Fig. 2.5.).

When the beam meets the interface at an angle other than 90°, the pulse is reflected in such a way that the angle of reflection equals the angle of incidence (Ginther, 1995). The pulse does not return to the transducer, resulting in misinterpretation of the interface since it is not detectable by this way (Meire and Farrant, 1995). In that case the transducer's position must be changed (Ginther,

1995) in order to image this structure. Only in cases of a right angle of the sound beam towards the reflecting interface is it possible for the reflected component to coincide with the route of the incident beam. Consequently, the amplitude of the returned echo is very dependent on the orientation of the sound beam towards the interface (Taylor, 1978).

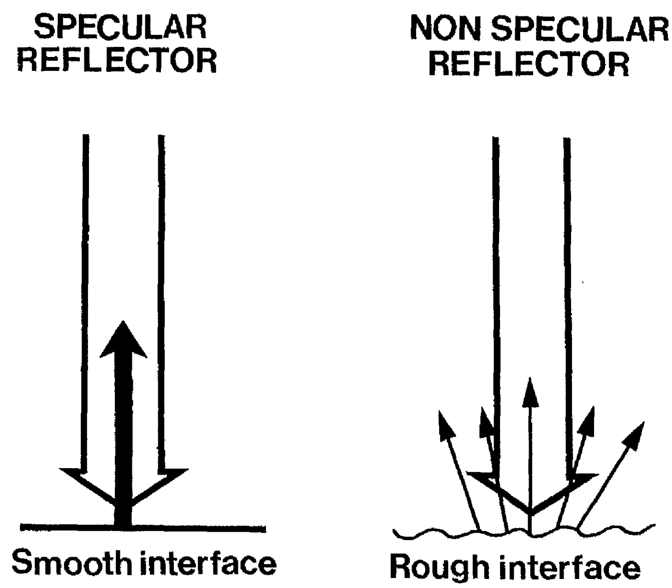

Fig. 2.5. Specular and nonspecular reflections.

Nonspecular reflections:

They appear when the ultrasound beam faces a rough interface, that is smaller than the beam. They are created even in cases, where the beam does not meet interfaces perpendicularly and are displayed on the screen as structures of differing echogenicities; consequently, soft tissues lying close to each other might be distinguished due to their own pattern, texture or speckling. In addition nonspecular reflections displayed on screens do not always reflect real tissue structures. As a result, the different echotextures that different kinds of tissues give are those which determine most times the characteristic appearance of an organ in real-time ultrasound imaging (Ginther, 1995) (Fig. 2.5.).

The intensity of nonspecular echoes is independent of the angle of the sound beam in as much as the latter surrounds the interface. But, still, the intensity of nonspecular echoes is less than specular ones, since the interfaces are smaller and are not able to reflect a large proportion of the sound beam (Bartrum and Crow, 1977).

Anisotropy:

The imaging of characteristic echotexture of tendons is directly related to the angle at which the transducer is being held (Craychee, 1995). It has been reported to be degraded in cases where the ultrasound beam is not perpendicular to the imaged tissues (Penninck, 1995). This is an artifact occurring when the transducer is not placed orthogonal to the structure imaged and, consequently, it appears hypoechoic (Winter, 1998), which may lead to the loss of imaging details and, sometimes, to false diagnosis of a tendinous disease (Martinoli et al., 1999).

A misleading image of a tendon can be observed in cases of an oblique position of a tendon in correlation to the skin surface (Martinoii et al., 1999). A stand-off pad can be useful in preventing the beam's obliquity (Penninck, 1995), because otherwise an anisotropy artifact could be misdiagnosed as tendinitis (Winter, 1998). Nevertheless, a real tendinitis can be distinguished if the lower echogenicity observed is combined with an increase in the volume of the tendon, the latter appearing rounder than usual in cross section (O' Keefe and Mamtora, 1992). A clinician should move the transducer accurately in order to avoid a confusion of this kind. The latter is suggested, especially in cases of imaging the long head of the biceps tendon (Winter, 1998).

2.4. Transducers

Ultrasonographic equipment used to be poor in its ability to detect disorders of the musculoskeletal system. This had an impact on the research performed in this particular field of ultrasound knowledge.

The transducers used in practice emitted a specific frequency, which determined the resolution of the ultrasound waves. The higher the frequency the better the resolution and also the better the view of superficial tissues (Nyland et al., 1995). It is therefore essential to match the type of the transducer used to each case examined (Meire and Farrant, 1995). Muscles and especially tendons however can be situated in both superficial and deeper surfaces; consequently, the need for the use of different frequencies in order to better visualise the structures around joints is of great importance.

In the past the frequency emitted by an individual transducer could not be altered by the ultrasonographer, as changing of the frequency usually required a simultaneous change of the transducer (Nyland et al., 1995).

There are currently however transducers able to have a multifrequency operation. This results in obtaining the maximum resolution (thus, the best quality) for a

given depth with a transducer. There is also a possibility of the clinician determining the focal point depth and obtaining the best resolution in different tissue depths (Nyland et al., 1995).
Mechanical sector scanners were widely in use until recently for ultrasound imaging. The beam was produced in accordance with the movement of the piezoelectric crystal (usually vibration). Despite their reasonable price and the ability of producing high frequency sound waves (Nyland et al., 1995), their use turned out to be limited, because they were greatly at risk to damage at frequent intervals.

Different kinds of array transducers (transducers that contain a large number of piezoelectric elements) are mainly used in small animal practice. Both seem to have advantages and disadvantages, which are listed below (Evans and McDicken, 2000):

Such transducers are preferred by the clinicians for use in practice since they do not have moving parts and the position of the focused beam may be electronically controlled and, consequently, moved fairly quickly. Moreover, the large number of elements is compatible with current computer technology which makes beam guidance easier (Evans and McDicken, 2000).

Array transducers may, on the other hand, require the addition of cylindrical lenses so that the sound beam focuses in the out-of-plane direction. Furthermore, it has proved more difficult to produce very high frequency array transducers (Evans and McDicken, 2000).

Linear array transducers:

Linear array transducers are characterised by the parallel arrangement of crystals along the transducer surface. Both the examining region and the image displayed on the screen are rectangular (Ginther, 1995). This means that the scan lines are organised in a vertical, linear and parallel way (Poulsen Nautrup, 2000) (Fig.2.6.).

This kind of transducer is valuable in that it can offer a large field of view even in superficial tissues (Barr, 1990); consequently, it can be useful for musculoskeletal system imaging. This is also supported by the narrow space between piezoelectric crystals providing emission of closely situated sound beams and, thus, a fine view of anatomical details (Ginther, 1995). Moreover, a linear array transducer does not have moving parts that could be subject to damage, which reduces their maintenance cost (Boyd, 1995).

Linear transducers require however an extensive area of contact with the body (Barr, 1990) which could be problematic for the imaging of extremities. This kind of limitation can be seen even when shorter and smaller transducers are used (Poulsen Nautrup, 2000).

Curved linear or curved array transducers:

Curved array transducers appear to be a combination of linear and sector transducers (Poulsen Nautrup, 2000). They appear to have piezoelectric crystals positioned in a linear array, but they have a convex rather than a flat footprint (Barr, 1995). They are different from linear probes in that their crystals are arranged in a curved arc-like line. The beam focusing is electronic (Poulsen Nautrup, 2000).

In this way, the field of view is increased and contact with the skin surface may be facilitated on some occasions (Evans and McDicken, 2000). Their main advantage remains their good near field resolution with the simultaneous use of a smaller footprint (Poulsen Nautrup, 2000).

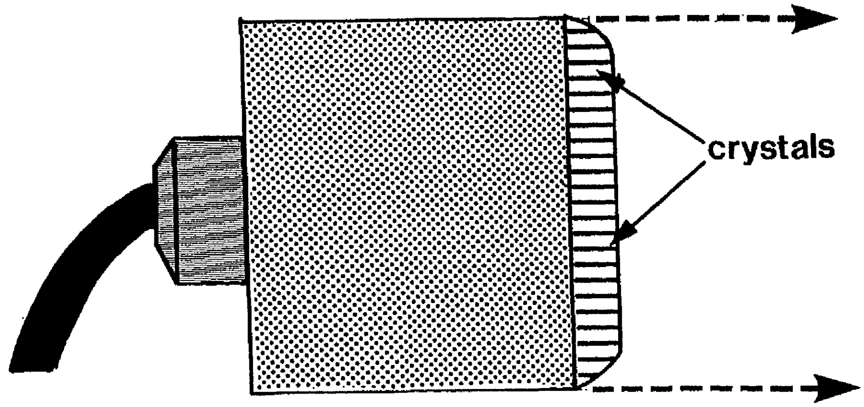

Linear Transducer

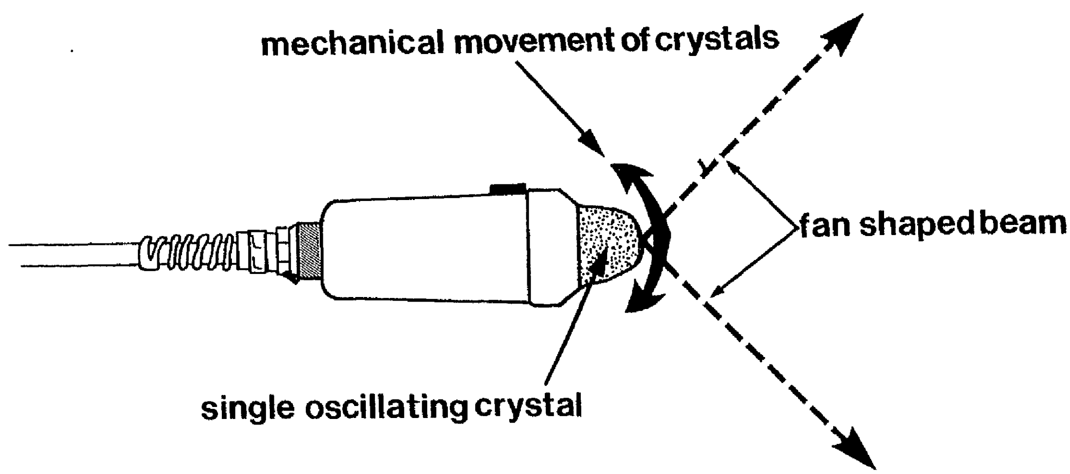

Sector Transducer

Fig. 2.6. Range of real time transducers.

Sector transducers:

Sector transducers are characterized by the use of a smaller footprint in order to acquire approximately the same image lengthwise as by using a linear array transducer (Ginther, 1995).

They are small, easy to use and by offering a smaller footprint and a fan-shaped field of view allow imaging of more structures (Barr, 1990), as well as the ability to image through narrow spaces, e.g. through the intercostal spaces (Ginther, 1995) by producing a wedge shaped display (Boyd, 1995).

However, they can suffer from poorer resolution, resulting in lack of precisely identifying different organs and tissues (Barr, 1990) especially in the near field (Boyd, 1995). This occurs at that level because of the scan line density and the narrow field of view at that level (Fig. 2.6.). Moreover, their use in the ultrasonography of superficial tissues turns out to be limited because of the necessity for the use of a stand-off pad (Poulsen Nautrup, 2000).

Phased array transducers:

Phased array transducers are characterised by the presence of a number of crystals in stable positions being activated sequentially (Barr, 1995). Their image quality is considered to be slightly inferior to that produced by linear transducers, since it is not easy to steer a beam without loss of energy due to the latter's transmission to different directions than the main ultrasound beam (Evans and McDicken, 2000). Furthermore, they are considered to be too expensive to be utilised in general small animal practice.

Two dimensional phased array transducers:

Two dimensional phased array transducers are responsible for the production of three dimensional scans, that constitute a brand new field in ultrasonographic imaging. They provide beam forming and steering in both elevation and azimuth, which helps provide flexible orientation of scan planes (Whittingham, 1997). They are difficult to produce in as much as multiple connections have to be made to the piezoelectric elements. Three dimensional imaging is still in its infancy, since problems like the long echo-collection time from a tissue have not been overcome yet (Evans and McDicken, 2000).

Annular array transducers:

Annular array transducers can achieve symmetrical electronic focusing about the axis of the transducer (Evans and McDicken, 2000). This can be accomplished by the spherical shape of the transducer that produces a small circular beam. Focusing occurs in all planes about the beam's axis for fine tissue quality throughout the image. Higher frequency probes may be used without a loss in penetration. By going to a higher number of rings (six to eight), remarkable control of tissue slice thickness and signal quality may be accomplished.

Because the image sector is steered mechanically, there is no off-axis reduction of the effective area of a transducer's transmit and receive surface at the edges of the sector as with linear phased arrays. Since the transducer is disc-shaped, larger effective areas of a transducer's transmit and receive surface with many rings can be designed that still have small contact areas.

Their main disadvantage is that they are required to function mechanically in order to scan a field of view (Evans and McDicken, 2000).

The deficiency in imaging deeply positioned structures close to each other using a sector type transducer can be addressed by the introduction of convex transducers. They are able to provide a combination of offering a small footprint as well as high resolution almost equal to that of a linear array transducer (Ginther, 1995) by having the piezoelectric crystals placed in such an order that reduces the contact surface required with minimal image distortion (Boyd, 1995).

The use of transducers offering smaller footprints and producing higher frequencies even up to 15-20 MHz has helped to reduce the limitations previously existing in musculoskeletal imaging. To date ultrasonography has been reported to be less accurate than arthrography. It has been proved to be difficult to use ultrasound to estimate abnormalities in the articular surface of the shoulder joint (Long and Nyland, 1999).

2.5. Scanning units

Display systems

Bi-stable systems: The bi-stable system preceded the gray-scale image display, which was first applied in 1974. Its major disadvantage proved to be that any echo below the given threshold disappeared, so that the image produced provided information concerning only organ boundaries and strong reflectors (Meire and Farrant, 1995).

Gray-scale systems: All modern ultrasound equipment uses gray-scale imaging. This refers to the range of intensities displayed on the screen according to the signal strength of the echoes: Weak echoes are represented with dark gray colour, whereas stronger echoes appear light gray. Extremely strong echoes originating from e.g. soft tissue-gas or soft tissue-bone interfaces are represented with white colour and non echogenic fluid-filled structures appear black on the screen (Farrow, 1996).

Display format:

There exist three basic display formats:

A-mode (amplitude mode): A-mode is now rarely used, except in cases of ophthalmic examinations and other applications requiring precise length measurements (Meire and Farrant, 1995), such as echoencephalography (Poulsen Nautrup, 2000). The echo's origin and strength are represented on the screen as spikes protruding from a baseline, where the transducer's location was represented at the far left of the baseline with increasing depth along the baseline to the right. The position of the spike represents the depth from which the echoes are derived, whereas the height of the spikes shows the intensity of the signals (Nyland et al., 1995).

B-mode (brightness mode): B-mode results in the display of the echoes returning to the transducer as dots whose brightness (scale of gray) corresponds to the amplitude of the echo and whose position reflects the depth of the structure that emitted the echo and lies within the beam's axis (Nyland et al., 1995). A strong signal produces a bright dot, whereas a weak signal will be converted to a darker dot (Herrtage, 1998). The B-mode system is usually displayed with the transducer surface to the top of the screen and the depth of the underlying tissues increasing to the bottom of the screen (Nyland et al., 1995).

M-mode (motion mode): M-mode is used for echocardiography in order to evaluate the heart's physical shape and functions (Farrow, 1996). A single line of B-mode dots with the same rules applying for gray-scale imaging is displayed against time on the screen (Nyland et al., 1995). M-mode has proved to be extremely useful for precise cardiac chamber and wall measurements, as well as motion measurements with time (Farrow, 1996). This is achieved by displaying the depth (or height) of structures in the vertical axis and the time in the horizontal axis (Poulsen Nautrup, 2000).

Real-time ultrasonography

Real-time refers to the ability of visualising motion on the ultrasound image appearing on the screen (Farrow, 1996). Real-time B-mode scanners can produce a moving image of cross-sectioned organs (Nyland et al., 1995). This kind of image is the result of successive complete sweeps of beams across all the piezoelectric crystals which are known as frame rate (Ginther, 1995). Sound pulses are sent and echoes come back to each element sequentially until a sector or rectangular image is formed (Nyland et al., 1995). Each line remains on the screen until it is renewed by the following sweep of the beam. Twenty to fifty images per minute may be displayed on a scanner screen (Poulsen Nautrup, 2000). Echoes originating from deeper structures need more time to return to the transducer and this results in a slower frame rate (Nyland et al., 1995).

Ultrasound controls

It is well known that the optimal image quality is obtained when the ultrasound machine used is efficient enough to either increase the intensity of the sound beam or decrease very strong echoes originating from the near field. The main purpose is to acquire a uniform image brightness in all fields of view (Nyland et al., 1995). The power or intensity control modifies the electrical current applied to the transducer and arranges the intensity of the echoes produced. If it is increased, it may result in the amplification of most of the returning echoes. Consequently, the power control must be arranged to be as low as possible in order to achieve the best degree of resolution in combination with minimal artifacts (Nyland et al., 1995) especially in the case of the current study which dealt with the imaging of superficial structures. Latest research, though, has shown that in canine and feline ultrasonography, where the use of 5 or more MHz transducers is very common, a high adjustment of the intensity control up to 100% may be required in order to display an image (Poulsen Nautrup, 2000).

The time-gain compensation control refers to the concept of adding selective amplification to small distant echoes to compensate for tissue attenuation (Bartrum and Crow, 1977). It can be explained by means of a simplified graphical representation of the amplitude of echoes from interfaces spaced evenly throughout the depth of a field of view. Time-gain compensation controls first apply to the near field of view (Nyland et al., 1995), where the pulse remains strong in superficial tissues (Meire and Farrant, 1995) and they usually function to decrease strong echoes arising from these tissues (Nyland et al., 1995) or provide no further adjustment (Poulsen Nautrup, 2000). Furthermore, the second part of time-gain compensation control, known as slope delay control, begins to be set at any depth beyond which the time-gain compensation controls increase the intensity of weaker echoes since the time required for their return to the transducer is now more.

The far gain control refers to the ability of some scanners to adjust any weaker echoes coming from any depth beyond that controlled by the slope rate control (Nyland et al., 1995). In this study near field and slope rate controls were of major importance, since a variety of structures with different echogenicities had to be imaged on the screen, which resulted in a great degree of attenuation of many echoes.

The zoom or image magnification control refers to a selection of a part of the screen by the operator and the placement of a "box-shape" construction, the area inside which may be enlarged with the help of another control of the keyboard (Farrow, 1996).

The gain control is responsible for equal amplification of all returning echoes from every depth of the imaging field. Extremely high or low gain settings might lead to loss of image quality (Poulsen Nautrup, 2000).

The echo enhancement control results in the increase of the intensity of separate weak echoes making the structures appear more prominent (Poulsen Nautrup, 2000).

"The difference between the weakest and the strongest registered echo intensity is called the dynamic range" according to Poulsen Nautrup. The greatest range should be used for abdominal scannings, whereas a middle range is adequate for echocardiography (Poulsen Nautrup, 2000).

Extended field of view:

This refers to a recently developed facility, which displays expansive planes of various organs in real time (Ghate et al., 1999), by using specialised computer processing via software algorithm (Fornage et al., 2000). These panoramic images visually link continuous organs into one image, eliminating the need to mentally piece together a picture of anatomical structures, as is currently required with conventional ultrasound systems (Ghate et al., 1999, Weng et al., 1997). Furthermore, it enables the operator to safely conduct measurements of large structures that do not fit on the monitor and, thus, be confident in evaluating organ size (Fornage et al., 2000), since results of measurement testing have demonstrated a remarkable accuracy (+_ 5%) (Weng et al., 1997). This may lead to more easily understood images of the anatomical relationship of structures than with a series of conventional ones (Deane, 2000). Another great advantage constitutes the ability to scan a volume of slices and post-scanning reconstruct slices in any way desirable (Beissert et al., 1998).

Imaging using an extended field of view system is thought to be of benefit in the examination of large organs and masses (e.g. spleen, liver, fetus position and volume of the placenta), extended vascular structures (e.g. the extent of venous thrombi, aneurysms of the aorta), musculoskeletal injuries (e.g. tendon ruptures and the surrounding inflammation), the side-by-side comparison of paired organs from one image or large pathologic volumes (e.g. ascites, pleural effusion, peritoneal tumours, retroperitoneal masses) (Beissert et al., 1998). This may be accomplished by allowing the imaging of surrounding tissue and architecture, which enables the detection of subtle lesions due to the image contrast (Ghate et al., 1999). The fact that the operator can image the organs of interest by free-hand scanning should also be taken into account (Hara et al., 1999).

The size of the anatomical structure that can be imaged in a single extended field of view scan is limited by the memory of the scanner and depends on the type of the probe and the depth and width of the field of view. The computer compares the image of the current frame with that of the previous frame, which enables the accurate positioning of the current frame in relation with the previous ones (Fornage et al., 2000). Other limitations of extended field of view imaging capacity consist of movement artifacts (which are mainly encountered in organs like the heart), the need for long surfaces for transducer contact, as well as limitations that also exist for conventional imaging, such as the need for clipping and lack of imaging due to strongly reflecting surfaces - bone and air. Its very high cost owing to the optimal quality computer system required is considered to be daunting for many practitioners (Beissert et al., 1998).

Three dimensional ultrasonic imaging

The three dimensional reconstruction of ultrasound images has become a widespread option in ultrasound equipment (Downey et al., 2000) and this main attribute is the fact that the clinician is able to directly visualise the anatomical structure under examination in all its three dimensions, rather than subconsciously convert them from individual two dimensional images. Several clinical applications, for example to the liver, the gallbladder and some central and peripheral vessels in humans have been described (Campani et al., 1998).

There are several advantages of a three dimensional ultrasound facility over the two dimensional equivalent. Three dimensional images can be obtained by a single sweep of the ultrasound beam across organs, so that the exact position and relationship of various anatomical structures can be determined easily and quickly. The above is important, taking into account the fact that the clinician who uses two dimensional ultrasound needs more time and mental effort in order to acquire multiple two dimensional images back and forth across the organ of interest and then develop a three dimensional impression of the underlying anatomy or pathological condition (Downey et al., 2000).

Sometimes the patient's anatomy or positioning makes it impossible to orientate the transducer for optimal visualisation between two structures. However, three dimensional ultrasound allows unrestricted access to an infinite number of viewing planes (Hamper et al., 1994).
Three dimensional images are better suited in order to monitor postoperative or healing effects, by enabling the comparison of two full data sets over time. Using two dimensional ultrasound does not guarantee standard patient positioning and imaging technique which are necessary for a reliable follow-up (Downey et al., 2000).

This recently developed technique enables the image produced to be displayed in various ways and processed for quantitative volume estimates (Downey et al., 2000) with just a single sweep of the sound beam (Farrell et al., 2000). There exist three different image displays which can be used to acquire more information about a diagnosis. Their value is evident in cases of confirmation of normal conditions, when a risk of recurrence of a specific problem is raised (Farrell et al., 2000).

The multi-planar display is able to process 3 orthogonal planes in the same time, in order to produce a volume image on the screen. Then it can be displayed in every axis desirable including the third dimension. This is responsible for the ability to rotate the stored volume in every dimension desired making sure that the object of interest is imaged in the best way so as to make a diagnostic interpretation (Farrell et al., 2000).

The surface mode can produce an almost photographic image of the features present on a structure's surface (Farrell et al., 2000).

The transparent display is able to provide the clinician with an accurate view of a three dimensional aspect of hyperechoic structures, for example the fetal skeleton (Farrell et al., 2000).

The use of three dimensional ultrasound to measure organ volumes has been applied to various organs in humans, including fetal organs. Its effects are superior compared to those acquired by conventional ultrasound, because the latter tends to give inaccurate readings for either distance or volume results when the object of interest tends to be irregular (Farrell et al., 2000). The clinical utility of three dimensional ultrasound is increased with accurate measurements, because there exists increased reliability and standardisation of measurements, which would improve the confidence on serial measurements (Riccabona et al., 1995).

The role of three dimensional ultrasound has proved to be valuable in biopsy procedures. The exact needle position in relation to the lesion is accurately determined. Furthermore, the volume data obtained can be stored with information about an anatomical region, including pathological details. This feature seems very promising for the future, since these data may be obtained and studied years later without any loss of quality (Weismann, 2000).

Limitations of three dimensional ultrasound do exist. Most of them refer to the time required to store images or retrieve them from the optical disk and the reconstruction time of the three dimensional scene display, which is more than that required for a conventional scanner. This additional time may prove to be annoying to ultrasound users who are accustomed to having the images appear on the screen instantaneously. Furthermore, many of the viewing programmes require a sophisticated image manipulation in order to achieve high quality images (Downey et al., 2000).

Operators should be alert in order to avoid artifacts created by false settings of surface-rendering and volume-rendering algorithms. They should be able to review the original raw data to clarify any possible abnormalities (Downey et al., 2000).

Three dimensional ultrasound may sometimes be confusing in the diagnostic process, in as much as it may eliminate image artifacts which occur with conventional scanning and are extremely helpful in the confirmation of a diagnosis (e.g. acoustic shadowing in the case of calculi) (Downey et al., 2000).

A previous argument against three dimensional scanning was the fact that all of the then current three dimensional ultrasound data acquisition equipment (e.g. transducers) were more cumbersome than conventional ultrasound equipment (Hamper et al., 1994).

The fact that three dimensional ultrasound images are effective in showing the real extent of lesions especially when the maximum amount of normal tissue surrounding them is included should also be taken into account. But this larger data inevitably requires more computer memory, storage capacity and faster data processors. Furthermore, larger data sets can be affected by motion and reconstruction artifacts and transmitting them over networks can be time consuming (Downey et al., 2000).

CHAPTER 3.

MATERIALS AND METHODS

3. MATERIALS AND METHODS

3.1. The animals

Cadavers

A number of adult, normal cadavers were used for operator training at the start of the project. The dogs were selected as belonging to the Greyhound breed, which ensured the minimum amount of fat or adipose tissue. They were chosen as in good physical condition and with no known abnormalities, having been received by the Department of Veterinary Anatomy from Dogs and Cats' Homes where they were euthanased for reasons unrelated to the current project.

In order to further validate the scan planes concerning the imaging of the various anatomical structures for the project, one Greyhound was selected for studies where an echo contrast agent was used.

Live animals

(A)Animals used for the project

Five Greyhound dogs, which were housed in the Glasgow University Small Animal Hospital and facilitated student work, were used for this study. The group contained adult, normal animals that ranged from six to ten years of age and were both neutered males and intact females.

In the initial training stages the dogs were used to establish imaging of the scan planes and anatomical structures. Once confidence had been ensured, two dogs were selected for more detailed study. The study was to include measurement of individual structures, which made the small number of selected dogs suitable for repeatability of measurements. One of these animals was a 9 year old neutered male Greyhound dog, which had no previous history of shoulder, stifle or tarsus joint abnormality or any other musculoskeletal disorders and was in good health and condition. The other dog selected was a 10 year old neutered male Greyhound dog, that was chosen for the same reasons as mentioned above. Nevertheless, it had to be withdrawn during the examination procedures, since it developed pathology of the shoulder joint.

(B) Animals used as clinical cases

Five dogs that were referred to the orthopaedic department of the Glasgow University Small Animal Hospital with suspected pathology of the musculoskeletal system were used for this study. These animals were examined within the period of May 2000 to January 2001 and were retained as in-patients during the period of examination. They will be listed in detail in chapters 4 and 5.

3.2. The scanning units

Four ultrasound systems were used in this study; the Toshiba Justvision Imaging Scanner (Toshiba Medical Systems, Crawley, UK), the Toshiba Corevision Imaging Scanner (Toshiba Medical Systems, Crawley, UK), the Dynamic Imaging Diasus (Dynamic Imaging Limited, Livingstone, Scotland, UK) and the Siemens Sonoline Elegra Ultrasound System (Siemens Medical Systems, Erlangen, Germany).

Toshiba Justvision 200 was a portable ultrasound machine. It was chosen when working with the cadavers at the preliminary stages of the project. The cadavers had to be dealt with in the Laboratory of Veterinary Anatomy, which made the use of a portable scanner more suitable than that of a non-portable one from the Small Animal Hospital.

This scanner was a high quality B-mode ultrasound machine, that had a small parts preset facility, making it appropriate for musculoskeletal imaging. This enabled the acquisition of optimum images, and, by using a consistent set up, the imaging of the same scan planes was readily repeated. It possessed a freeze mode, a magnification or zoom control and gain setting control.

A 7.5 MHz convex linear transducer was used with the Toshiba Justvision 200 ultrasound machine. It had 192 lines of information suggestive of the potential for a high quality image and its range of frequencies varied between 5 and 8 MHz.

Toshiba Justvision 200 allowed the recording of two dimensional ultrasound on video tapes. It had also the capability of using a thermoprinter, so that the sonographer could obtain prints of the organs of interest. The scans of the cadaver selected were recorded on SVHS video tape using a VCR video recorder (Panasonic) with playback facilities. For documentation a thermal printer (Sony UP-811) was connected to Toshiba Justvision and selected frames were printed on thermoprint paper.

Toshiba Corevision was located in the Small Animal Hospital and was used in the initial stages of training in order to become familiar with the normal anatomical scan planes. It was also used for measuring the dimensions of various anatomical structures, as well as for the imaging of the five clinical cases used in the study.

This machine constituted a high quality B-mode scanner, which was able to provide digital image processing in order to deliver clear and sharp images. It was equipped with a small parts preset, which was indicative of the potential for an advanced quality imaging which could be reliable enough for consistently repeated scan planes. Its depth of field could reach up to 24 cm and it could produce 63 frames per second.

A 5 to 8 MHz electronic linear array transducer with 192 lines of information and 45 mm of active length and 9 mm of active width was used in the Toshiba Corevision system. This transducer was used as emitting a frequency of 8 MHz for the musculoskeletal work.

Scans taken with the use of Toshiba Corevision were recorded on SVHS video tapes with the use of a Sony SVO-9500 MDP video recorder. A Sony UP-850 thermoprinter was also utilised so that the sonographer could obtain prints of the organs of interest. Measurements of structures were carried out with the help of electronic calipers which could be manipulated from the keyboard. Frames of measurements of the structures of the three joints involved in the study, performed with Toshiba Corevision were also saved in digital form, which ensured the best possible quality of photographs.

Dynamic Imaging Diasus constituted a recent scanning development specially designed for musculoskeletal ultrasonography. This machine was used for imaging of the normal anatomical structures in live Greyhounds, as well as for the conduction of measurements where appropriate. Although this machine offered the potential for ultra high resolution and, thus, accuracy in the diagnosis of musculoskeletal disorders, it was not possible to scan the clinical cases referred to the Small Animal Hospital, because it was on loan from the manufacturers. Therefore, the time limits for the conduction of this present study with Diasus were narrow.

Dynamic Imaging Diasus offered better resolution due to the use of very high frequency transducers, although its depth of view was inevitably limited to 10 cm and it could produce 30 frames per second. Its image quality was considered as optimal for recent advancement in ultrasound imaging.

The two linear transducers used for the current study with Dynamic Imaging Diasus were technically advanced, with their frequencies ranging from 8 to 16 MHz and 10 to 22 MHz respectively, both with an active length of 26 mm. Both had 128 crystal elements and their penetration depth was limited to 60 and 40 mm respectively, but with increased resolution due to the high frequencies. The 8 to 16 MHz transducer was used for normal anatomical imaging and measurements, whereas the 10 to 22 MHz was used under certain circumstances for the imaging of very superficial structures, such as the common calcanean tendon, which lay just underneath the skin in the talocrural region.

The Diasus imaging scanner contained a computer PC hard disk, which was able to save images and allow their downloading to floppy disks for further studying. As a result, all the images of anatomical structures were saved in the Diasus hard disk and downloaded to floppy disks. Where required, the images containing measurements were saved by this method.
The Siemens Sonoline Elegra Ultrasound System is a machine with very high computer specifications, which explains its use in this project for the advanced imaging of anatomical structures and measurements using extended field of view and three dimensional ultrasound capabilities. Access to this particular scanner was restricted, but, when available, was used for scanning of some clinical cases.

The Siemens Sonoline Elegra Ultrasound System had been designed in order to offer signal processing, flexible electronics and high quality display. High speed computation and processing power had made the development and implementation of sophisticated image processing algorithms for data sampling and signal management possible. This highly sophisticated machine had been equipped with the extended field of view facility, a major development in ultrasound technology that acquired and displayed expansive image views of internal organs in real time, allowing, thus for an overall estimation of the diseased structure. Moreover, three dimensional ultrasound offered the ability to acquire imaging information in two planes simultaneously and reconstruct the third dimension. The system software was completed with applications and transducer-specific imaging presets. The Siemens Sonoline Elegra system also provided custom imaging presets. This allowed the user to construct a constant foundation of predefined imaging parameters for a specifically-targeted study.

The transducer used with the Siemens Sonoline Elegra Ultrasound System was a linear transducer with a frequency range between 5 and 12 MHz and 40 mm of active length and 5 mm of active width.

The Siemens Sonoline Elegra ultrasound system offered video recording facilities (Sony SVO-9500 MDP video recorder), thermal printing (Sony UP-850) as well as computing facilities that allowed the loading of stored software upgrades and the ability to save patient information and images into optical disks.

3.3. Examination procedures

3.3.1. Cadaver work

The Greyhound cadaver selected for evaluation of scan planes by use of the echocontrast agent was positioned in right lateral recumbency and clipped over the left shoulder, stifle and tarsal joints. Hair was removed and the forementioned regions were cleaned with spirit in order to dissolve any existing grease on the skin. Acoustic coupling gel (Henleys Medical, Herts, UK) was then applied to facilitate adequate contact between the transducer and the skin.

An aqueous solution of dye and spherical albumin microcapsules with a diameter of 7 μm was prepared and drawn into a syringe with a hypodermic needle. The microcapsules have been used experimentally as an echocontrast agent as they produce hyperechoic signals when injected into the body tissues, which are then imaged with B-mode ultrasound. When the structure of interest was located ultrasonographically, the needle of the syringe was guided to the structure and 0.1 ml of this particular solution was injected into the precisely selected structure in the cadaver.

The trunk and limbs of the cadaver were frozen with the joints extended so as to simulate a normal standing position. Subsequently, the trunk and the pelvic region with the appropriate limbs were sectioned through the limbs in order to establish the validity of the injection sites as correct anatomical structures. The right limb was sectioned in long axis and the left limb in short axis and sections were made at 1 cm intervals in the regions of interest. Their cut faces were photographed and these photographs were compared to the ultrasound images that were recorded at the time of the injection.

The structures where echocontrast agent was used were:

Left forelimb - Shoulder joint:

M. supraspinatus at the level of the middle of the spine of the scapula and at the level of the musculotendinous junction.

M. infraspinatus at the level of the middle of the spine of the scapula (Fig. 3.1.a., 3.1.b.) and at the level of the musculotendinous junction.

Tendon of origin of the m. biceps brachii at the level of the intertubercular groove (Fig. 3.2.a., 3.2.b.)

M. teres minor at the level of the acromial process as it lay deep to the m. deltoideus

Left hindlimb - Stifle Joint:

Patellar ligament

Cruciate ligaments

Tendon of origin of the m. extensor digitorum longus

Left hindlimb - Tarsus joint;

Common calcaneal tendon at the level of the bifurcation of the lateral saphenous vein (Fig. 3.3.a., 3.3.b.)

Common calcaneal tendon at the level of the calcaneal tuberosity

3.3.2. Live animal normal anatomical scanning

Normal anatomy scanning was then performed in order to verify what structures could be imaged with each ultrasound machine that was available. The dogs were positioned in right lateral recumbency and clipped at the regions of the left shoulder, the left stifle and the left tarsus region. Clipping was kept to a minimum and was not repeated every day, due to the high sensitivity of the skin of the Greyhound breed and to aesthetic reasons. Spirit and acoustic coupling gel were applied onto the surfaces to be scanned. The room was darkened so that a wider range of gray-scale image could be visualised to result in optimal image quality and assessment (Fig. 3.4.).

The normal anatomical structures that were scanned were the same with all the three machines used for the project. Scan planes were taken with Toshiba Corevision of the mm. supraspinatus, infraspinatus, deltoideus, biceps brachii and teres minor as far as the shoulder joint was concerned. The patellar ligament, the infrapatellar fat pad, the tendons of origin of the m. extensor digitorum longus and the tendon of insertion of the m. quadriceps femoris and the abaxial aspects of the menisci were visualised. Imaging of the cranial cruciate ligament was attempted with Diasus and Elegra systems. The common calcanean tendon with 3 different layers was also able to be imaged. The use of a stand-off pad was considered necessary for the initial identification of very superficial structures of the stifle and tarsal joints, such as the patellar ligament, the tendon of origin of the m. extensor digitorum longus or the common calcaneal tendon.

Diasus as a high resolution machine made for accurate imaging of very superficial regions or structures of similar echogenicity and provided the operator with high quality images on screen. Consequently, more anatomical structures were able to be visualised in detail.

In the shoulder joint, the mm. supraspinatus, infraspinatus with its bursa surrounding its tendon, the acromial and scapular part of the m. deltoideus, the m. biceps brachii with the bursa (synovial sheath extension of the joint capsule) surrounding its tendon of origin and the shoulder joint capsule and joint space were successfully visualised with the 16 MHz probe.

Imaging of the stifle joint comprised the visualisation of the m. quadriceps femoris with its bursa, the patellar ligament, the infrapatellar fat, joint fluid, the tendon of origin of the m. extensor digitorum longus with its synovial pouch, the medial and lateral collateral ligaments, the cruciate ligaments and the abaxial aspects of both menisci with great accuracy with the 16 MHz transducer. A stand-off pad was used in order to obtain images of very superficial structures, such as the collateral and patellar ligaments, the menisci and the tendon of origin of the m. extensor digitorum longus.

The common calcanean tendon was imaged both with and without the use of a stand-off pad with the 16 and 22 MHz probes. The synovial bursa that lay underneath the tendon proximally to the calcaneal tuberosity was able to be detected.

3.3.3. Extended field of view imaging

With extended field of view imaging the transducer used with the Siemens Sonoline Elegra scanner was a linear format of 12 MHz frequency. As with all linear formatted transducers the foot print was rectangular in shape. To create an extended field of view image the transducer was generally drawn over the body surface so that the length of the footprint travelled in the long axis proximal to distal over the required distance to produce an extended panoramic image. This could extend up to 30 cm, but was usually curtailed to fit the structure under investigation. As the transducer travelled over the body surface the extended image could be seen being built up on the screen.

There was a time limit during which the information could be acquired and the image processing could cope only if the movement was even in pace without hesitation or major deviation from a straight line across the body surface. In other words the imaging processing could not cope with sharp curvatures or erratic movement such as when encountering bony prominences. It was therefore necessary to explore the region with real- time B-mode initially to plan out the best track for the transducer and then make a practice run before recording for extended field of view imaging.

It was possible to make images for extended field of view by moving the long face of the footprint in short axis but due to the small areas involved in the dog limbs this did not prove an asset for providing additional information. Once the extended field of view image had been acquired on the screen it was frozen and was then available for closer examination. This could be done by looking at the entire panoramic view or by placing a cursor at a selected anatomical landmark, the single original image frame from that spot could be called up on the screen and examined in detail with measurements being made if required.

The mm. supraspinatus and infraspinatus in the shoulder joint, the patellar ligament in the stifle joint and the common calcaneal tendon in the tarsal joint were able to be represented on extended field of view images.

3.3.4. Three dimensional scanning

To produce three dimensional images the same transducer was used as with Siemens Sonoline Elegra extended field of view, but in this case the transducer was drawn over the body surface with the short dimension of the footprint (the width) travelling proximal to distal along the long axis. With the transducer travelling thus it accumulated information in two planes simultaneously and this information was stored and then processed to create the co-ordinates for the third dimension. Once this was accomplished the area under investigation was displayed on the screen as a reconstructed volume sample in gray scale. As with extended field of view collection, the transducer movement was time limited and intolerant of erratic or hesitant movement. There was an alternative method of moving the transducer whereby it could be rocked gently through an arc on the body surface and thus gathered information which created a wedge shaped reconstructed volume sample for three dimensional examination. This was of greater use when imaging joint spaces such as the stifle joint. If the reconstructed sample contained information extraneous to the structure under investigation it was possible to eliminate this unwanted material using an electronic scalpel package whereby a line was drawn around the unwanted area and it was eliminated from the reconstruction.

Once a suitable reconstructed volume sample had been acquired it could be rotated in any of the three planes allowing viewing of all three faces. The volume sample could then be sliced in any of the three planes so that cross sections from proximal to distal face, lateral to medial face and dorsal (or coronal) sections from dorsal to ventral face could be made and each slice viewed individually. It was possible to identify a precise area of interest on one of the plane slices and by moving a cursor through it view the area of interest simultaneously in the other two planes. It was also possible to again identify a precise area of interest and centre the cursor on that area and by rotating the cursor through 360 degrees, view slices of that area one at a time at all angles in all three dimensions. These techniques were utilised to investigate structures, such as the m. biceps brachii and its tendon of origin, the mm. supraspinatus and infraspinatus and the stifle joint.

3.3.5. Live animal measurements of anatomical structures

A number of the anatomical structures surrounding the three joints under review were considered to be of more clinical importance than others and, in some cases, it was thought to be appropriate to measure their dimensions. The dimensions of the structures selected were repeatedly measured. Each measurement took place on a different day, with the prospect of finding out the potential for consistency on successive measurements. Five sessions took place for all the three joints under review using all the three scanning machines which were available.

The left limb was chosen to be scanned, with the dog in right lateral recumbency. There was a prospect of measuring the normal anatomical structures on the right limb, if a consistency in successive measurements of the left limb was proved. The lack in such led to the omission of conducting measurements on the right limb.

Specific anatomical landmarks were used in order to ensure that the measurements of the anatomical structures involved were taken at the same place each time. The use of a stand-off pad was not considered necessary for the measurements. The results for each structure were tabulated and the measurements for each structure using different scanners were investigated to prove any degree of consistency on repeated examinations. The average, the median, the standard deviation and the margins of error of the average for the confidence coefficients of 0.90 and 0.95 were calculated for each set of measurements taken with all the three scanners.

3.3.5.1. Shoulder joint:

M. supraspinatus: Depth measurements were taken in a short axis view at the level of the middle of the spine of the scapula (Fig. 3.5.) and depth and width measurements were conducted at the level of the musculotendinous junction proximal to the greater tubercle of the humerus (Fig. 3.6.) with the Toshiba Corevision and Dynamic Imaging Diasus. Depth measurements were taken from long axis extended field of view images with Siemens Sonoline Elegra. The site for measurement was selected and the individual frame for that site was called up on the screen and the measurement was taken (Fig. 3.7.).

M. infraspinatus: Depth measurements were taken in a short axis view at the level of the middle of the spine of the scapula (Fig. 3.8.) and depth and width measurements were conducted at the level of the musculotendinous junction proximal to the greater tubercle of the humerus (Fig. 3.9.) with the Toshiba Corevision and Dynamic Imaging Diasus. Depth measurements were taken from long axis extended field of view images with Siemens Sonoline Elegra using the technique already described (Fig. 3.10.).

M. biceps brachii: Three measurements were obtained, two of them having been taken in a long axis view and the third in a short axis view. The depth of the tendon was measured at the level of the intertubercular groove (Fig. 3.11.) as well as at the level of the curve through the intertubercular groove towards the cranial surface of the humerus (Fig. 3.12.) with the Toshiba Corevision and Dynamic Imaging Diasus. The dimensions of the tendon were then measured in a short axis view (Fig. 3.13.) with the Toshiba Corevision and Dynamic Imaging Diasus.

Measurements with Siemens Sonoline Elegra were not able to be taken in extended field of view images, because a consistent and continuous sweeping of the transducer along the tendon could not be accomplished. This was due to the curvature of its position on the cranio-medial aspect of the humerus.

M. teres minor: Depth and width measurements were taken when imaging the m. teres minor in a short axis view. The transducer was placed at the level of the acromial process at an angle perpendicular to the axis formed between the supraglenoid tubercle of the scapula with the olecranon of the ulna (Fig. 3.14.) with the Toshiba Corevision and Dynamic Imaging Diasus. Measurements with Siemens Sonoline Elegra were not taken in extended field of view images, because of the small size of the muscle and its deep position.

3.3.5.2. Stifle joint:

Patellar ligament: The depth of this structure was measured in two standard locations, both of them in a short axis view: the former was distal to the patella (Fig. 3.15.) and the latter proximal to the tibial tuberosity (Fig. 3.16.) with the Toshiba Corevision and Dynamic Imaging Diasus. Depth measurements with Siemens Sonoline Elegra were taken in long axis extended field of view images and the individual frame was assessed and used for measuring (Fig. 3.17.).

M. extensor digitorum longus: This tendon of origin was imaged in a short axis view and depth and width measurements were taken at the level of the extensor groove, which lay laterally on the cranial part of the tibia (Fig. 3.18.), with the Toshiba Corevision and Dynamic Imaging Diasus. Measurements (depth measurement) were not taken in extended field of view images with Siemens Sonoline Elegra because of the relatively small size of the tendon of origin.

3.3.5.3. Tarsal joint:

Common calcaneal tendon: The tendon was imaged and three depth measurements were taken for its three layers at the level of the bifurcation of the lateral saphenous vein (Fig. 3.19.) and proximal to the calcaneal tuberosity (Fig.

3.20.) both in a short axis view with the Toshiba Corevision and Dynamic Imaging Diasus. Depth measurements were taken in long axis extended field of view images with Siemens Sonoline Elegra using a selected individual image frame to make the measurement for the tendon in its entity, because the technique could not be applied successfully for each one of the layers (Fig. 3.21.).

3.3.6. Clinical cases

Five dogs that had been referred to the orthopaedic section of the Small Animal Hospital were used for this study (Table 3.1.). They had a clinical work up, which included physical examination, radiography, and in some cases arthroscopy and scintigraphy. These examinations were carried out by other members of staff and only the ultrasonography was carrried out by the researchers involved in this project.

CASE	AGE (yrs)	WEIGHT (Kg)	BREED	SEX
1	4	19	Border Collie	EF
2	5	35	Weimaraner	NM
3	8	32.5	Greyhound	NM
4	2.5	51	Rottweiler	EM
5	10	32	Labrador	NF

EF: entire female, NF: neutered female, EM: entire male, NM: neutered male

Table 3.1. Age, weight, breed, and sex distribution of the 5 clinical cases presented.

The ultrasonographic examinations carried out were limited to the field of interest relevant to the clinical condition. The presentation of these clinical cases will be given in Chapters 4 and 5.

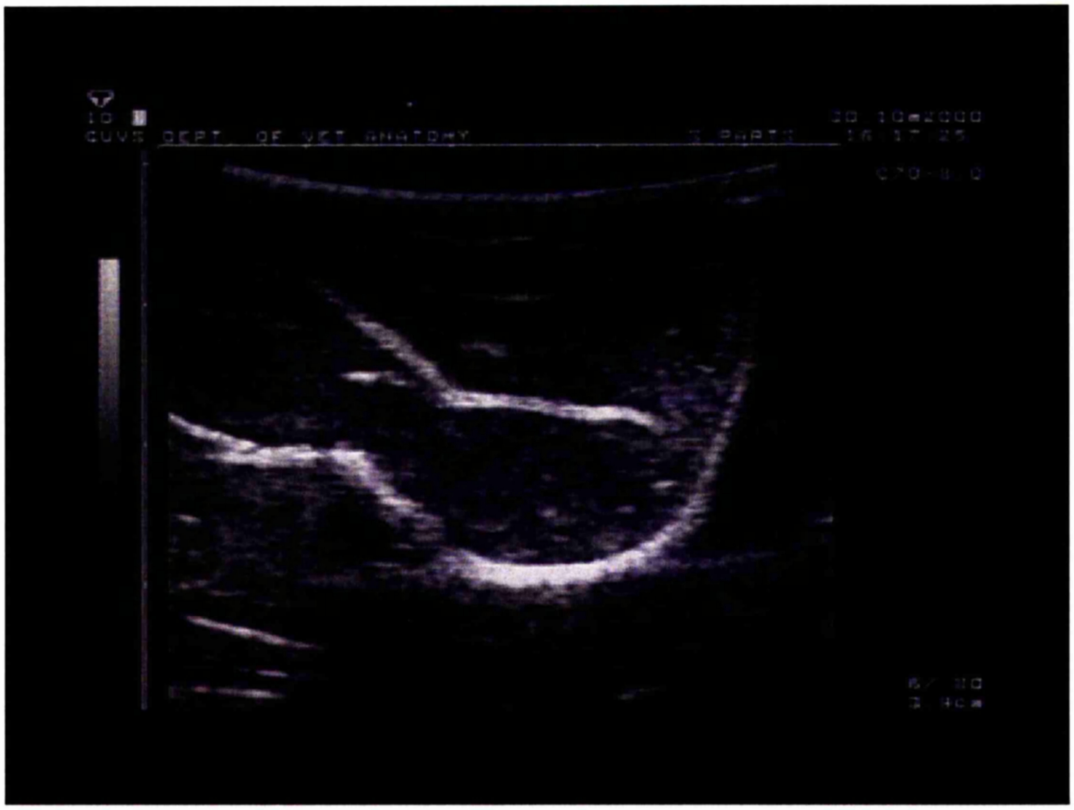

Fig. 3.1.a. Short axis view of the m. infraspinatus at the level of the middle of the spine of the scapula of a cadaver scanned with Justvision and a 7.5 MHz convex linear transducer. The hyper reflective spine of the scapula with anechoic acoustic shadowing distal to it appears to the right of the picture. The injected echocontrast agent is represented by a hyperechoic dot surrounded by an anechoic area lying to the left of the scapular spine and superficial to the hyperechoic line corresponding to the perimysium that appears in the middle of the muscle.

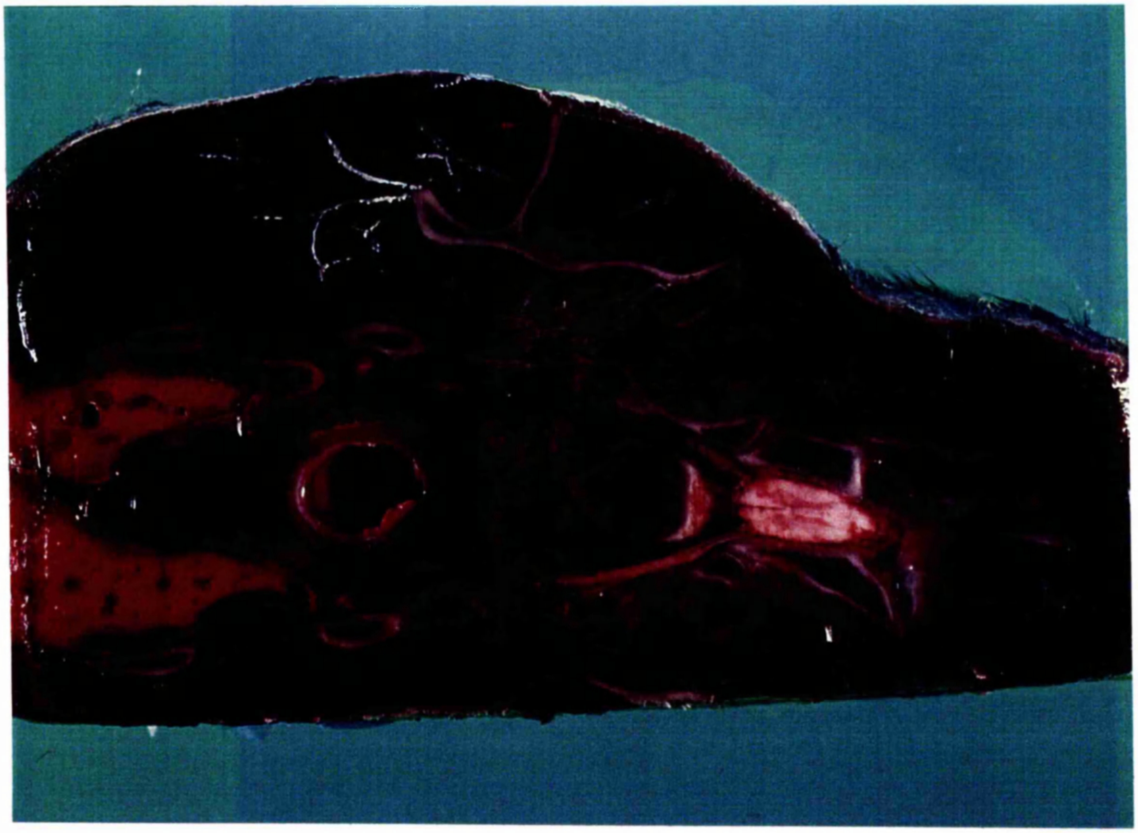

Fig. 3.1.b. Gross anatomy cross section of the left shoulder region of a Greyhound cadaver. The scapula with mm. supraspinatus and infraspinatus appear in the centre at the top of the picture and the echocontrast agent that has been injected in the muscles is displayed as a yellowish dot in the fleshy m. infraspinatus to the left of the scapular spine.

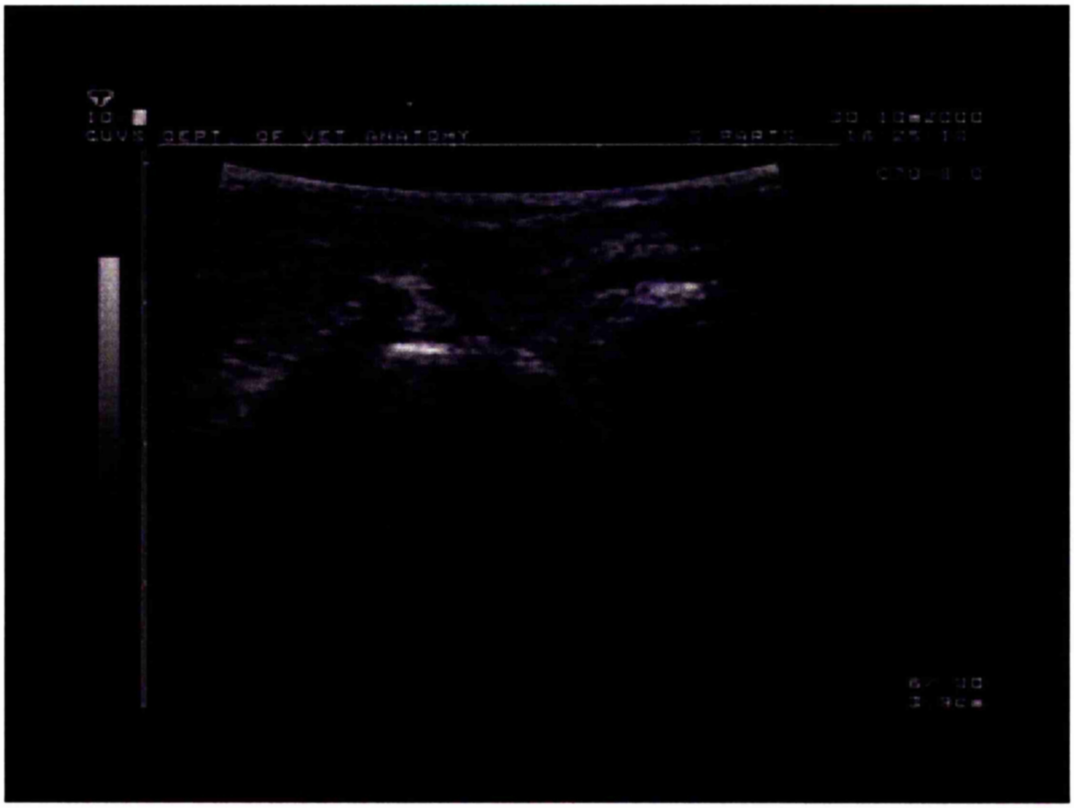

Fig. 3.2.a. Short axis view of the tendon of origin of the m. biceps brachii at the level of the intertubercular groove of a cadaver scanned with Justvision and a 7.5 MHz convex linear transducer. The hyper reflective intertubercular groove is displayed in the mid field with the tendon running over it being represented as a rounded hyperechoic structure to the left of mid field. The injected bolus of echocontrast agent is seen as a hyperechoic area lying on the superficial surface of the tendon.

Fig. 3.2.b. Gross anatomy cross section of the left shoulder region of a Greyhound cadaver. The humerus is displayed on the top left with the tendon of origin of the m. biceps brachii appearing as a rounded structure on its medial surface. The yellow dye with echocontrast agent is visible on the superficial surface of the tendon and within the m. teres minor that lies on the caudal lateral surface of the cross sectioned humerus.

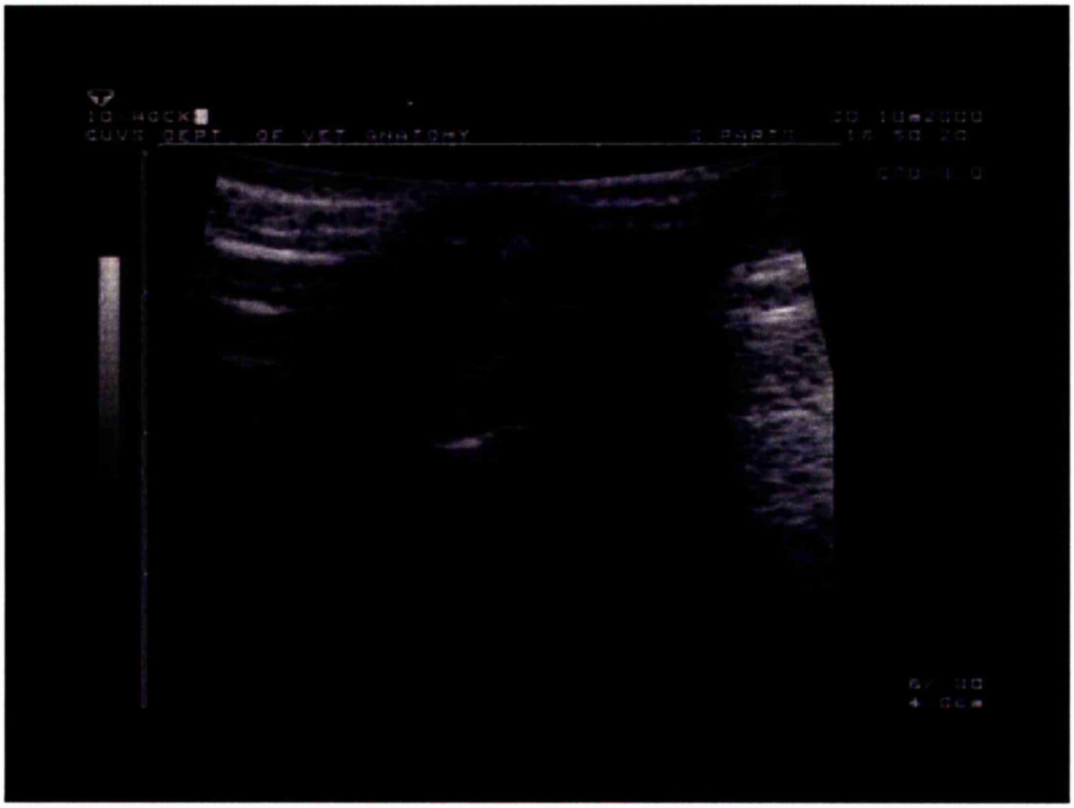

Fig. 3.3.a. Short axis view of the common calcanean tendon at the level of the bifurcation of the lateral saphenous vein of a cadaver scanned with Justvision and a 7.5 MHz convex linear transducer. The tendon appears in the top centre of the image and the injected echocontrast agent is represented by a hyperechoic dot in the tendon substance at 1 o'clock on the tendon circumference.

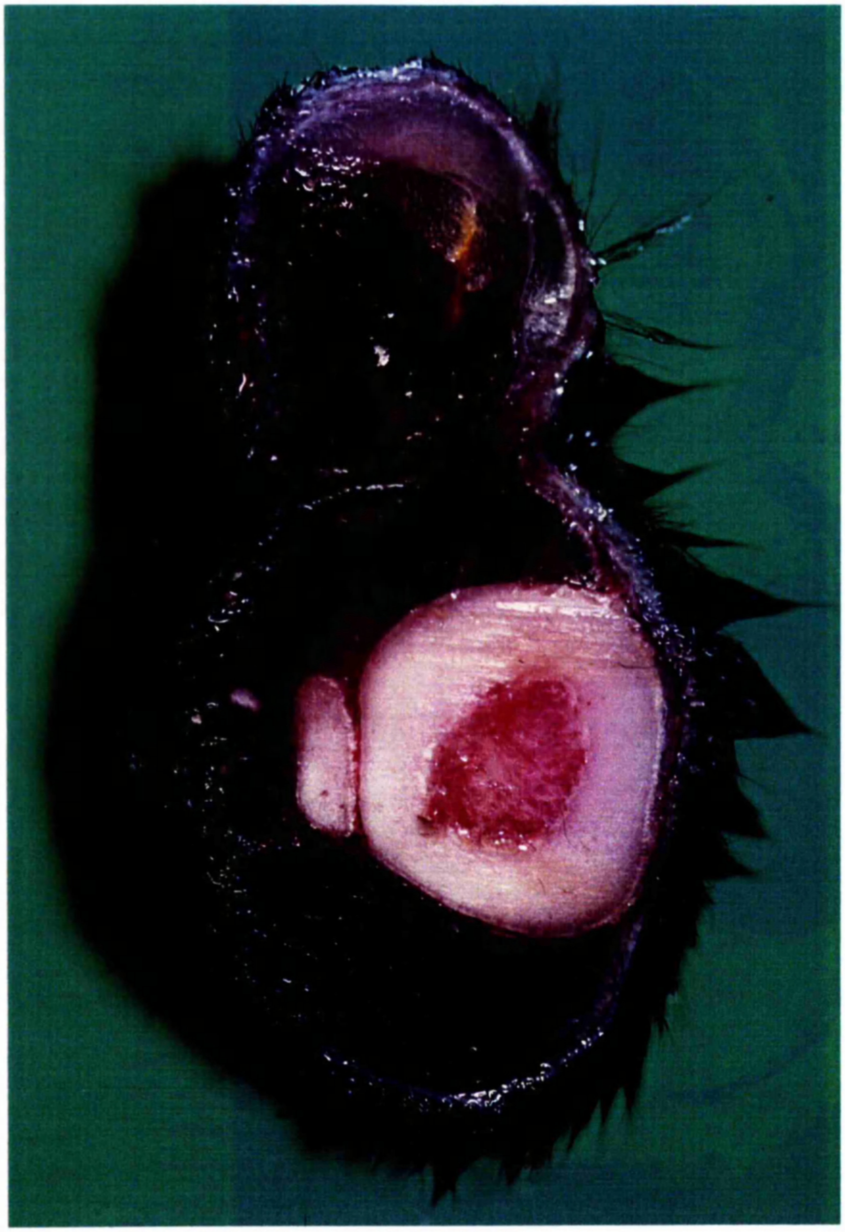

Fig. 3.3.b. Gross anatomy cross section of the left tarsal joint of a Greyhound cadaver. The tibia and fibula lie in the lower field, whereas the common calcaneal tendon is to the top of the picture with the injected dye and echocontast agent lying within its substance.

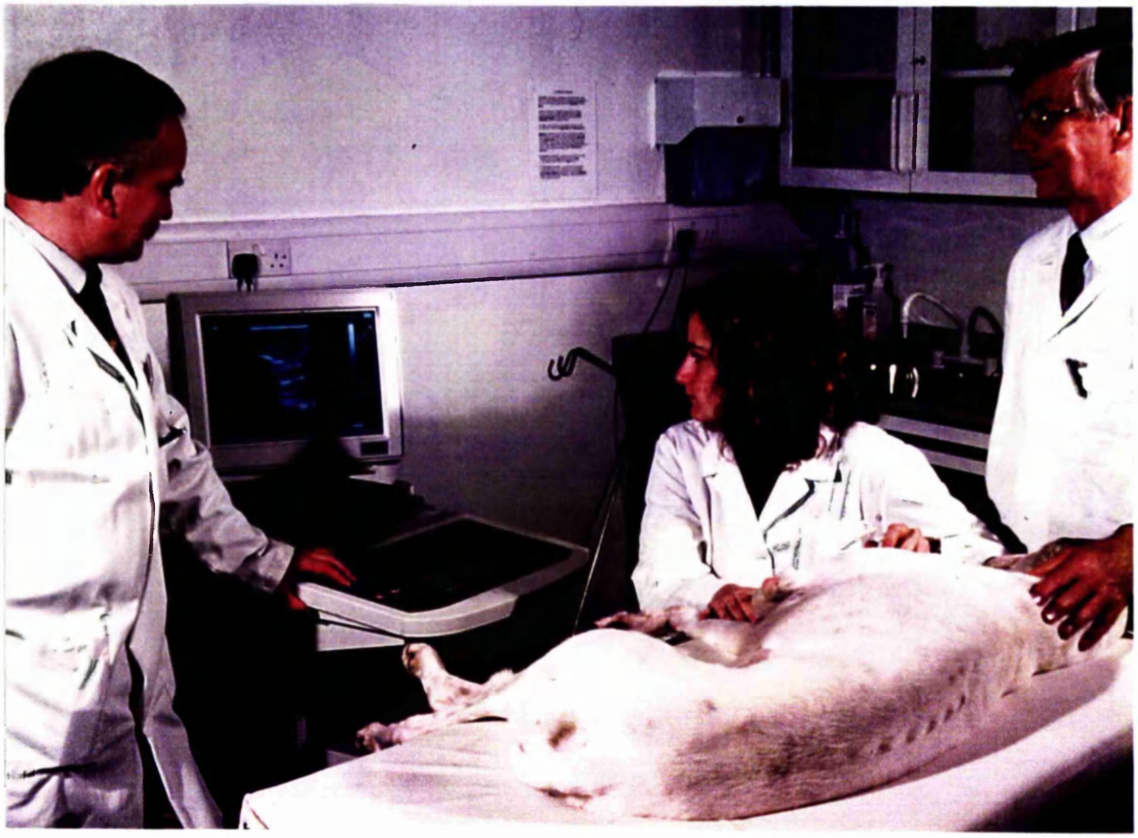

Fig. 3.4. Researchers involved in the project scanning a Greyhound with the Diasus scanner. The dog is in right lateral recumbency and the transducer is applied to the prepared clipped area of the shoulder joint.

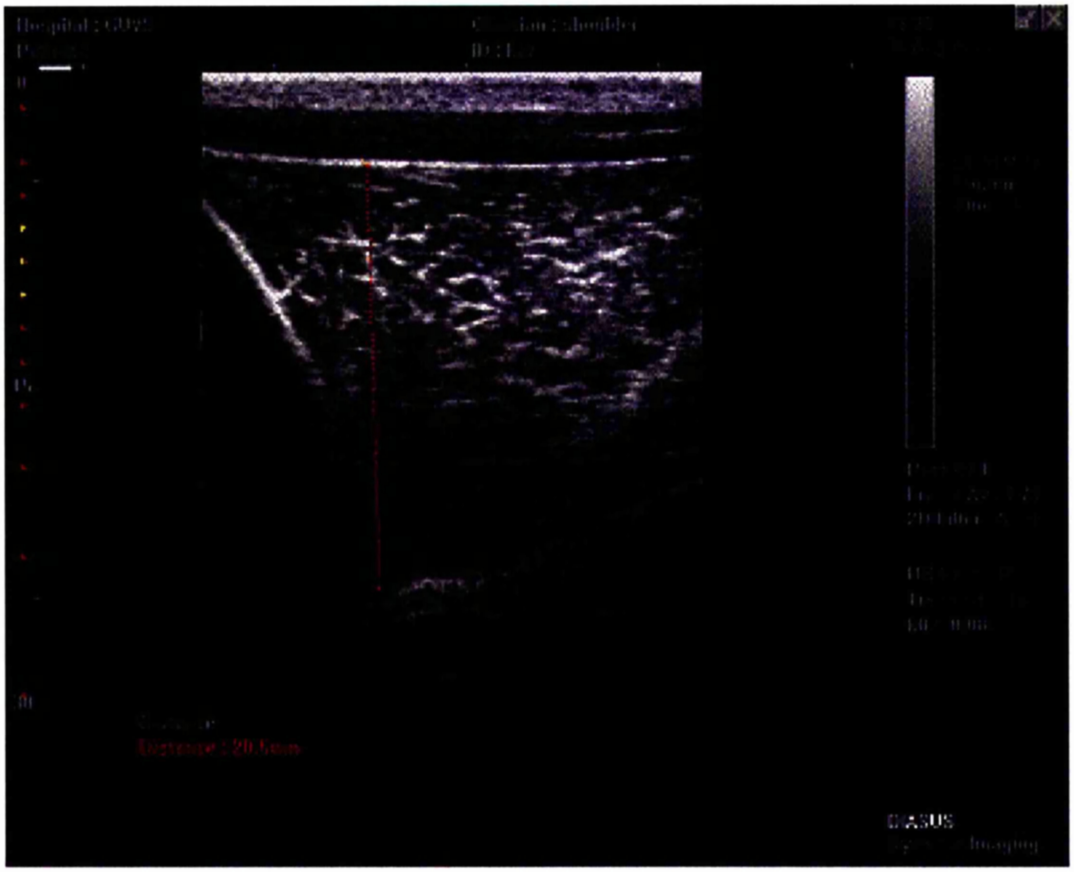

Fig. 3.5. Depth measurement of the m. supraspinatus of the left forelimb of a dog at the level of the middle of the spine of the scapula in short axis view scanned with the Diasus scanner and a 16 MHz linear transducer. The linear hyper reflective spine of the scapula with an anechoic area of acoustic shadowing distal to it is imaged on the left and the muscle is displayed from left to right. The skin lies to the top of the image and the m. omotransversarius immediately deep to it.

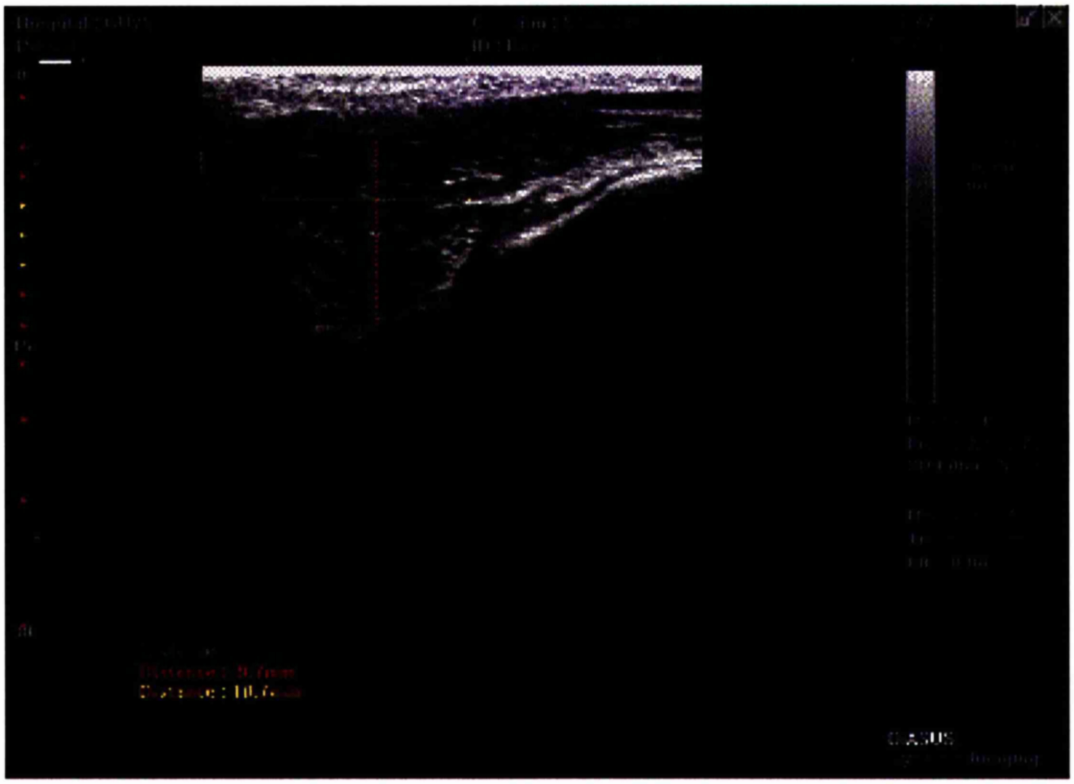

Fig. 3.6. Depth and width measurements of the m. supraspinatus of the left forelimb of a dog at the level of the musculotendinous junction in short axis view scanned with the Diasus scanner and a 16 MHz linear transducer. The muscle appears in the centre of the image.

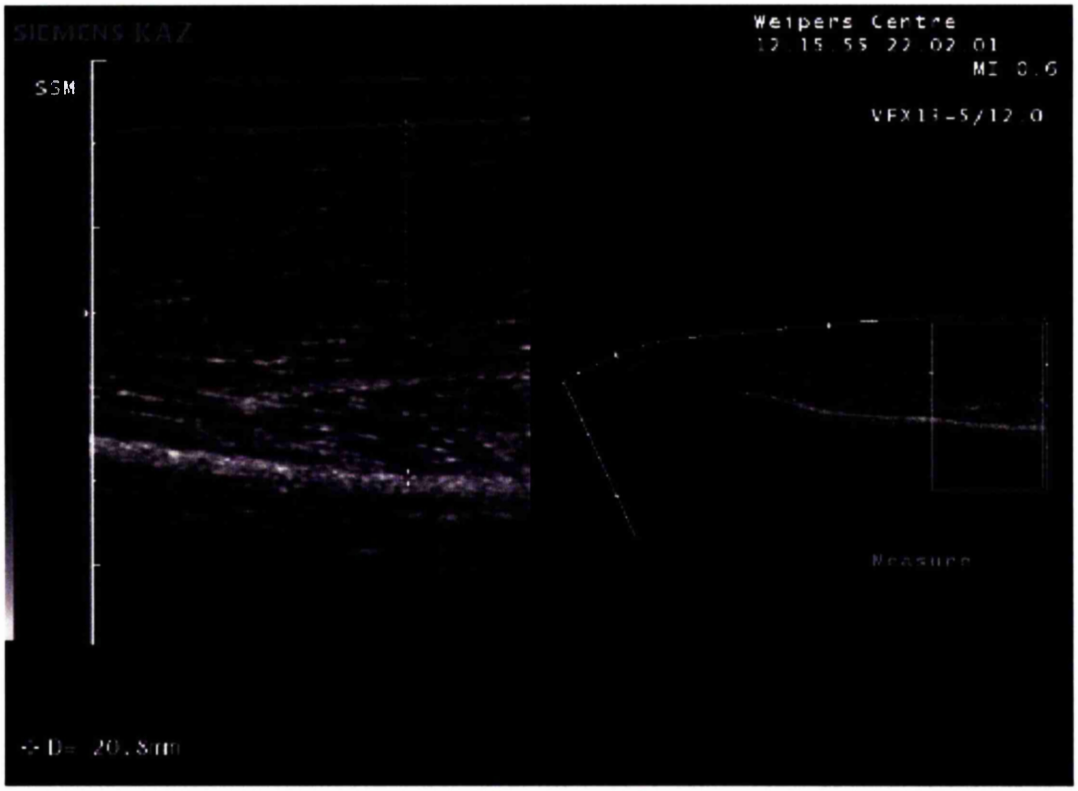

Fig. 3.7. Extended field of view image of the m. supraspinatus in the left forelimb of a dog using Elegra with a 12 MHz transducer. The panoramic view is displayed to the right of the picture with a box cursor placed over the area of interest for measurement. A single frame from that area of interest is displayed on the left with electronic measurement markers set at the superficial and deep surface of the muscle to give a measurement of depth of that muscle at that point.

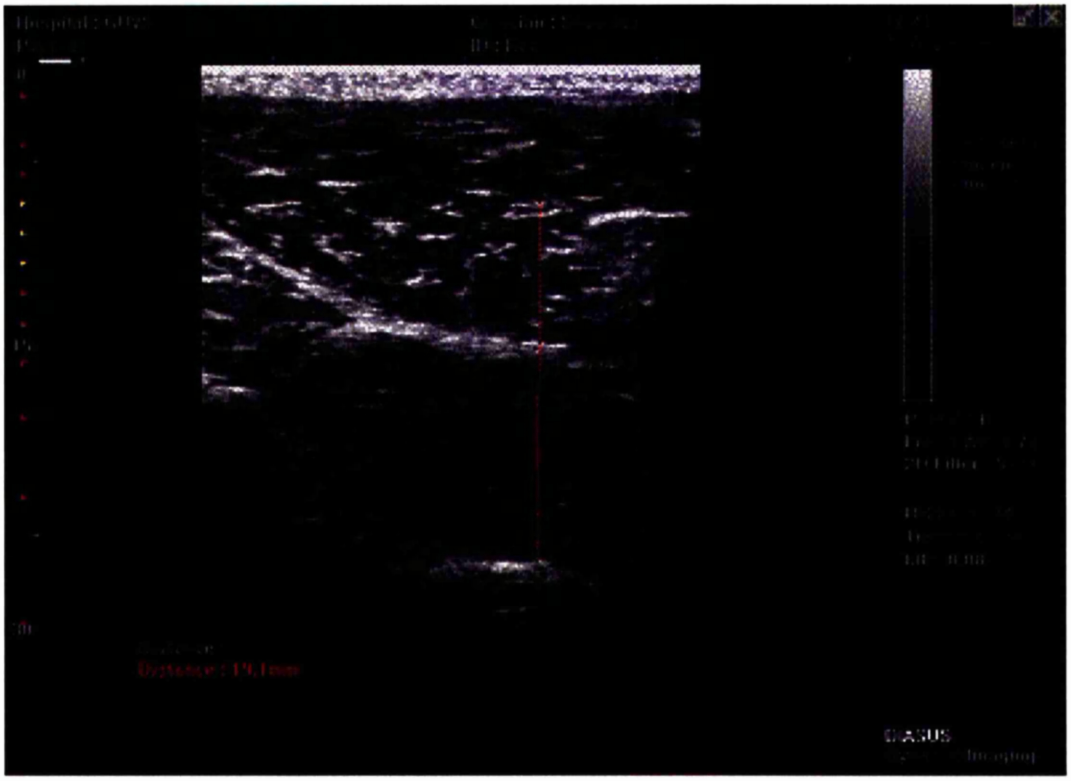

Fig. 3.8. Depth measurement of the m. infraspinatus of the left forelimb of a dog at the level of the middle of the spine of the scapula in short axis view scanned with the Diasus scanner and a 16 MHz linear transducer. The linear hyper reflective spine of the scapula with an anechoic area of acoustic shadowing distal to it appears on the extreme right with the muscle being displayed from left to right.

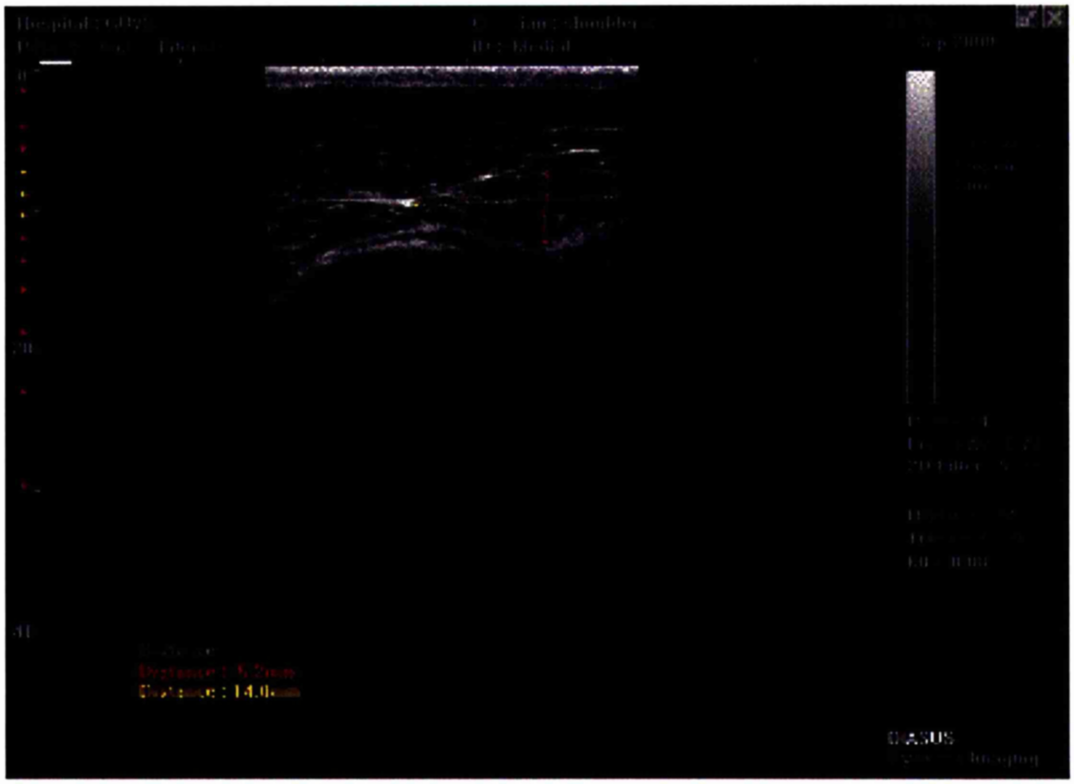

Fig. 3.9. Depth and width measurements of the m. infraspinatus of the left forelimb of a dog at the level of the musculotendinous junction in short axis view scanned with the Diasus scanner and a 16 MHz linear transducer. The muscle is displayed on the right of the screen and the hyper reflective greater tubercle of the humerus with an anechoic area of acoustic shadowing distal to it lies to the bottom of the image.

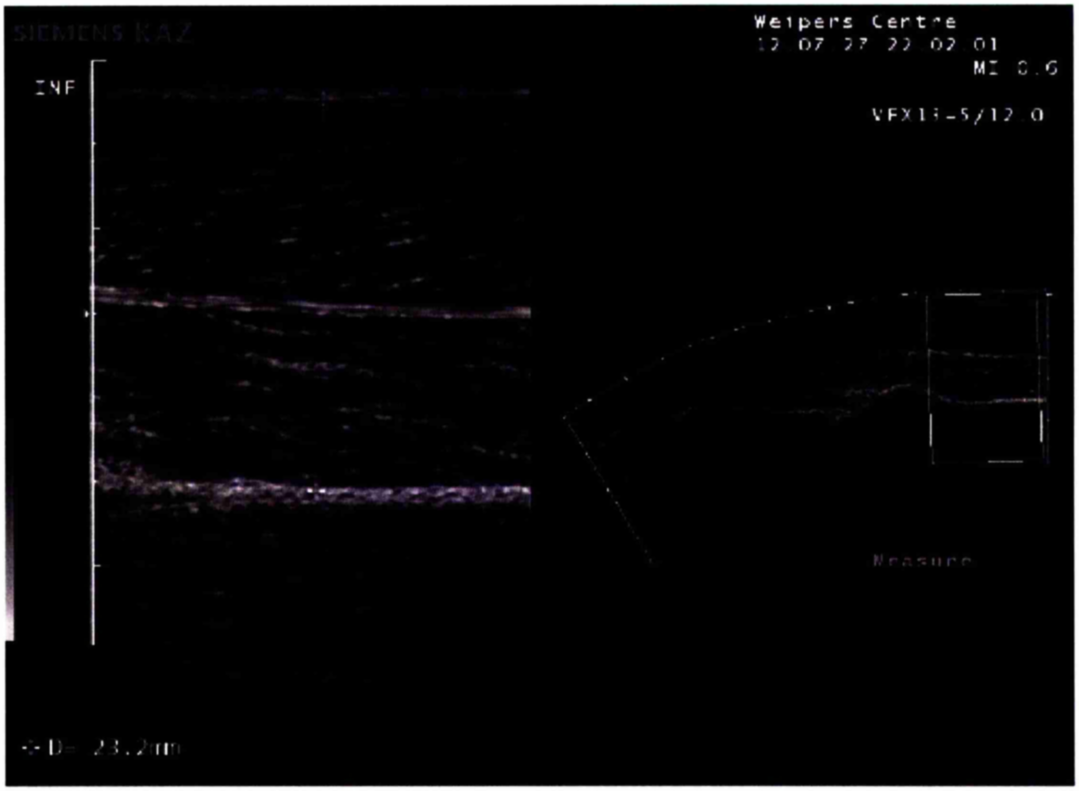

Fig. 3.10. Extended field of view image of the m. infraspinatus in the left forelimb of a dog using Elegra with a 12 MHz transducer. The panoramic view is displayed to the right of the picture with a box cursor placed over the area of interest for measurement. A single frame from that area of interest is displayed on the left with electronic measurement markers set at the superficial and deep surface of the muscle to give a measurement of depth of that muscle at that point.

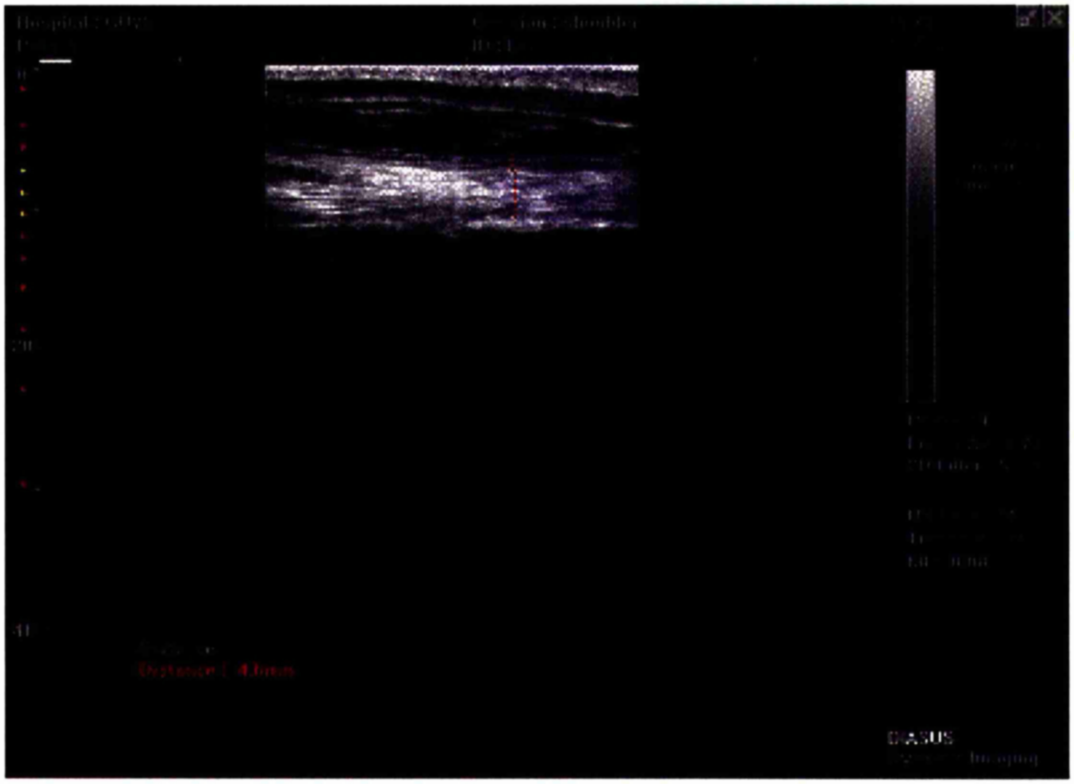

Fig. 3.11. Depth measurement of the tendon of origin of the m. biceps brachii of the left forelimb of a dog at the level of the intertubercular groove in long axis view scanned with the Diasus scanner and a 16 MHz linear transducer. The hyperechoic tendon lies on the hyper reflective intertubercular groove with an anechoic area of acoustic shadowing distal to it, that corresponds to the bottom of the picture.

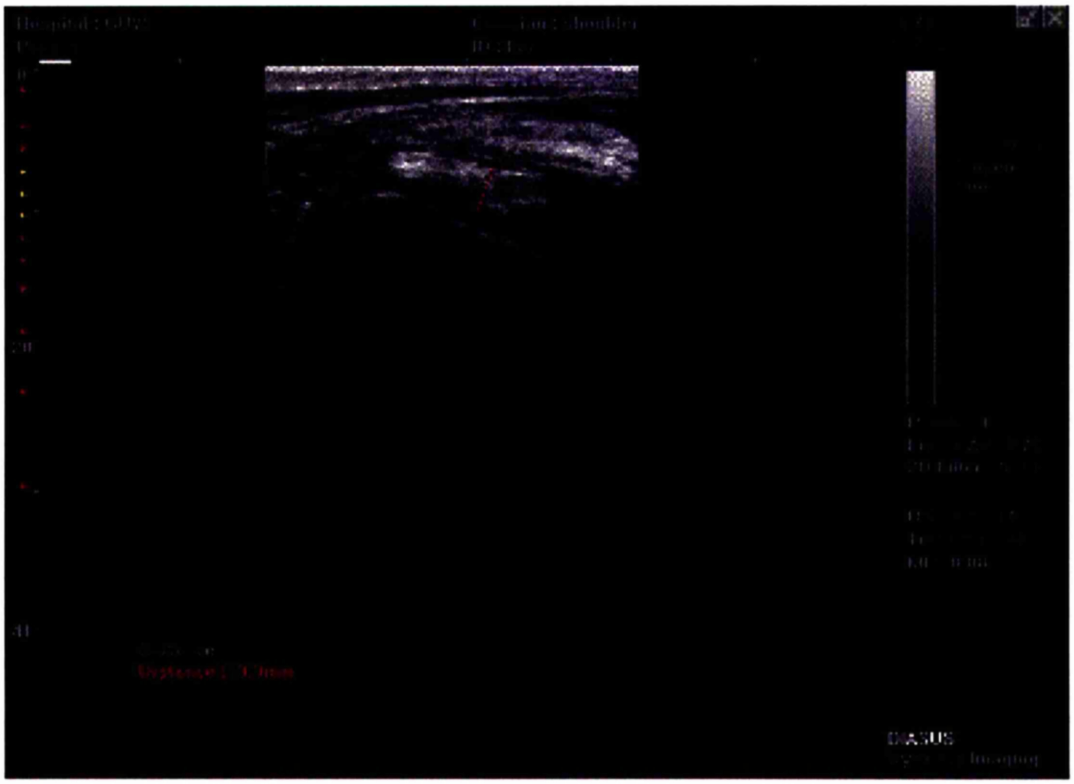

Fig. 3.12. Depth measurement of the tendon of origin of the m. biceps brachii of the left forelimb of a dog at the level of the curve in the long axis view scanned with the Diasus scanner and a 16 MHz linear transducer. The hyperechoic tendon is displayed in the mid field on top of the hyper reflective humerus at the level of the curve. An anechoic area of acoustic shadowing distal to the humerus corresponds to the bottom of the picture. The anisotropy artifact is evident along the tendon.

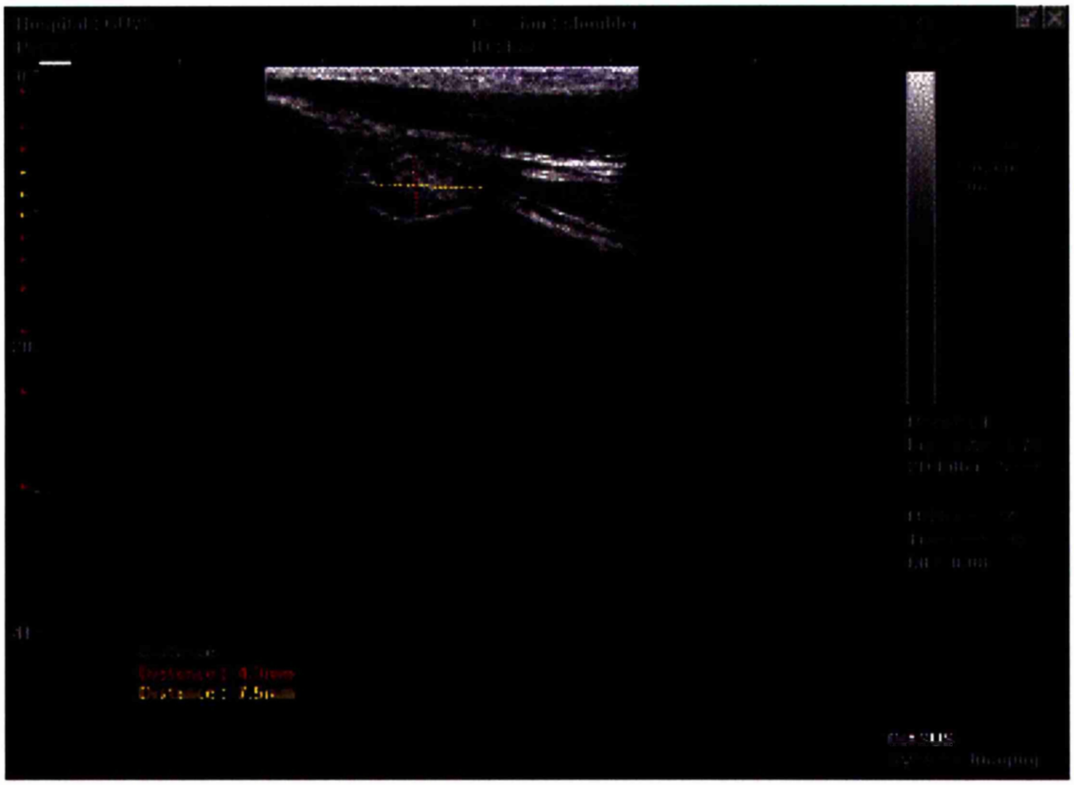

Fig. 3.13. Depth and width measurements of the tendon of origin of the m. biceps brachii of the left forelimb of a dog at the level of the intertubercular groove in short axis view scanned with the Diasus scanner and a 16 MHz linear transducer. The hyperechoic tendon is displayed in the hyper reflective intertubercular groove with an anechoic area of acoustic shadowing distal to it.

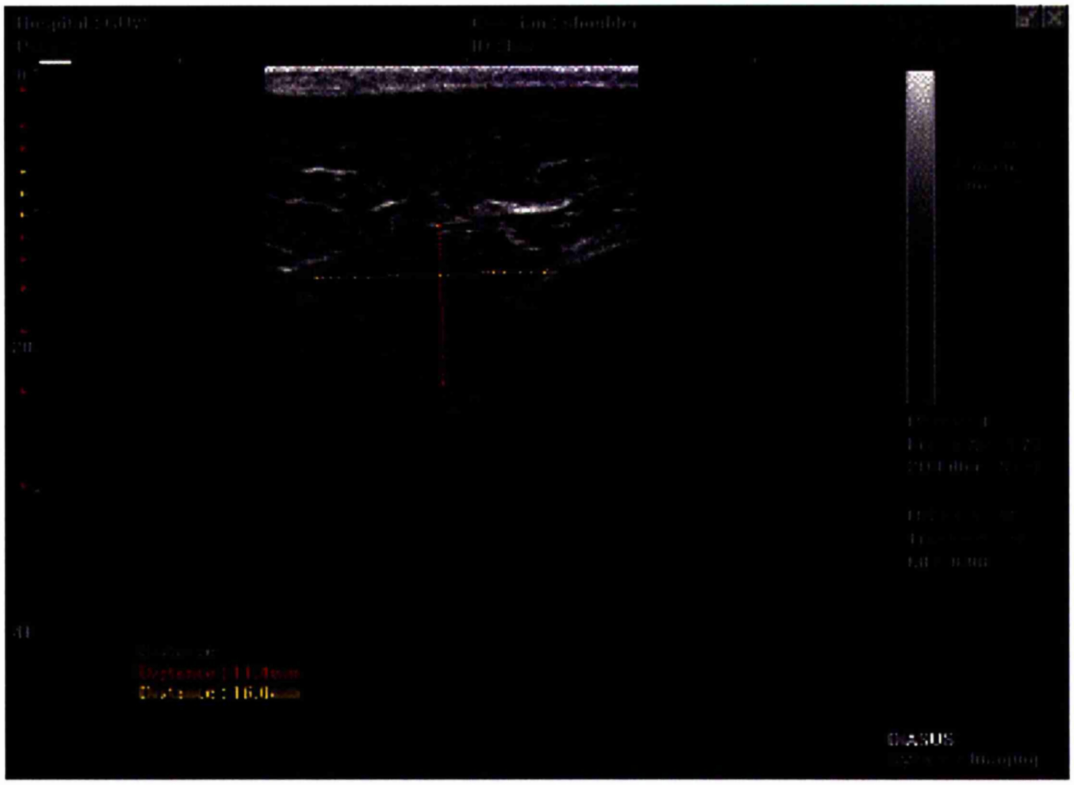

Fig. 3.14. Depth and width measurements of the m. teres minor of the left forelimb of a dog in short axis view scanned with the Diasus scanner and a 16 MHz linear transducer. The moderately hypoechoic muscle is displayed in the middle of the screen with the hyper reflective greater tubercle of the humerus on the right with an anechoic area of acoustic shadowing distal to it.

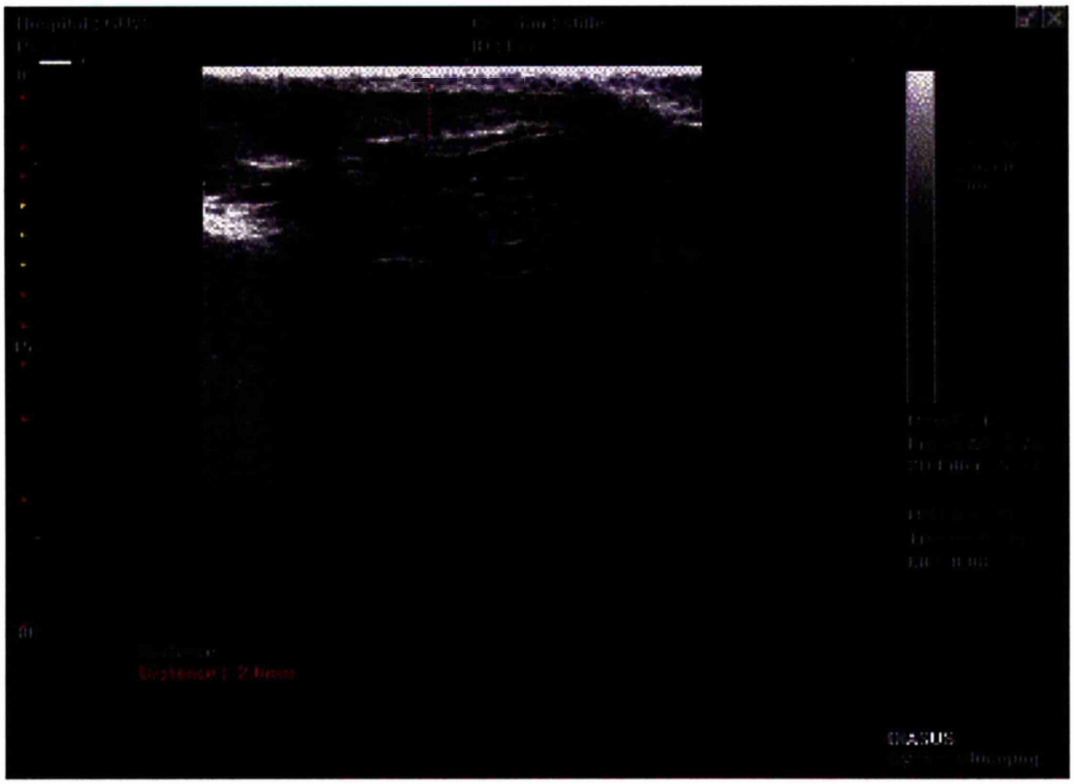

Fig. 3.15. Depth measurement of the patellar ligament of the left pelvic limb of a dog distal to the patella in short axis view scanned with the Diasus scanner and a 16 MHz linear transducer. The hypoechoic patellar ligament lies to the top with the echogenic infrapatellar fat in the mid field.

Fig. 3.16. Depth measurement of the patellar ligament proximal to the tibial tuberosity of the left pelvic limb of a dog in short axis view scanned with the Diasus scanner and a 16 MHz linear transducer. The hypoechoic patellar ligament lies to the top with the echogenic infrapatellar fat in the mid field.

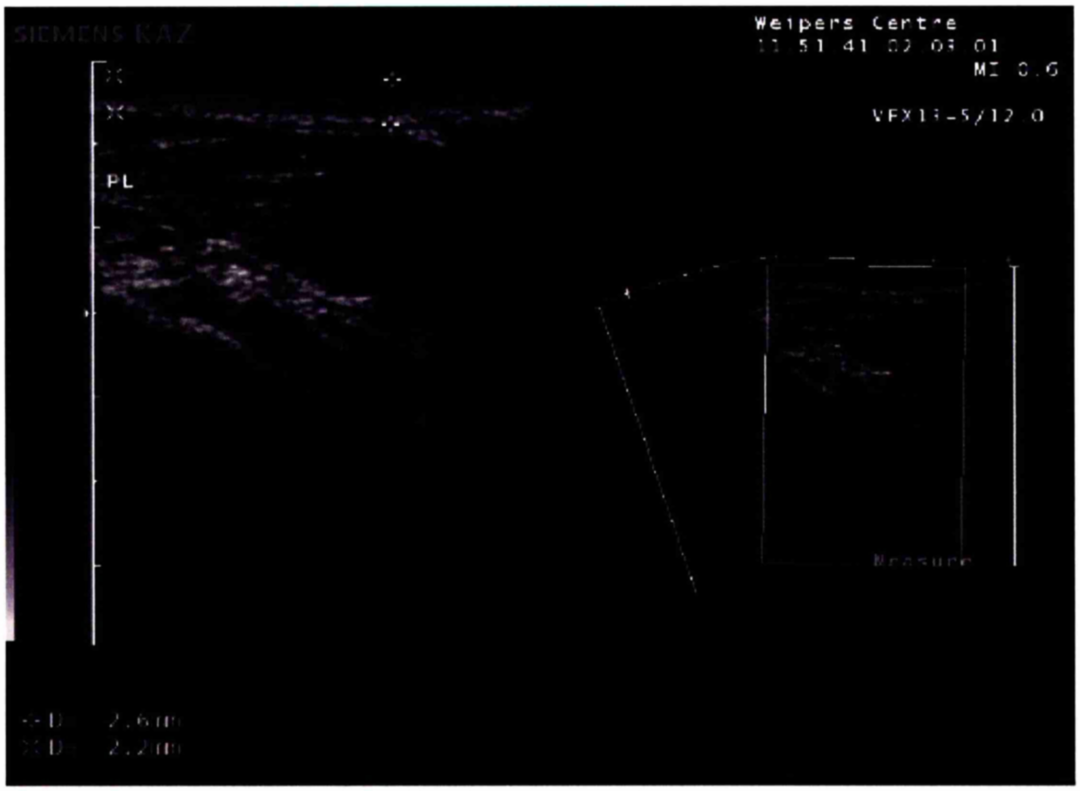

Fig. 3.17. Extended field of view image of the stifle joint using Elegra with a 12 MHz transducer. The panoramic view is displayed to the right of the picture with a box cursor placed over the area of interest for measurement. A single frame from that area of interest is displayed on the left with electronic measurement markers set at two positions on the patellar ligament. The markers are measuring the thickness of the patellar ligament at its origin from the patella to the right and its insertion onto the tibial tuberosity to the left.

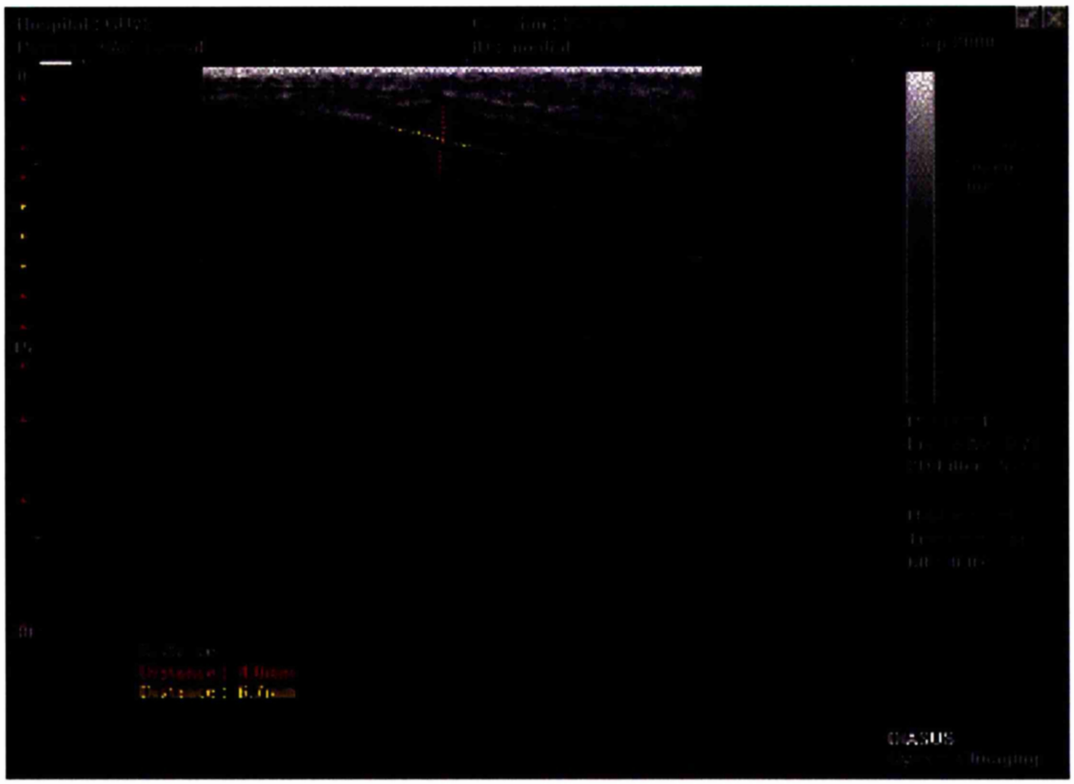

Fig. 3.18. Depth and width measurements of the tendon of origin of the m. extensor digitorum longus of the left pelvic limb of a dog at the level of the extensor groove in short axis view scanned with the Diasus scanner and a 16 MHz linear transducer. The round hyperechoic tendon lies on the top of the picture in the hyper reflective extensor groove with an anechoic area of acoustic shadowing distal to it.

Fig. 3.19. Depth measurement of the common calcaneal tendon at the level of the bifurcation of the saphenous vein of the left pelvic limb of a dog in short axis view scanned with the Diasus scanner and a 16 MHz linear transducer. Its three hyperechoic layers are displayed on the left of the picture.

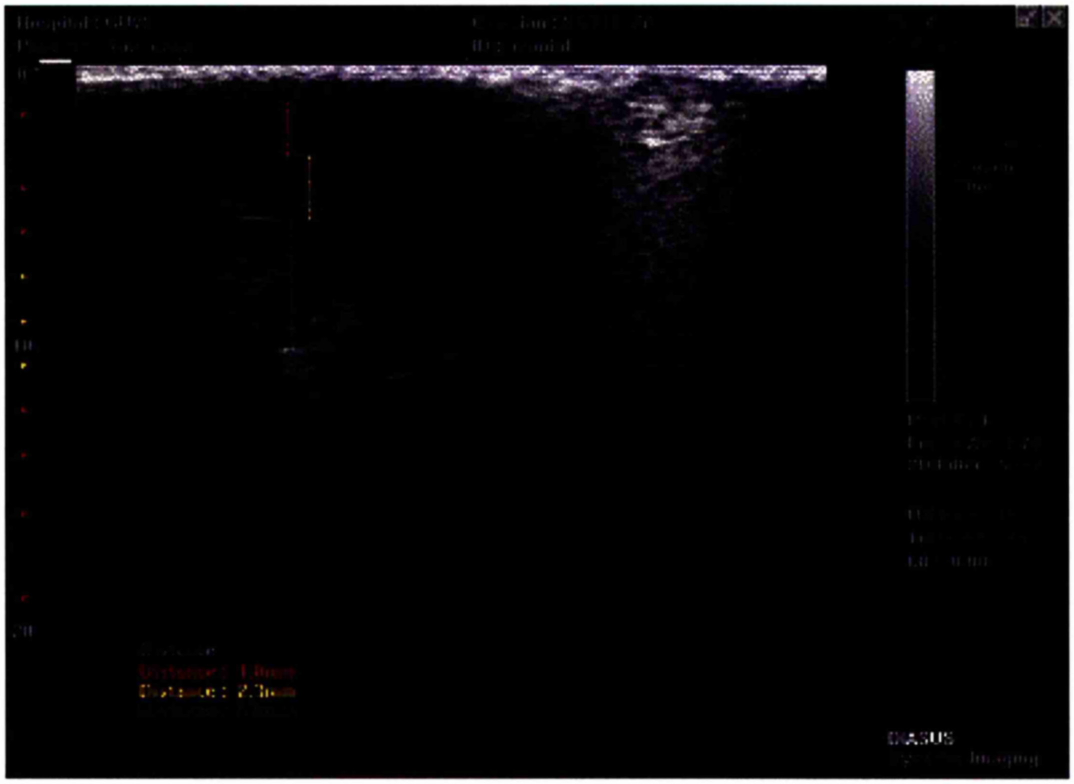

Fig. 3.20. Depth measurement of the common calcaneal tendon at the level of the calcaneal tuberosity of the left pelvic limb of a dog in short axis view scanned with the Diasus scanner and a 16 MHz linear transducer. Its three hyperechoic layers are displayed on the left of the picture.

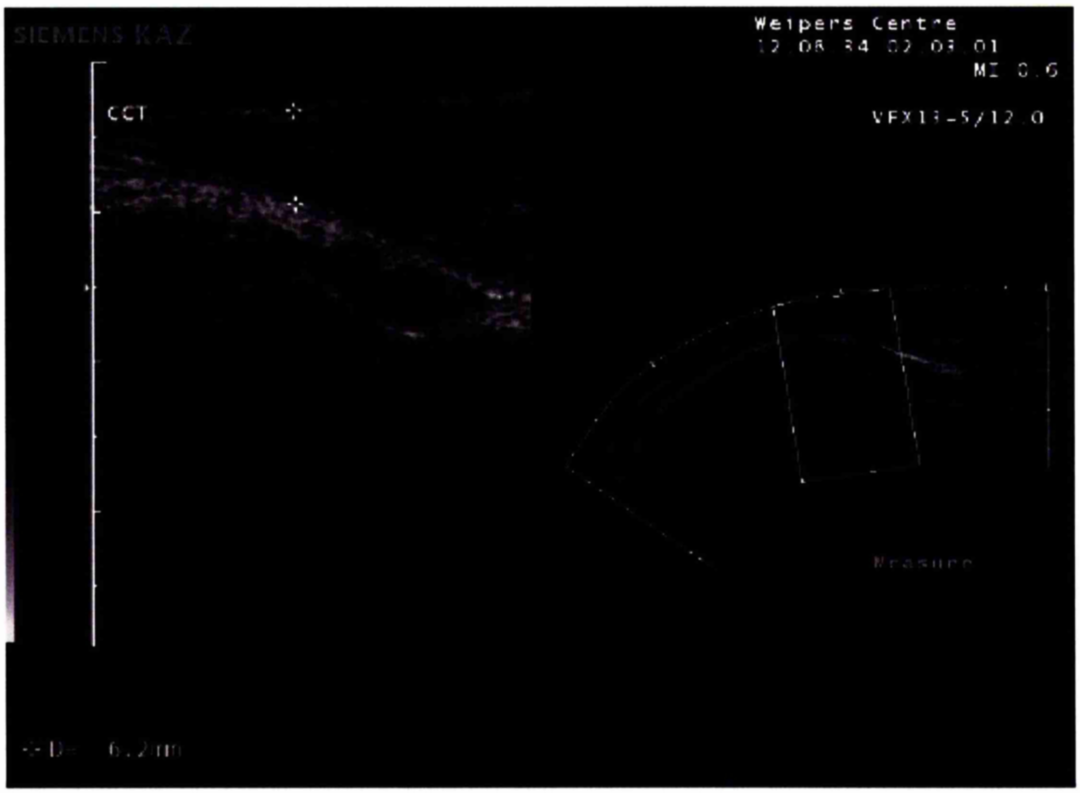

Fig. 3.21. Extended field of view image of the common calcanean tendon using Elegra with a 12 MHz transducer. The panoramic image is displayed to the right with a box cursor placed over the area of interest for measurement. A single frame from that area of interest is displayed on the left with electronic measurement markers set at the point of the musculotendinous junction to measure the thickness of the muscle at that point.

CHAPTER 4.

RESULTS

4. RESULTS

4.1. Cadaver work

The comparison of images using echocontrast agent with anatomical sectioning correlated well and gave confidence in identification of specific structures. This was of particular use in the case of multiple structures, such as the common calcanean tendon.

4.2. Live animal normal anatomical scanning

Various anatomical structures were able to be visualised with all the three scanners used in the study.

4.2.1. Shoulder Joint:

M. supraspinatus: The m. supraspinatus was successfully visualised underneath the m. omotransversarius. It was imaged as a moderately hypoechoic structure both in long and short axis with Corevision. A hyperechoic line represented the perimysium, which divided the entire muscle into two parts. Finely hyperechoic areas representing collagen bundles were scattered throughout the parenchyma. The epimysium was imaged as a smooth hyperechoic line surrounding the entire muscle. The muscle structure became more hyperechoic as the transducer moved towards the tendon, which appeared homogeneously hyperechoic, the collagen bundles surrounding it being represented in this way.

The use of Diasus enabled accurate imaging of the m. supraspinatus both in long and short axis, due to the high resolution that the high frequency probe offered. The images produced revealed a moderately hyperechoic structure, that had hyperechoic dots scattered around the parenchyma, but were distinct and their margins well defined. The perimysium and epimysium were imaged as hyperechoic lines around the muscle bundles and the whole muscle itself (Fig. 4.1.). The tendon of insertion of the m. supraspinatus appeared brightly hyperechoic on the screen, due to the near optimum resolution.

When imaged with the extended field of view system of Elegra, the m. supraspinatus appeared as a complete structure on the screen in long axis. It looked hypoechoic with bright echoes in its parenchyma. The perimysium was not evident and only the presence of the hyperechoic epimysium was confirmed. The short hyperechoic tendon of insertion was accurately imaged on most of the scans performed (Fig. 4.2.).

The m. supraspinatus was a suitable structure for producing three dimensional volume samples and thus the muscle belly could be investigated in multiple planes and the tendon of insertion viewed in three dimensions. The dorsal (coronal) plane had the poorest image quality but it was of use to register the position of the tendon relative to the bone surface.

M. infraspinatus: The m. infraspinatus was clearly imaged both in long and short axis with Toshiba Corevision. It appeared as a moderately hypoechoic structure with hyperechoic dots scattered throughout the parenchyma. The perimysium, which divides the muscle into two parts, was evident as a smooth hyperechoic line when imaged both in long and in short axis. The epimysium of the entire muscle appeared to be of the same echogenicity. The m. infraspinatus appeared to be more hyperechoic when it was imaged at the level of the musculotendinous junction. Its tendon was hyperechoic (which corresponded to the higher echogenicity of the collagen layers surrounding it) when imaged in long axis. Its point of insertion was also accurately detected. The infraspinous bursa was not consistently visualised.

Imaging with Diasus revealed a more detailed view of the m. infraspinatus both in long and in short axis. The entire organ was viewed as a homogeneously hypoechoic structure with precisely defined hyperechoic foci around the parenchyma. The perimysium was detected as a hyperechoic line, as well as the epimysium (Fig. 4.3.). The tendon of insertion appeared hyperechoic and clearly defined, whereas the infraspinous bursa was able to be visualised as a small anechoic round structure, lying beneath the tendon (Fig. 4.4.).

Extended field of view imaging with the Elegra Ultrasound System revealed the muscle as an entity on the screen in long axis. The muscle was imaged as a hypoechoic structure with hyperechoic foci scattered in the parenchyma. The perimysium and epimysium were both visualised as smooth hyperechoic lines extending throughout the entire muscle. The tendon of insertion was imaged inserting onto the greater tubercle of the humerus. The infraspinous bursa was not consistently visualised (Fig. 4.5.).

Imaging in three dimensions to create a volume sample was also possible with the m. infraspinatus thus allowing reviewing of the structure in multiple planes.

<u>M. deltoideus:</u> Both parts of the m. deltoideus were visualised both in long and short axis with Corevision as moderately hypoechoic structures overlying the m. infraspinatus. Hyperechoic dots were scattered around its parenchyma.

Imaging with Diasus revealed a more detailed presentation of the same muscle both in long and short axis. Better resolution resulted in the accurate imaging of both parts, as well as of their junction (Fig. 4.6.).

M. deltoideus was not visualised with the Elegra System, because of the inability to image the whole muscle with only one sweep of the ultrasound beam.

M. biceps brachii: The m. biceps brachii was visualised as a longitudinal hypoechoic structure in long axis, being the continuation of its tendon of origin, which was able to be imaged with Corevision. The tendon was visualised as a linear hyperechoic structure lying in the intertubercular groove and at the curve formed by the greater tubercle of the humerus when imaged in long axis views. It should be mentioned that the structure appeared more hyperechoic at the points where the transducer was placed perpendicular to the tendon. All other regions looked more hypoechoic without being pathologic, because of the anisotropy artifact, which could not be avoided, even when the Diasus scanning machine was used. It could also be imaged in short axis views in the intertubercular groove as a round hyperechoic structure surrounded by a small amount of fluid, that represented its synovial sheath.

The tendon of origin of the m. biceps brachii was clearly imaged both in long and short axis with Diasus scanner. its high echogenicity due to the highly reflective collagen bundles both in long and short axis was evident (Fig. 4.7., 4.8.). The synovial sheath of the tendon contained a small amount of anechoic fluid and was imaged in fine detail (Fig. 4.8.). The transverse humeral ligament was also able to be detected as a small moderately hyperechoic linear structure that held the tendon in the intertubercular groove (Fig. 4.9.).

There was some difficulty in imaging the tendon of the m. biceps brachii with the extended field of view modality, due to its medial position and the curved path required to be taken by the transducer to acquire images, but with practice an extended field of view could be built up, which had the benefit of demonstrating the topography of the tendon in the groove but the tendon detail did not match up to that acquired with Diasus.

A three dimensional volume of the proximal end of the belly of the muscle lying against the bone cortex and the tendon of origin running through the intertubercular groove was produced and the detail of the tendon in the groove with its surrounding sheath was able to be followed in multiple planes (Fig. 4.10., 4.11., 4.12., 4.13., 4.14., 4.15., 4.16., 4.17., 4.18.).

M. teres minor: The m. teres minor was detected with Corevision, although its size is considered to be small. It was detected distocaudally on the scapula and was covered by the mm. infraspinatus and deltoideus. Its imaging in long axis was not consistent during ail scannings, because of its size, whereas its imaging in short axis proved to be easier. It appeared as an opposite triangular structure with moderate to low echogenicity and hyperechoic dots around its parenchyma.

The same muscle was visualised with greater accuracy in short axis with Diasus. Its margins and hyperechoic dots were defined with greater accuracy due to the near optimal resolution of the scanning machine (Fig. 4.19.). Imaging in long axis was not consistent, in as much as the size of the muscle proved to be a handicap in it, even though the resolution of the used transducer was much better than that of the one used with Corevision.

The m. teres minor proved to be difficult to visualise with the extended field of view modality because of its small size.

As this muscle lay deep to the m. deltoideus it was difficult to create a volume sample with the three dimensional modality for the muscle alone without using extensive scalpel facility to take out extraneous muscle from the sample. This made it unproductive to use the three dimensional modality for this muscle.

Joint space: The shoulder joint capsule was able to be detected in long axis with the Diasus scanner. That was due to the high resolution of the scanner which enabled the imaging of small structures with significant accuracy. The shoulder joint capsule was imaged as a thin hyperechoic line lying over the head of the humerus that defined the longitudinal anechoic joint space (Fig. 4.20.).

Due to the narrow acoustic window offered at this joint by the overhang of the acromial process and the proximal extent of the greater tubercle laterally and the layers of muscle medially it proved to be difficult to obtain any size of image with the extended field of view and three dimensional modalities.

4.2.2. Stifle joint:

M. quadriceps femoris: The insertion of the m. quadriceps femoris onto the patella was imaged in long axis with Corevision. The mm. vastus medialis, vastus lateralis and rectus femoris, which form three of its components, were visualised as hypoechoic structures by the use of a stand-off pad, because they lay very superficially. Their merging towards the patella and thus the patellar ligament produced a hyperechoic image.

Mm. vastus medialis, vastus lateralis and rectus femoris were visualised both in long and short axis with Diasus as moderately hypoechoic structures, which then turned to more hyperechoic ones, merging onto the patellar ligament (Fig. 4.21., 4.22.). The almost round anechoic bursa lying underneath the m. quadriceps femoris was successfully detected (Fig. 4.23.).

This muscle was not imaged in its entity with extended field of view Elegra System, since it would not be possible to image all the components of the muscle from their origin to their insertion with a single sweep of the transducer.

Patellar ligament: The patellar ligament was successfully visualised as a moderately hyperechoic structure, due to the presence of the parallel longitudinal echogenic collagen fibres. Its shape was linear when imaged in long axis with Corevision. The structure looked more hypoechoic when imaged in short axis and was oval shaped. A stand-off pad enabled the imaging of the origin of the patellar ligament in the patella (being in fact the tendon of insertion of the m. quadriceps femoris) and its insertion onto the tibial tuberosity.

The patellar ligament appeared as a moderately hyperechoic structure both in long and short axis with Diasus. Hyperechoic dots corresponding to the collagen fibres were more distinct and accurately presented on the screen. It was clearly distinguished from the overlying skin, as well as the infrapatellar fat (Fig. 4.24.).

The patellar ligament was successfully visualised in long axis with the extended field of view Elegra system, as a moderately hyperechoic structure originating from the patella (being the continuation of the tendon of the m. quadriceps femoris) and inserting onto the tibial tuberosity (Fig. 4.25).

The patellar ligament was successfully visualised in three dimensional images. The whole structure was able to be rotated together with the structures lying beneath (infrapatellar fat and cruciate ligaments) and be presented on screen in all the three planes (Fig. 4.26., 4.27., 4.28., 4.29., 4.30.).

Infrapatellar fat: The infrapatellar fat was imaged as a hyper reflective structure both in long and short axis with Corevision. Its margins were poorly defined in the far field.

The same structure was more precisely defined as a hyperechoic structure lying deep to the patellar ligament both in long and short axis with the Diasus scanner. The hyperechoic dots representing fatty tissue were more distinct.
This particular structure was visualised in long axis with extended field of view Elegra System, while imaging the patellar ligament. It looked moderately hyperechoic as described with the previous machine (Fig. 4.25.).

M. extensor digitorum longus: The tendon of origin of the muscle was imaged with Corevision. It could be visualised in short axis views. Long axis views were not consistent, because of its superficial position at the extensor groove. They could only be obtained with the use of a stand-off pad. The tendon of origin was imaged as a hyperechoic structure iying within a hyper reflective surface, corresponding to the extensor groove.

The tendon of origin of the muscle was optimally imaged with Diasus. The tendon was able to be followed through its long axis as a moderately hyperechoic linear structure. Its best point for imaging was between the lateral epicondyle of the femur and the extensor groove of the tibia (Fig. 4.31.). The synovial pouch of the meniscotibial portion of the stifle joint capsule (the so called capsular synovial bursa or, in some texts, the synovial sheath, as it curves around the tendon) that corresponds to the tendon was detected when the structure was imaged in long axis (Fig. 4.32.).

The tendon of origin of the muscle was not imaged with extended field of view Elegra system. This occured because of its relatively small size.

Cruciate ligaments: These structures were not clearly imaged using Corevision, but with Diasus they were apparent when the joint contents were imaged in long axis with the transducer placed over the patellar ligament or slightly lateral to it with the joint in strong flexion. Deep to the patellar ligament lay the infrapatellar fat, which became more hyperechoic as it lay deep within the joint. Deep to it the cruciate ligaments were seen as hypoechoic bands running across the long axis of the joint. The cranial cruciate ligament was more readily imaged as it originated from cranial on the tibiai plate and it could be followed as it ran towards the intercondylar space of the femur. The caudal cruciate ligament was only partially imaged as it crossed over the cranial ligament in the mid joint space but its attachments on the tibial plate and femur were not imaged. With Diasus the ligament appeared to be hypoechoic but with a linear fibre pattern (Fig. 4.33.).

With extended field of view imaging it was possible to image the entire joint space in long axis so that interpretation of topography was made easier with the other units.

In this case the cruciate ligaments were imaged in the same scan plane as they crossed in mid joint appearing as hypoechoic linear areas iying deep to the hyperechoic fat pad (Fig. 4.34.).

With three dimensional imaging a wedge shaped volume sample was created and the cruciate ligaments were visualised deep within the reconstructed sample and thus could be serially sliced and rotated to observe their form in three planes (Fig. 4.26., 4.27., 4.28., 4.29., 4.30.).

<u>Collateral ligaments</u>: An attempt was made to image the medial and lateral collateral ligaments with Corevision in long axis. Their imaging was not consistent, because of their close proximity to the underlying bones and their narrow width. They were more successfully imaged with the use of a stand-off pad as homogeneous hypoechoic bands.

The medial and lateral collateral ligaments were more accurately imaged in long axis with the Diasus scanner. They were presented as moderately hypoechoic structures lying between the skin and the bony components of the stifle joint. The medial collateral ligament fused with the medial meniscus and the joint capsule (Fig. 4.35.). The lateral collateral ligament was imaged passing over the tendon of origin of the m. popliteus, as it crossed the joint cavity (Fig. 4.36.). Their origin from the medial and lateral epicondyle of the femur and their insertion to the medial tibial condyle and the fibula respectively was observed.

These structures were not able to be imaged with extended field of view with the Elegra scanner, because of their small size.

<u>Menisci</u>: The menisci were able to be imaged with Corevision in long axis. The imaging of both medial and lateral menisci was facilitated by the use of a stand-off pad. They were both imaged as homogeneous, hyperechoic and triangular shaped

structures lying between the femur and the tibia. They were not able to be imaged in their entity, because of the extremely narrow acoustic window provided within the joint space.

A more accurate presentation of menisci was obtained with Diasus scanning system in long axis. Their margins were defined more precisely. More hyperechoic dots appeared from their parenchyma (Fig. 4.35.).

Extended field of view Elegra System only images in extended sweeps of a transducer. Menisci were too small structures to offer a target for this type of imaging.

4.2.3. Tarsal Joint:

Common calcaneal tendon: The common calcanean tendon has contributions from several muscle groups, including the m. gastrocnemius, which is located on the caudal aspect of the stifle and tibia and the mm. biceps femoris, semitendinosus and gracilis, which arise from further proximally in the limb. These fuse to form the main two components of the tendon before inserting onto the proximal aspect of the calcaneus where the common calcaneal tendon terminates. The tendon of the m. flexor digitorum superficialis is located caudally and passes over the caudal aspect of the calcaneus immediately below the skin surface before continuing distally into the pes.

The common calcaneal tendon was imaged both in long and short axis with Corevision. All the tarsal muscles forming the tendon were visualised as successive layers of hypoechoic linear structures. The perimysia and epimysia surrounding them were represented as smooth hyperechoic lines. The three layers of the common calcanean tendon, the most superficial of it corresponding to the m. flexor digitorum superficialis, the deeper one to the m. gastrocnemius and the deepest to the mm. semitendinosus, gracilis and biceps femoris, were all visualised in long axis as linear hyperechoic structures. When imaged in short axis, they were presented as oval structures.

When imaging with Diasus proximal the caudal aspect of the calcaneus appeared as a smooth, slightly convex, hyperechoic line with distal acoustic shadowing when imaged in long axis (Fig. 4.37.). The tendon of the m. flexor digitorum superficialis could be visualised as a hyperechoic band running across the calcaneus between it and the skin surface as it continued distally. The component of the common calcanean tendon arising from the medial head of the m. gastrocnemius could be visualised immediately deep to the tendon of the m. flexor digitorum superficialis as a narrow, hyperechoic band with a prominent linear, fibrous pattern. It could be followed to the caudal proximal aspect of the calcaneus where it inserted and was separated from the tendon of the m. flexor digitorum superficialis at this point by a bursa. The section of the common calcanean tendon formed from the remaining components was visualised deep to this and could be followed distally towards the calcaneus but it inserted onto the medial aspect of the proximal calcaneus and so the angle of the transducer had to be altered in order to visualise its point of insertion. There was a second bursa between these two components of the common calcanean tendon. The tendon was imaged both in long and short axis (Fig. 4.38., 4.39., 4.40., 4.41.).

The common calcaneal tendon was imaged in long axis with an extended field of view system and the entire structure from the musculotendinous junction to the insertion on the tuber calcanei could be seen on the one screen. The three hyperechoic layers were present on the screen, but the small bursa lying deep to the tendon could not be visualised on the panoramic view, but when individual frames were called up for the distal insertion the bursa was evident as an anechoic space deep to the tendon.

Acquiring a three dimensional volume for the tendon was possible but difficult due to the narrow width of the structure and the tendency of the transducer to slide off the linear axis and as the detail proved by Diasus was so effective, the three dimensional modality did not further contibute to examination for detail.

4.3. Measurements:

The results of the five measurements taken for each anatomical structure of the three joints under investigation were tabulated and processed with basic statistical methods. Advanced methods did not take place, because of the small number of measurements, which constituted a handicap for their high degree or reliability. The average, the median and the standard deviation (mentioned in the tables as St. Dev.) as well as the 90% and 95% margins of error (mentioned in the tables as 90% ME and 95% ME respectively) of the five individual measurements were calculated. The average refers to the sum of values divided by the number of values. The median refers to the middle value; half the values are smaller and half are larger. The standard deviation indicates how closely a set of observations cluster round their mean. The margin of error for the estimate mean (that is, the average of the current measurements) can be computed for any confidence coefficient. it helps the researcher to conclude that the average has a certain value and he is 90% or 95% confident (because these are the most frequently calculated confidence coeficients) that this average is within the limit calculated and, therefore, there is a probability of 10% or 5% that a certain value is outwith those limits (Table 4.1., 4.2., 4.3., 4.4., 4.5., 4.6., 4.7., 4.8., 4.9., 4.10., 4.11).

	Measurements (mm) of the m. supraspinatus at the level of the middle of the spine of the scapula (short axis view)		Measurements (mm) of the m. supraspinatus at the level of the musculotendinous junction (short axis view)			
Sessions	Corevision	Diasus	Corevision		Diasus	
			Depth	Width	Depth	Width
1	21.5	20.5	12.0	15.8	7.6	14.6
2	21.9	22.9	10.2	18.7	9.7	10.7
3	21.2	19.1	9.2	16.9	10.1	15.5
4	20.1	21.1	9.3	14.0	10.4	20.8
5	21.0	21.6	8.4	13.7	11.1	18.6
Average	21.1	21.0	9.8	15.8	9.8	16.0
Median	21.2	21.1	9.3	15.8	10.1	15.5
St. Dev.	0.673	1.399	1.375	2.078	1.322	3.876
90% ME	0.641	1.333	1.310	1.979	1.259	3.692
95% ME	0.837	1.739	1.709	2.583	1.644	4.819

Table 4.1.

	Measurements (mm) of the m. supraspinatus at the level of the middle of the spine of the scapula (long axis view)
Sessions	Sonoline Elegra
1	20.3
2	20.8
3	20.2
4	20.2
5	20.5
Average	20.4
Median	20.3
St. Dev.	0.255
90% ME	0.243
95% ME	0.317

Table 4.2.

	Measurements (mm) of the m. infraspinatus at the level of the middle of the spine of the scapula (short axis view)		Measurements (mm) of the m. infraspinatus at the level of the musculotendinous junction (short axis view)			
Sessions	Corevision	Diasus	Corevision		Diasus	
			Depth	Width	Depth	Width
1	19.5	20.3	5.7	13.4	3.3	18.5
2	19.3	19.1	5.9	14.2	5.5	15.6
3	20.3	20.3	6.1	14.3	5.1	14.9
4	19.4	22.5	7.1	13.6	5.8	18.1
5	20.5	20.7	5.3	11.4	5.2	14.0
Average	**19.8**	**20.6**	**6.0**	**13.4**	**5.0**	**16.2**
Median	**19.5**	**20.3**	**5.9**	**13.6**	**5.2**	**15.6**
St. Dev.	**0.557**	**1.230**	**0.672**	**1.171**	**0.978**	**1.987**
90% ME	**0.531**	**1.172**	**0.640**	**1.115**	**0.932**	**1.893**
95% ME	**0.692**	**1.529**	**0.835**	**1.456**	**1.216**	**2.470**

Table 4.3.

	Measurements (mm) of the m. infraspinatus at the level of the middle of the spine of the scapula (long axis view)
Sessions	Sonoline Elegra
1	23.2
2	23.3
3	23.2
4	22.8
5	23.0
Average	23.1
Median	23.2
St. Dev.	0.200
90% ME	0.191
95% ME	0.249

Table 4.4.

	Measurements (mm) of the depth of the tendon of origin of the m. biceps brachii at the level of the intertubercular groove (long axis view)		Measurements (mm) of the depth of the tendon of origin of the m. biceps brachii at the curve (long axis view)		Measurements (mm) of the tendon of origin of the m. biceps brachii at the level of the intertubercular groove (short axis view)			
Sessions	Corevision	Diasus	Corevision	Diasus	Corevision		Diasus	
					Depth	Width	Depth	Width
1	3.8	4.6	3.1	3.3	5.2	8.4	4.3	7.5
2	4.6	4.0	4.5	3.7	5.7	7.2	3.9	5.0
3	4.2	4.2	4.1	4.7	4.3	6.6	3.3	4.9
4	5.1	5.8	5.2	3.6	4.0	6.9	4.2	5.8
5	5.6	3.8	4.0	3.0	4.1	8.3	5.0	7.7
Average	4.7	4.5	4.2	3.7	4.7	7.5	4.1	6.2
Median	4.6	4.2	4.1	3.6	4.3	7.2	4.2	5.8
St. Dev.	0.713	0.795	0.766	0.643	0.750	0.823	0.619	1.344
90% ME	0.679	0.757	0.730	0.612	0.714	0.784	0.590	1.280
95% ME	0.886	0.988	0.952	0.799	0.932	1.023	0.770	1.671

Table 4.5.

	Measurements (mm) of the m. teres minor at the level of the acromial process (short axis view)			
Sessions	Corevision		Diasus	
	Depth	Width	Depth	Width
1	3.3	16.2	11.4	16.0
2	7.4	9.6	9.4	17.0
3	7.7	14.5	7.5	12.3
4	7.6	15.3	8.9	14.8
5	8.8	12.4	7.2	16.2
Average	7.0	13.6	8.9	15.3
Median	7.6	14.5	8.9	16.0
St. Dev.	2.117	2.641	1.684	1.832
90% ME	2.017	2.516	1.604	1.745
95% ME	2.632	3.283	2.094	2.278

Table 4.6.

	Measurements (mm) of the depth of the patellar ligament distal to the patella (short axis view)		Measurements (mm) of the depth of the patellar ligament proximal to the tibial tuberosity (short axis view)	
Sessions	Corevision	Diasus	Corevision	Diasus
1	3.0	2.6	2.1	1.8
2	2.4	2.3	2.6	2.0
3	3.7	3.0	2.7	2.2
4	2.8	2.7	2.3	2.0
5	3.7	2.6	3.1	2.1
Average	3.1	2.6	2.6	2.0
Median	3.0	2.6	2.6	2.0
St. Dev.	0.572	0.251	0.385	0.148
90% ME	0.545	0.239	0.367	0.141
95% ME	0.711	0.312	0.479	0.184

Table 4.7.

	Measurements (mm) of the depth of the patellar ligament distal to the patella (long axis view)	Measurements (mm) of the depth of the patellar ligament proximal to the tibial tuberosity (long axis view)
Sessions	Sonoline Elegra	Sonoline Elegra
1	2.6	2.2
2	2.5	2.0
3	2.6	2.0
4	2.5	2.2
5	2.4	2.1
Average	2.5	2.1
Median	2.5	2.1
St. Dev.	0.084	0.100
90% ME	0.080	0.095
95% ME	0.104	0.124

Table 4.8.

	Measurements (mm) of the tendon of origin of the m. extensor digitorum longus at the level of the extensor groove (short axis view)			
Sessions	Corevision		Diasus	
	Depth	Width	Depth	Width
1	4.2	8.8	5.3	3.0
2	5.6	7.1	2.6	6.2
3	5.2	6.2	2.4	6.3
4	5.6	6.5	4.0	6.7
5	3.3	7.3	1.6	4.9
Average	**4.8**	**7.2**	**3.2**	**5.4**
Median	**5.2**	**7.1**	**2.6**	**6.2**
St. Dev.	**1.006**	**1.008**	**1.467**	**1.512**
90% ME	**0.958**	**0.960**	**1.397**	**1.440**
95% ME	**1.251**	**1.253**	**1.824**	**1.880**

Table 4.9.

	Measurements (mm) of the depth of the common calcaneal tendon at the level of the bifurcation of the saphenous vein (short axis view)						Measurements (mm) of the depth of the common calcaneal tendon at the level of insertion to the calcaneal tuberosity (short axis view)					
Sessions	Corevision			Diasus			Corevision			Diasus		
	1st layer	2nd layer	3rd layer	1st layer	2nd layer	3rd layer	1st layer	2nd layer	3rd layer	1st layer	2nd layer	3rd layer
1	3.7	5.3	2.3	2.4	2.4	1.2	1.9	2.5	2.0	2.4	1.5	1.0
2	3.5	2.1	5.3	2.1	4.6	1.5	2.0	2.5	8.1	2.6	1.7	1.7
3	2.6	4.5	1.9	0.9	1.8	1.9	2.4	2.7	8.2	1.6	1.6	1.5
4	2.2	2.3	1.6	2.1	1.2	4.5	3.0	2.0	7.4	2.1	1.2	1.5
5	3.4	2.4	1.5	2.6	2.8	1.9	2.8	2.0	8.2	1.7	2.4	6.8
Average	3.1	3.3	2.5	2.0	2.6	2.2	2.4	2.3	6.8	2.1	1.7	2.5
Median	3.4	2.4	1.9	2.1	2.4	1.9	2.4	2.5	8.1	2.1	1.6	1.5
St. Dev.	0.646	1.474	1.585	0.661	1.292	1.319	0.482	0.321	2.693	0.432	0.444	2.418
90% ME	0.615	1.404	1.510	0.630	1.231	1.256	0.459	0.306	2.565	0.412	0.423	2.303
95% ME	0.803	1.833	1.971	0.822	1.606	1.640	0.599	0.399	3.348	0.537	0.552	3.006

Table 4.10.

	Measurements (mm) of the depth of the common calcaneal tendon at the level of the musculotendinous junction (long axis view)
Sessions	Sonoline Elegra
1	6.3
2	6.2
3	6.3
4	6.2
5	6.3
Average	6.3
Median	6.3
St. Dev.	0.055
90% ME	0.052
95% ME	0.068

Table 4.11.

From the observation of the statistical results for each of the measurements that were held the following conclusions can be made:

The comparison between the average and the median can offer an indication about the shape of the distribution of the observations. If there are outlying observations only in one direction the distribution is said to be a skewed distribution. If these are small, the distribution is skewed to the left and, then, the average is smaller than the median. On the contrary, if the outstanding values are large, the distribution is considered to be skewed to the right and the average is larger than the median. A symmetric distribution is one in which the distribution has the same shape on both sides of the mean.

Most of the results in the current study, concerning Corevision and Diasus scanners, were either skewed to the right or skewed to the left, which indicates the presence of outstanding values among the 5 measurements. Consequently, consistency in measurements is excluded in those cases. Symmetrical distribution was observed and the values were equally distributed. As a result, the comparison between the average and the median cannot be of great value to this particular study.

The observation of the values of the standard deviation and the margins of error for each of them in correlation to the average suggests a significant difference between the potentials of the transducers and the software facilities of the three scanners used in this study. The scanning technique proved to be able to influence the statistical results and, thus, the accuracy of measurements.

The results obtained by Corevision suggest a scattered distribution of the values, which has contributed to large numbers of the numerical summaries mentioned above. With the possible exception of the measurements concerning the patellar ligament, it is proved that conventional ultrasonography cannot provide the clinician ligament, it is proved that conventional ultrasonography cannot provide the clinician with the ability of performing consistent measurements for the specific anatomical structures. This may be attributed to the difficulty in orientating the angle of the transducer and detecting exactly the same one repeatedly in all sessions. Moreover, the poor resolution results in the lack of definition of the margins of each anatomical structure, which is extremely important in the case of small or physically slight structures. This also happens because of image pixelation errors that take place when measuring structures on screen.

The transducer used when scanning with Diasus has smaller active length, which makes it less cumbersome and easier to handle by the operator, and higher resolution, because of the higher frequency. The results obtained, though, prove that the aforementioned advantages over Corevision are not sufficient in order to acquire consistency in repeated measurements. The angling of the transducer cannot be alike in all individual sessions, which inhibits the display of the various anatomical structures in the same way each time. Furthermore, the large number of bony prominences, in combination with the narrow acoustic windows of the joints under investigation, constitute obstacles that cannot be totally overcome even when a high resolution transducer is used.

When the results obtained with the Elegra transducer when the extended field of view capability was applied are observed, the difference in consistency is evident. The values of standard deviation and of the margins of error are very small, which indicates a small distribution of the values around the average and, thus, a potential for consistency on individual sessions. It is proved that when anatomical landmarks are spotted with the extended field of view modality, and had the potential of calling up that particular single original image frame, consistency can be obtained since they can be found on repetitive sessions.

4.4. Clinical cases

4.4.1. Case 1

Subject: Border Collie, 4 years old, entire female. Weight 19 kg.

History and clinical signs:

The dog sustained bilateral fractures of unknown origin of the radius and ulna 11 days prior to the ultrasound examination. Furthermore, there was a swollen left shoulder with crepitus elicited medially on palpation.

Radiography:

The thoracic radiographs that were performed gave indication of mild pneumomediastinum.

When the radius and ulna were radiographed, a left comminuted radial fracture in the distal third with minimal overriding and displacement was observed. In addition, a right oblique ulnar fracture and a comminuted radial fracture in the middle of the diaphysis had taken place. Soft tissue swelling was present in both legs.

As far as the left shoulder joint was concerned, a mild subluxation was detected, but it was thought that it could have been positional (Fig. 4.42.). A separate bone fragment on the medial aspect of the glenoid tubercle could be seen (Fig. 4.43.).

Postoperative radiographs revealed the presence of a Dynamic Compression Plate on the cranial aspect of the left radius which was placed there after ulnar osteotomy. A Dynamic Compression Plate was also put on the cranial aspect of the right radius. Excellent alignment had taken place on both.

Radiological diagnosis: Fracture of the radius and ulna.

Differential or additional diagnoses: Shoulder subluxation and chip fracture.

Ultrasonography:

Right limb: The tendon of origin of the m. biceps brachii was imaged in the intertubercular groove with a minimum of fluid in the bursa surrounding it.

Left limb: The tendon of origin of the m. biceps brachii was imaged in the intertubercular groove but the groove was disrupted and round hyperechoic bone fragments, that created acoustic shadowing, were visualised around the lesser tubercle. The bursa of the tendon was distended with anechoic fluid. The moderately hypoechoic transverse ligament was intact, but a hypoechoic area was detected superficial and medial to it, overlying the transverse ligament (Fig. 4.44., 4.45.).

Ultrasonographic diagnosis: Fracture involving the lesser tubercle and the intertubercular groove of the left limb, which could be causing instability of the tendon of origin of the m. biceps brachii.

Further examination and treatment:

The dog was operated on and an 8 hole Dynamic Compression Plate was placed in the right fracture (3.5 mm), as well as a 7 hole Dynamic Compression Plate in the left fracture after ulnar osteotomy (3.5 mm). The dog was treated with carprofen and cephalexin for two weeks after the operation and was kept in the Glasgow University Small Animal Hospital for postoperative care for three weeks. As far as the dog's left shoulder was concerned, no special treatment was performed, but both its forelegs were dressed for one week and the left one continued to be dressed using a gutter splint for a month.

The dog was admitted to the Small Animal Hospital three weeks later, since it was still lame on the left forelimb. The left shoulder was painful in flexion and extension, as well as on palpation.

Radiography:

A mineralised fragment was detected 0.5 to 1 cm medial to the lesser trochanter of the left shoulder. It was clearly seen on skyline view with a corresponding lucent zone in the region of the lesser trochanter. A rim of sclerosis was also detected medial to this. The edges of the fragment were not sharply defined, confirming that it was not a recent fracture.

Postoperative radiographs showed that a lag screw was placed from medial to lateral in the lesser trochanter. Moreover, a screw and a washer were placed from medial to lateral in the proximal third of the humeral diaphysis for relocation of the tendon of the m. biceps brachii. Gas was detected in subcutaneous tissues.

Radiological diagnosis: Fracture of the lesser tubercle of the left shoulder.
Differential or additional diagnoses: Not recent fracture. Reduction and fixation with lag screw. Relocation of the tendon of the m. biceps brachii.

Ultrasonography:

The left shoulder of the dog was scanned. The m. supraspinatus was imaged proximal to the shoulder joint. Hyperechoic bone fragments that caused acoustic shadowing were detected at the level of the joint space. The tendon of origin of the m. biceps brachii was imaged in the intertubercular groove and was intact and of normal echogenicity, but its attachment on the supraglenoid tubercle was hyperechoic. The bursa of the tendon of origin of the m. biceps brachii was distended with anechoic fluid. When imaging towards the lesser tubercle, hyperechoic bone fragments that caused acoustic shadowing, as well as an anechoic interval, representing the interrupted contour of the hyperechoic and highly reflective intertubercular groove surface on the medial aspect, were observed (Fig. 4.46.).

Ultrasonographic diagnosis: Fracture involving the lesser tubercle and the intertubercular groove of the left limb, which could be causing instability of the tendon of origin of the m. biceps brachii.

Arthroscopy:

Arthroscopy of the left shoulder was indicative of an angled and possibly torn appearance of the medial glenohumeral ligament.

Arthrotomy:

A fracture of the lesser tubercle was observed. It was reattached to its normal position with a 3.5 mm long screw and washer. The tendon was ruptured and was adhered to the intertubercular groove. A tenodesis was performed with a 3.5 mm long screw.

Further treatment:

The dog was kept under restricted exercise for a week in the Small Animal Hospital and was treated with carprofen for 6 weeks and a combination of amoxycillin and clavulanic acid for 10 days. It was then dismissed with directions for limited exercise to the owner. A re-examination was suggested in 6-8 weeks. The case is still ongoing.

4.4.2. Case 2

Subject: Weimaraner, 5 years old, neutered male. Weight 35 kg.

History and clinical signs:

The dog slipped while running 3 weeks before referral. It became lame and was radiographed by the referring vet, who suggested a detached tendon of origin of the m. biceps brachii and was treated with carprofen and rest. The clinical examination which was held at the Glasgow University Veterinary Hospital revealed lameness on the right forelimb, some muscle wasting over the right shoulder and pain on shoulder extension and flexion.

Radiography:

On both elbow radiographs no specific abnormality was detected.

On shoulder radiographs the right supraglenoid tubercle was irregular and mottled. Patches of new bone in the right intertubercular groove were imaged (Fig. 4.47.). A smooth osteophyte was detected on the medial humeral head on the right (Fig. 4.48.).

An arthrogram was also performed showing a narrowed contrast column through the right medial bursa of the tendon of origin of the m. biceps brachii. Contrast agent was present medial and lateral to the distal scapula and acromion, whereas irregular filling defects were presented throughout (Fig. 4.49.).

Radiological diagnosis: Bicipital bursitis

Ultrasonography:

The tendon of origin of the right m. biceps brachii was found to be thickened and hypoechoic compared to the left one. The synovial bursa was thickened and hyperechoic and was filled with echogenic material. The joint capsule was thickened as well (Fig. 4.50.).

The tendon of origin of the left m. biceps brachii was imaged more clearly. Some bright echoes were observed in the tendon. The bursa was clear (Fig. 4.51.).

Ultrasonographic diagnosis: Tenosynovitis on the right side.

Fluid analysis:

No bacterial presence was detected.

Further examination and treatment:

The dog was discharged and the owners were advised to treat the dog with carprofen, a combination of amoxycillin and clavulanic acid and keep it under restricted exercise.

Since no improvement took place, the dog was admitted one week later for arthroscopy.

Arthroscopy:

The examination showed severe synovitis, as well as a partial detachment from the supraglenoid tubercle of the tendon of origin of the m. biceps brachii. The tendon appeared abnormally thinned.

Further examination and treatment:

The joint was thoroughly flushed with approximately 1 litre of fluids and the dog was discharged on carprofen and Cosequin ® (feed additive), as well as restricted exercise.

The dog was rechecked in three weeks' time and it was found to have improved significantly. The owners were advised to build up lead exercise over the following four weeks and to continue administering Cosequin ® (feed additive).

However deterioration occured three weeks later, sufficient to indicate the necessity for an arthrotomy.

Arthrotomy:

Tenodesis and transposition of the tendon of origin of the m. biceps brachii took place. The wound was covered and two post-operative radiographs were taken to confirm the positioning of screws.

Further examination and treatment:

The dog was using the leg well post-operatively and so was discharged the following day. The owners were asked to restrict it to short lead walks and give him cephalexin and carprofen. The sutures were removed after a couple of weeks and on a further examination that took place a week later its condition was significantly improved.

Outcome:

Subsequently the dog made an uneventful recovery.

4.4.3. Case 3

Subject: Greyhound, approximately 8 years old, neutered male. Weight 32.5 kg.

History and clinical signs:

An haematology and biochemistry test done in September showed that the dog was neutropenic and had mild hypocalcaemia. A month after this examination the dog was found to be neutropenic and leukopenic and it was decided that it could not be used as a blood donor any more. 30 days later it presented as lame on its left fore and it exhibited pain in its shoulder at the region of the deltoid rim. There was also a graze on the medial aspect of the right metacarpus. It was decided to treat the dog with meloxicam (Metacam ®) until further diagnostic procedures took place.

Radiography:

There was a reduction in opacity of the left proximal humerus with a mottled appearance and multiple punctate lucencies were observed. The caudal bone cortex had a thinning and ragged appearance and in the associated area. There existed irregular new bone formation. There was a separate region of irregular mineralisation of approximately 1.5 cm in length located in the soft tissue adjacent to the greater tubercle (Fig. 4.52.).

Radiographic diagnosis: Bone tumour. Primary osteosarcoma most likely.

Ultrasonography:

A hyperechoic lesion was detected at the level of the musculotendinous junction of the m. infraspinatus. The head of the humerus had an irregular and mottled appearance, whereas the cortex of tihe humerus deep to m. deltoideus was raised and roughened as well (Fig. 4.53., 4.54., 4.55.). The bursa of the tendon of origin of the m. biceps brachii was dilated and filled with moderately hyperechoic material (Fig. 4.56.). Calcified lesions were detected near the tendon of origin of the m. biceps brachii in the intertubercular groove.

Ultrasonographic diagnosis: Bone tumour.

Further examination and treatment:

It was decided that the dog should not go under further treatment and, so as not to suffer any more pain, was euthanased. A post mortem examination was performed.

Post mortem examination:

A soft mass of 1.5 inches long by 1 inch wide was present attached to the caudal aspect of the cranial metaphysis of the humerus, medial to the intertubercular groove. The periosteum was seen to be lifted off by the mass. Haemorrhage extended for about 0.5 inch into the bone marrow (Fig. 4.57.).

4.4.4. Case 4

Subject: Rottweiler, 2.5 years old, entire male. Weight 51 Kg.

History and clinical signs:

The dog presented lame on both its front legs, the right one being worse. Medication with meloxicam (Metacam ®) and carprofen did not help the dog. The left shoulder was painful on extension, whereas the dog showed mild discomfort on right elbow flexion.

Radiography:

Radiographs showed mild osteoarthritis of both elbows. Moreover, a cluster of small, well defined mineralised opacities was observed forming a line overlying the cranial aspect of the greater tubercle of the humerus (Fig. 4.58.).

Arthrography:

Arthrography confirmed that these were outwith the normal appearing bursa of the tendon of origin of the m. biceps brachii.

Radiographic diagnosis: Soft tissue mineralisation possibly of the m. supraspinatus.

Ultrasonography:

Both limbs were scanned.

Hypoechoic areas in the m. supraspinatus at the level of the musculotendinous junction were found at the right forelimb. Hyperechoic areas in the m. biceps brachii and around its tendon were observed in the intertubercular groove, which were suggestive of calcification. The m. infraspinatus was clear. The m. deltoideus was scanned as well and some roughening of the humeral cortex was detected deep to the muscle.

In the left forelimb, hyperechoic areas at the musculotendinous junction of the m. supraspinatus were found, as well as in the m. biceps brachii and around its tendon in the intertubercular groove (Fig. 4.59.). The mm. deltoideus and infraspinatus were clear.

Ultrasonographic diagnosis: Calcification within the muscle and around the musculotendinous junction.

Further examination and treatment:

Conservative management was suggested and the dog was discharged. Re-examination was suggested after a month. The dog returned to the Glasgow University Veterinary Hospital with a report of improvement at the beginning of the month, but deterioration by the end of the month. There was definite pain on flexion of the right elbow, but there was no swelling or shoulder pain. The same treatment was decided to be continued and, if no improvement occured, to perform other diagnostic tests.

The dog came back after two weeks and scintigraphy, computed tomography, electromyelography and arthroscopy were performed. These tests revealed a degree of elbow osteoarthritis, but it proved to be not significant enough to cause the extent of lameness the dog showed.

Outcome:

The dog went back home under the same medication and was advised to come back in 4 weeks time. The case is still ongoing.

4.4.5. Case 5

Subject: Labrador, 10 years old, neutered female. Weight 32 kg.

History and Clinical signs:

The dog had a long history of developing lameness over the last six months before presentation. During that period the dog became definitively lame on its left fore.

During the clinical examination, pain irritability and local increased temperature was observed during palpation. A reluctance to flex and extend the shoulder joint was evident.

Laboratory tests:

No specific abnormality was detected on the blood tests performed.

Radiography:

Both shoulder joints appear radiographically unremarkable (Fig. 4.61.).

Radiographic diagnosis: None

Ultrasonography:

The m. infraspinatus of the left forelimb looked more hyperechoic than usual and mineralisation in the form of hyperechoic foci was observed (Fig. 4.61.). The tendon of the m. biceps brachii was intact, but the bicipital bursa was dilated and full of anechoic fluid. The m. teres minor was unremarkable.

Ultrasonographic diagnosis: Calcifying tendinopathy

Arthroscopy:

A lot of flocculent fluid was found which rendered the examination inconclusive. The joint was flushed.

Further examination and treatment:

The dog was treated with meloxicam (Metacam ®) for a month and no further manifestation of the problem was reported.

Outcome:

The dog made an uneventful recovery.

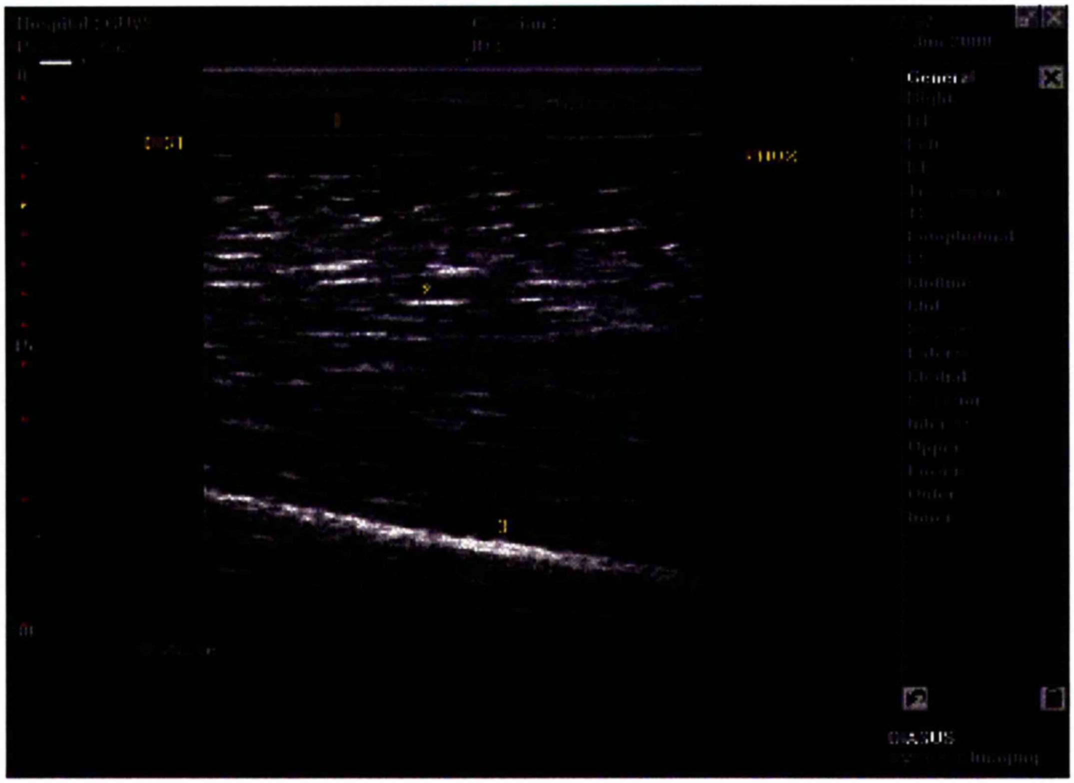

Fig. 4.1. Long axis view of the left thoracic limb of a dog using Diasus with a 16 MHz linear transducer. The middle portion of the m. supraspinatus is displayed running from right to left through the picture.

1) M. omotransversarius

2) M. supraspinatus

3) Scapula

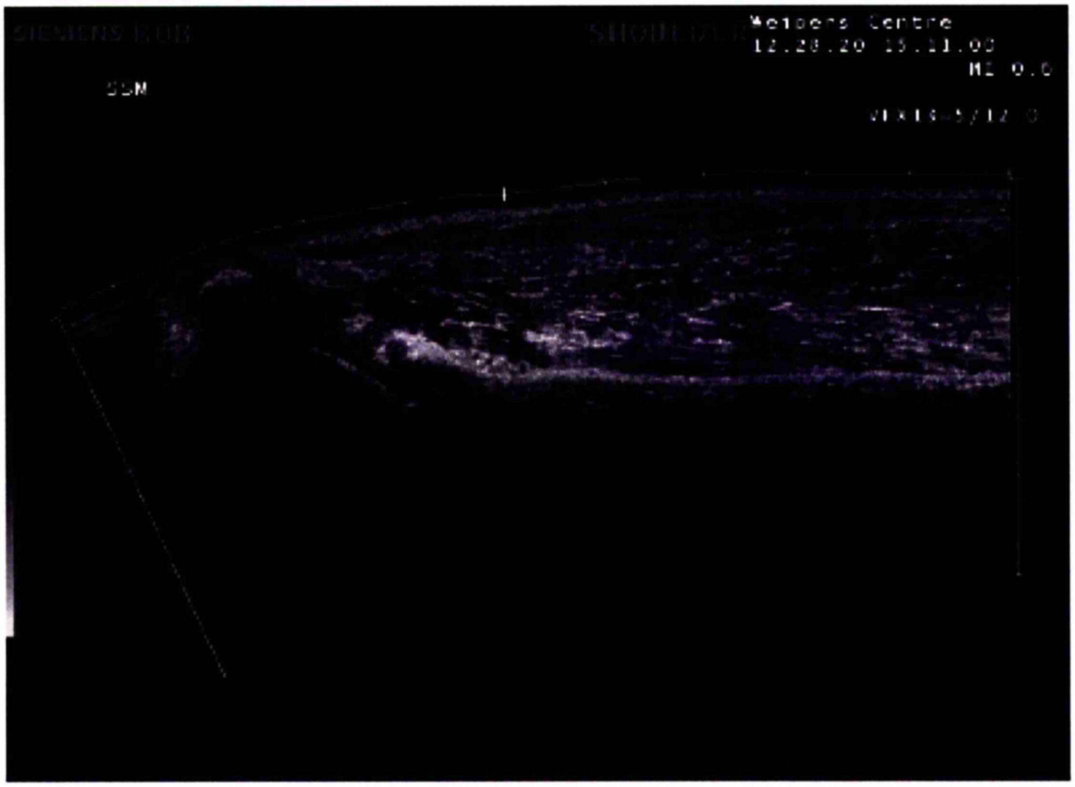

Fig. 4.2. Extended field of view image of the left forelimb of a dog using Elegra with a 12 MHz linear transducer. The distal end of the m. supraspinatus and its tendon of insertion lie from right to left of the picture. The skin with the m. omotransversarius immediately deep to it is imaged at the top of the field, proximal is to the right, distal to the left and the deeper scapula is in the middle depth of the field being imaged as a hyperechoic line with an anechoic area of acoustic shadowing distal to it. The greater tubercle is imaged at 9 o' clock with the moderately echogenic tendon running across the joint space, which is seen as a hyperechoic curved line (humeral head) covered by a layer of non echogenic cartilage.

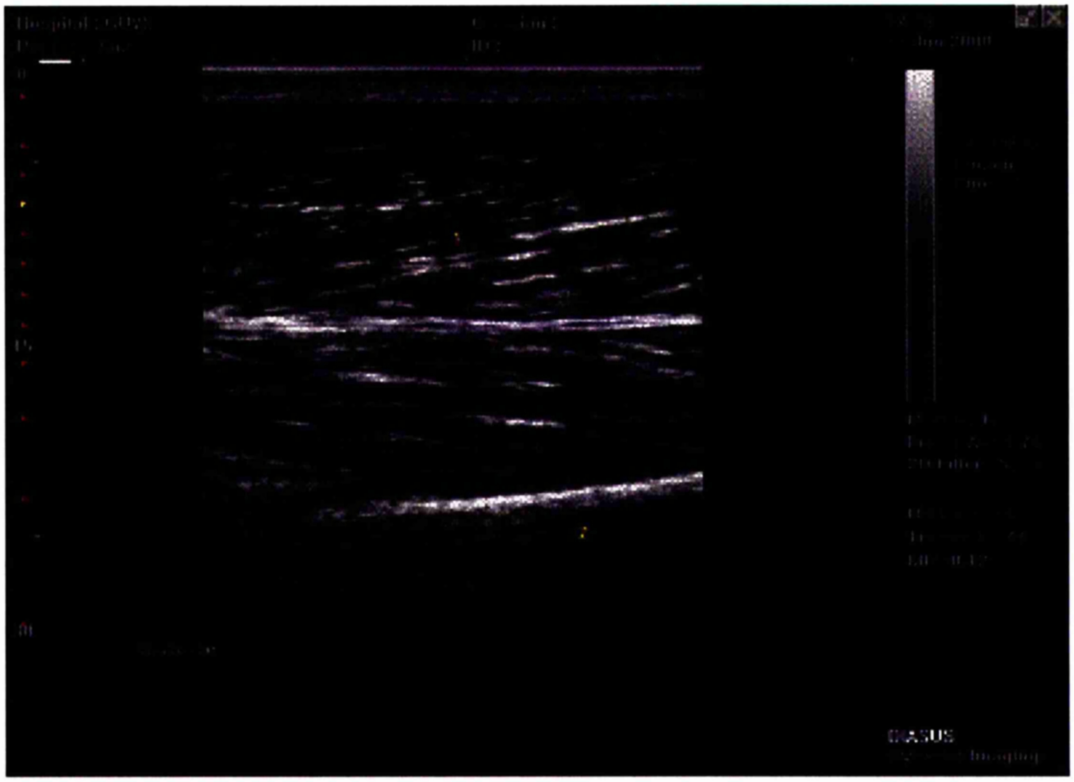

Fig. 4.3. Long axis view of the left thoracic limb of a dog using Diasus with a 16 MHz linear transducer. The middle portion of the m. infraspinatus is displayed running from right to left through the picture.

1) M. infraspinatus

2) Scapula

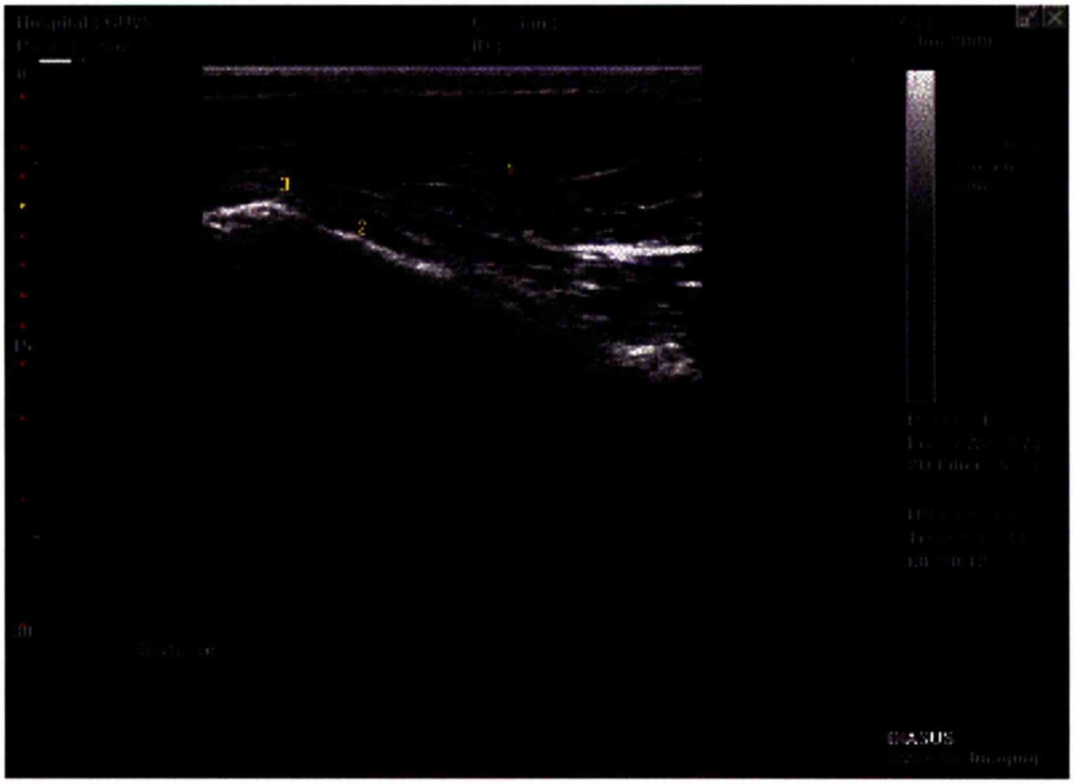

Fig. 4.4. Long axis view of the left thoracic limb of a dog using Diasus with a 16 MHz linear transducer. The distal portion of the m. infraspinatus is displayed running from right to left through the picture. The infraspinous bursa is displayed underneath the hyperechoic tendon of insertion, which is imaged on the left of the screen.

1) M. deltoideus

2) Infraspinous bursa

3) Tendon of insertion of the m. infraspinatus

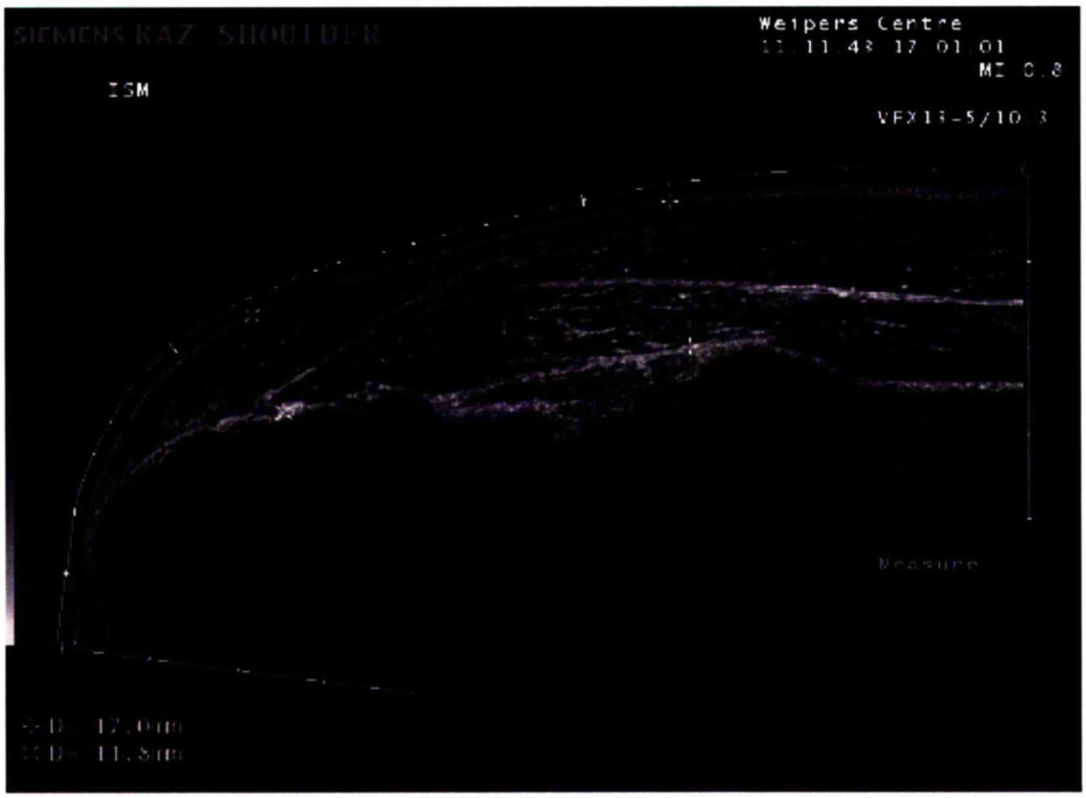

Fig. 4.5. Extended field of view image of the left forelimb of a dog using Elegra with a 12 MHz transducer. The distal end of the m. infraspinatus and its tendon of insertion lie from right to left of the picture. The skin is imaged at the top of the field, proximal is to the right, distal to the left and the deeper scapula is in the middle depth of the field being imaged as a hyperechoic line with an anechoic area of acoustic shadowing distal to it. The greater tubercle is imaged at 9 o' clock with the moderately echogenic tendon running across the joint space, which is seen as a hyperechoic curved line (humeral head) covered by a layer of non echogenic cartilage.

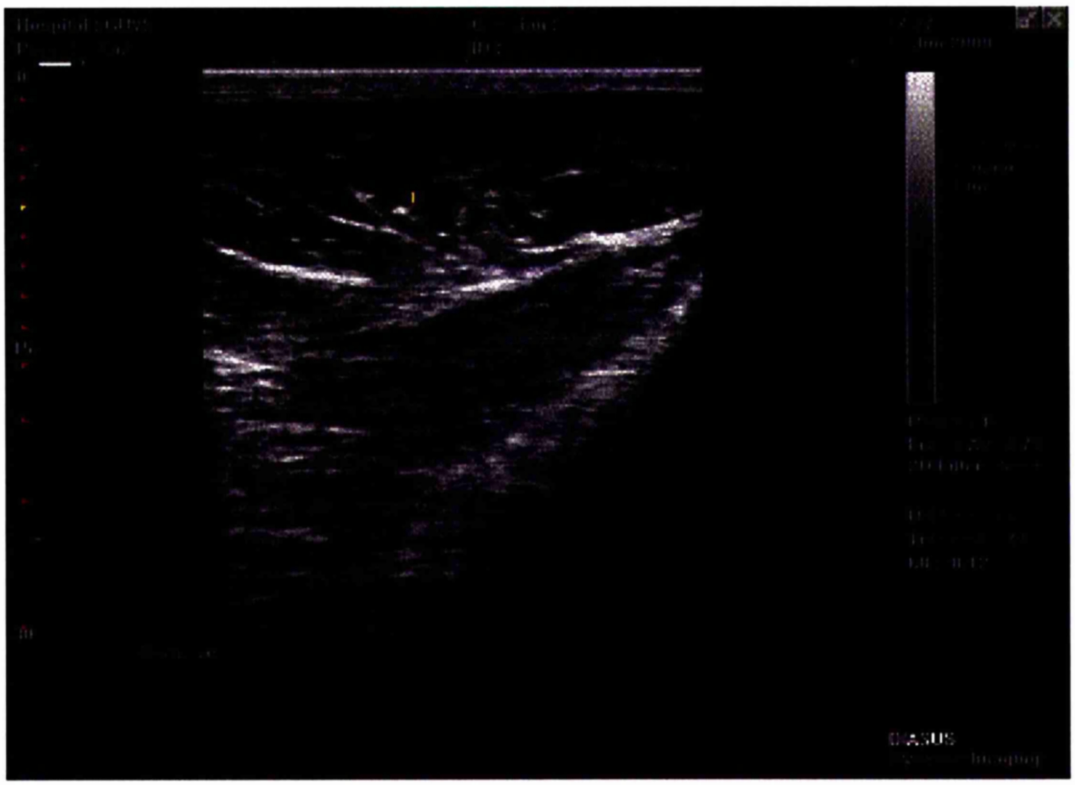

Fig. 4.6. Short axis view of the left thoracic limb of a dog using Diasus with a 16 MHz linear transducer. The portion of the m. deltoideus lying at the level of the acromial process is displayed running from right to left through the picture.

1) M. deltoideus

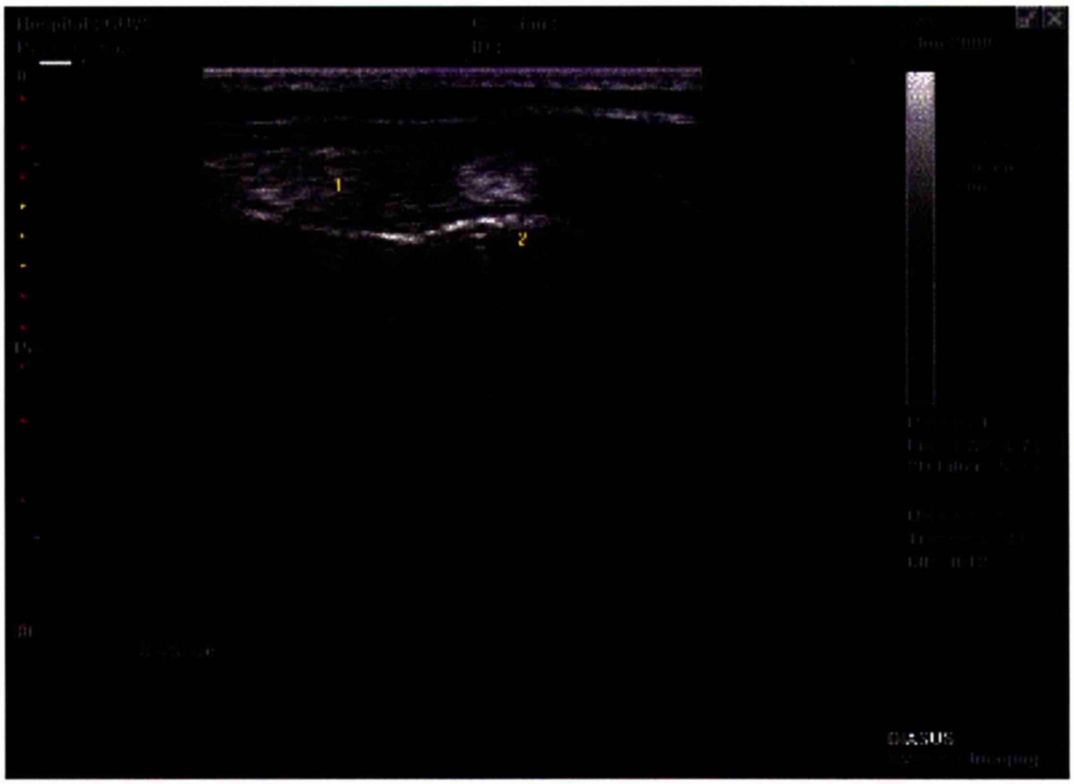

Fig. 4.7. Long axis view of the left thoracic limb of a dog using Diasus with a 16 MHz linear transducer. The hyperechoic tendon of origin of the m. biceps brachii is displayed running from right to left through the picture in the hyper reflective intertubercular groove with an anechoic area of acoustic shadowing distal to it.

1) Tendon of origin of the m. biceps brachii

2) Intertubercular groove

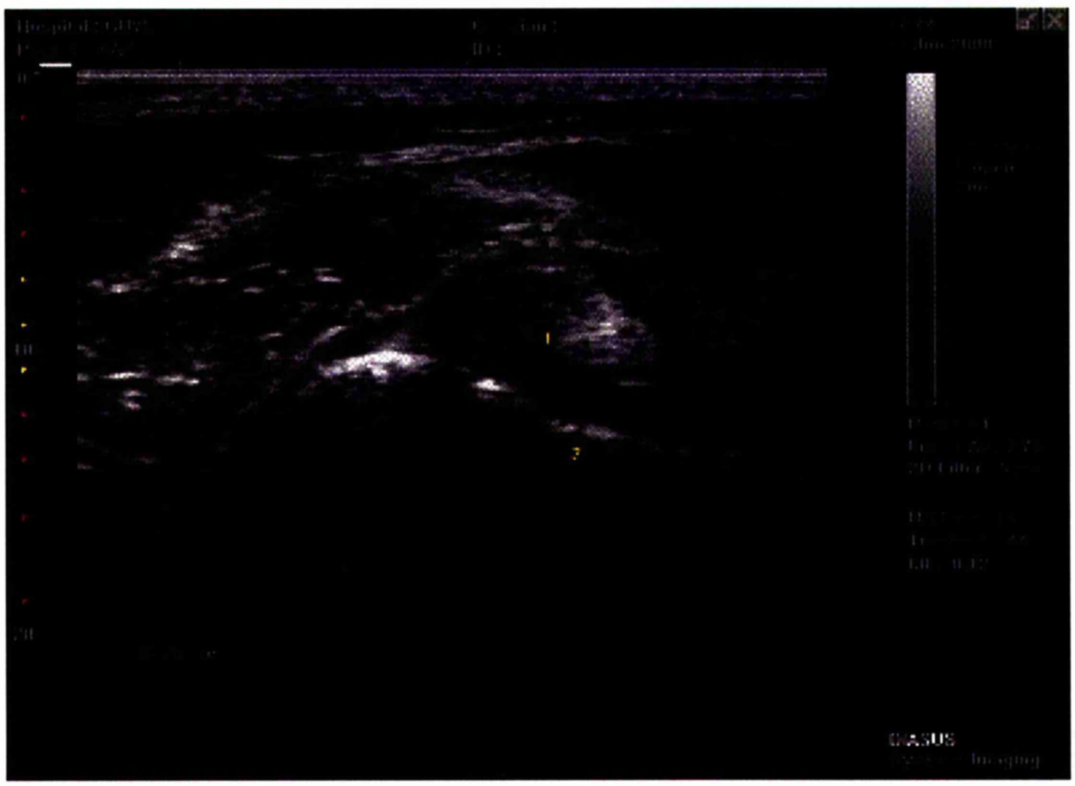

Fig. 4.8. Short axis view of the left thoracic limb of a dog using Diasus with a 16 MHz linear transducer. The round hyperechoic tendon of origin of the m. biceps brachii is displayed to the right of centre of the picture. A small amount of fluid is surrounding the tendon and the hyper reflective intertubercular groove with an anechoic area of acoustic shadowing distal to it lies beneath the tendon.

1) Tendon of origin of the m. biceps brachii

2) Intertubercular groove

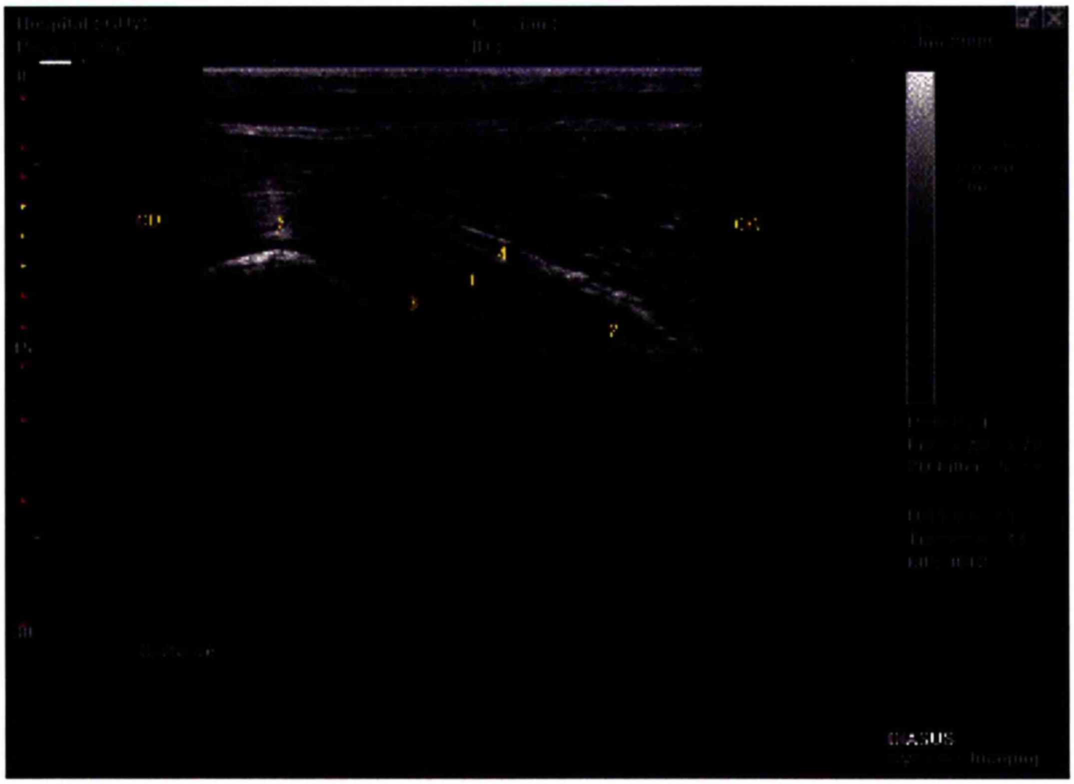

Fig. 4.9. Long axis view of the left thoracic limb of a dog using Diasus with a 16 MHz linear transducer. The hyperechoic tendon of origin of the m. biceps brachii is displayed on the left of the picture and its point of insertion is very clearly marked on the right. The anisotropy artifact is evident. The anechoic bursa of the m. biceps brachii lies around and deep to the tendon in the centre of the image and the hyperechoic transverse ligament is displayed superficial to the tendon.

1) Tendon of origin of the m. biceps brachii

2) Insertion of the tendon of origin of the m. biceps brachii

3) Bursa of the tendon of the m. biceps brachii

4) Transverse ligament

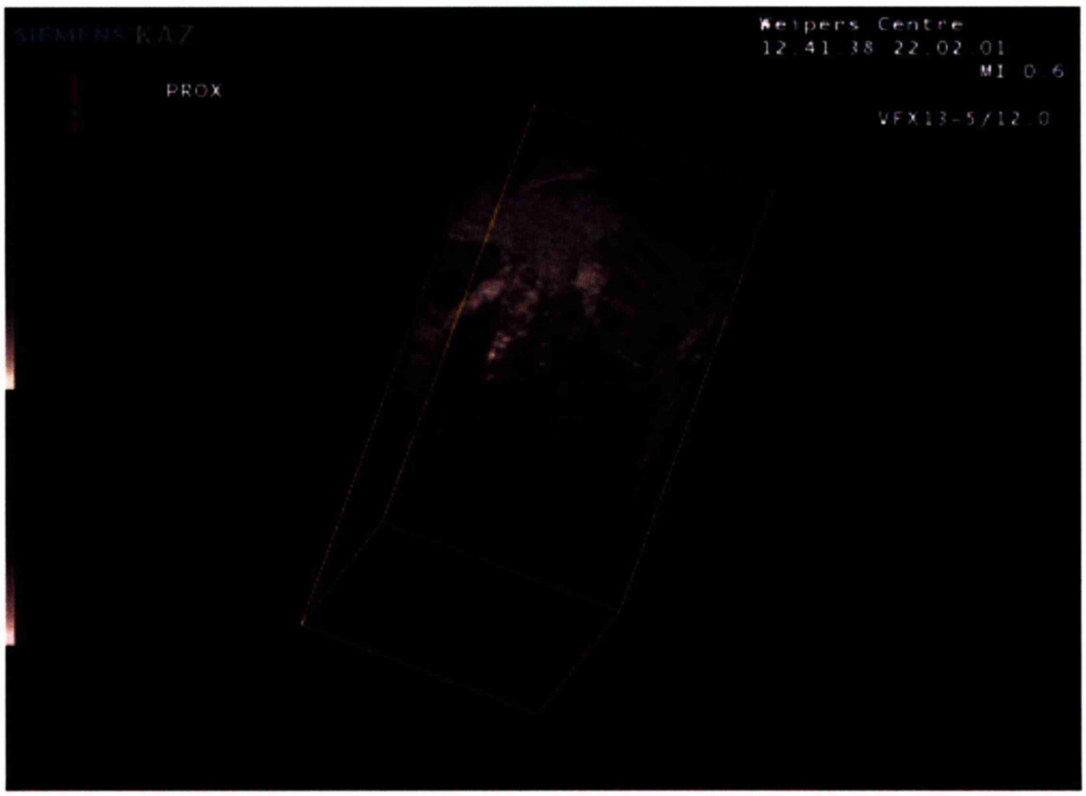

Fig. 4.10. Reconstructed three dimensional volume sample of the m. biceps brachii and its tendon of origin as they lie on the proximal humerus of the left leg of a dog using Elegra with a 12 MHz linear transducer. The sample is rotated on an equatorial axis so that the viewed surface of the cube is the proximal face, to the right is medial and to the left is lateral. On this face the skin and subcutaneous tissues lie at the top of the field with the m. biceps brachii in mid field and the humeral surface in the deep field.

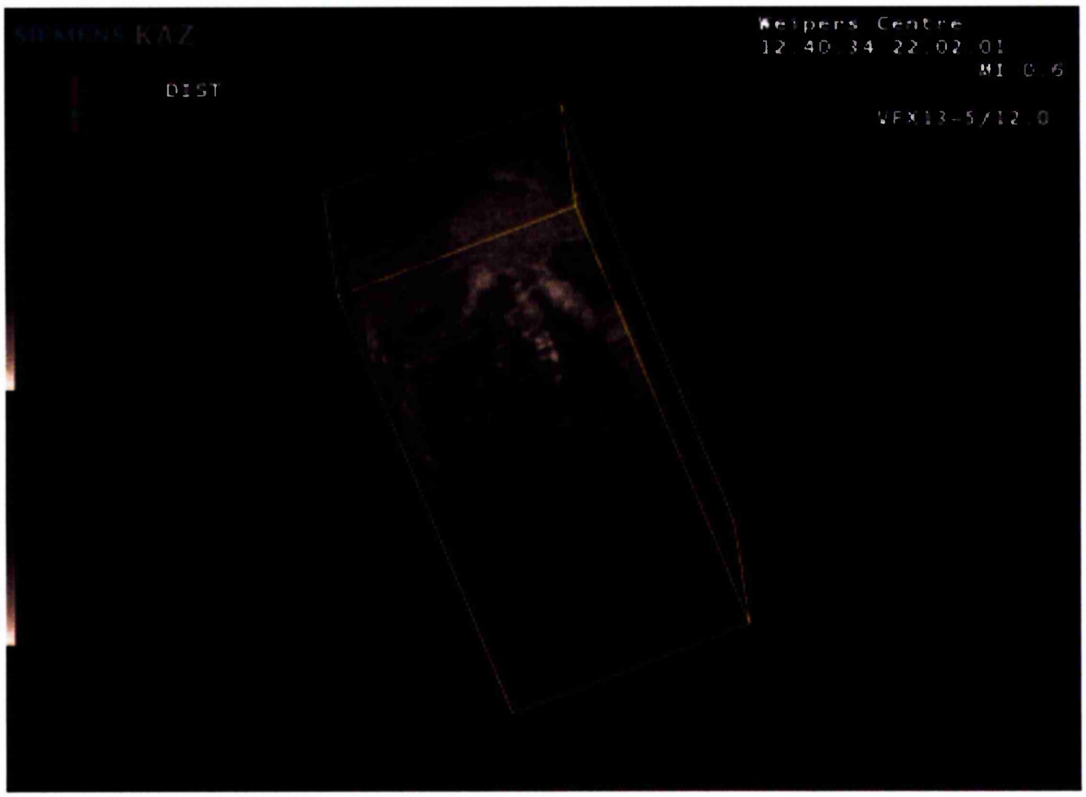

Fig. 4.11. Reconstructed three dimensional volume sample of the m. biceps brachii on the proximal humerus of the left leg of a dog using Elegra with a 12 MHz linear transducer. The sample is rotated in an equatorial plane so that the viewed surface of the cube is the distal surface, to the right is lateral and to the left is medial. The skin and superficial structures lie at the top of the field, the m. biceps brachii is in mid field and the humerus is at the bottom of the field.

Fig. 4.12. Reconstructed three dimensional volume sample of the m. biceps brachii on the proximal humerus of the left leg of a dog using Elegra with a 12 MHz linear transducer. The cube is rotated in an equatorial plane so that the viewed surface of the cube is the lateral face. The skin and the superficial structures lie at the top of the field, to the right is proximal, to the left is distal and the deeper structures are towards the bottom of the field. The tendon of origin of the m. biceps brachii is imaged as a hyperechoic line running from right to left through the centre of the field. The black area at the bottom of the field is due to the acoustic shadow created by the humeral body.

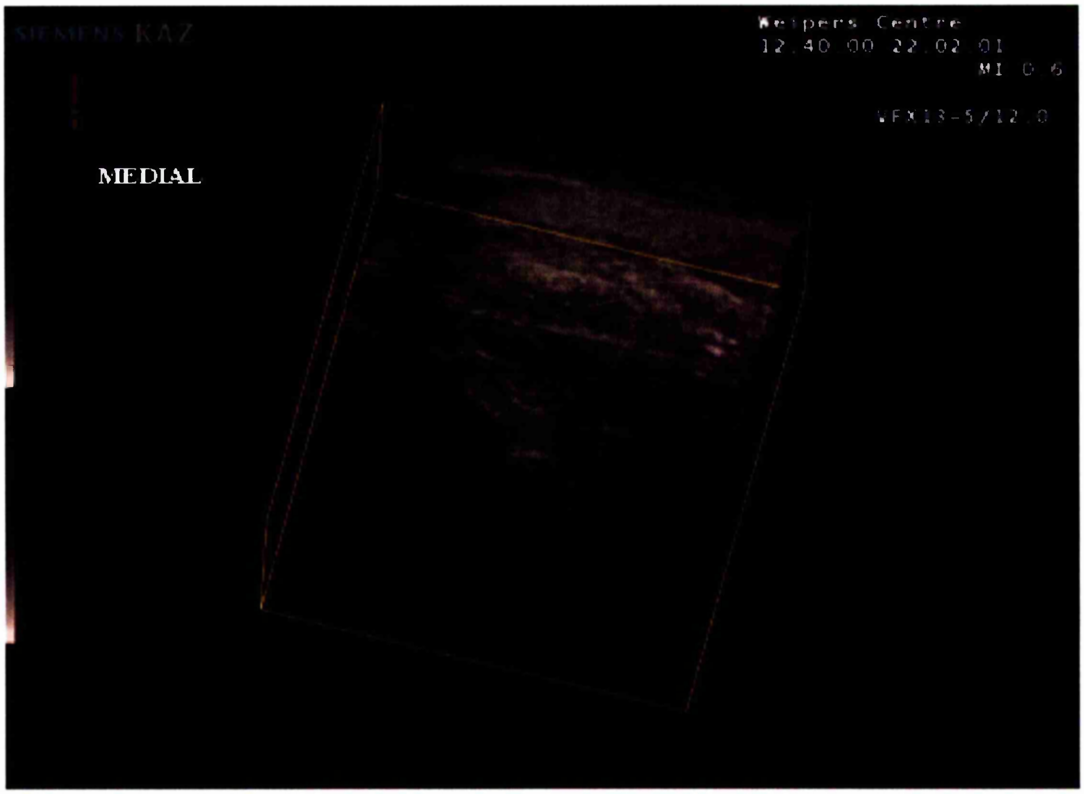

Fig. 4.13. Reconstructed three dimensional volume sample of the m. biceps brachii on the proximal humerus of the left leg of a dog using Elegra with a 12 MHz linear transducer. The sample is rotated in an equatorial plane so that the viewed surface of the cube is the medial surface. The skin and the superficial structures lie at the top of the field, to the left is proximal, to the right is distal and the deeper structures are towards the bottom of the field. The tendon of origin of the m. biceps brachii is imaged as a hyperechoic line running from left to right through the centre of the field. At 9 o' clock the tendon is surrounded by the anechoic synovial sheath, which connects with the joint capsule. The long surface of the intertubercular groove is seen in the lower regions of the field.

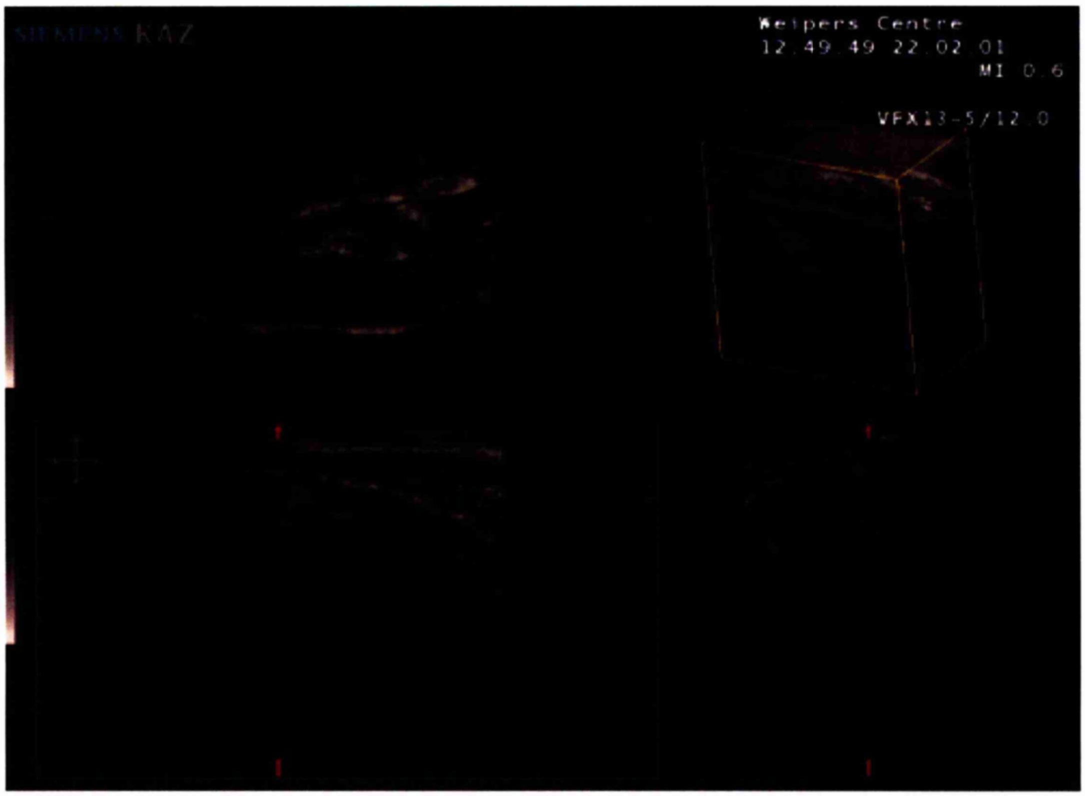

Fig. 4.14. The reconstructed three dimensional volume of the m. biceps brachii and its tendon of origin as they lie on the proximal humerus of the left leg of a dog using Elegra with a 12 MHz linear transducer is displayed in the upper right and the viewed face of the cube is medial. An arrow indicates the area of interest in the cube and this area is displayed in three planes including the appearance of the tendon of the m. biceps brachii in the intertubercular groove surrounded by the anechoic synovial sheath of the joint capsule. Upper left is dorsal (or coronal plane), lower left is long axis (sagittal plane) and lower right is short axis (transverse plane).

Fig. 4.15. The dorsal (coronal) plane taken at the point of interest in the reconstructed three dimensional volume sample of the m. biceps brachii and its tendon of origin as they lie on the proximal humerus of the left leg of a dog using Elegra with a 12 MHz linear transducer is indicated in the bottom right. The enlarged image is revealed in the centre of the picture with the hyperechoic tendon surrounded by the anechoic synovial sheath of the joint capsule.

Fig. 4.16. The sagittal plane taken at the point of interest in the reconstructed three dimensional volume sample of the m. biceps brachii and its tendon of origin as they lie on the proximal humerus of the left leg of a dog using Elegra with a 12 MHz linear transducer is indicated in the bottom right. The enlarged image is revealed in the centre of the picture with the hyperechoic tendon surrounded by the anechoic synovial sheath of the joint capsule.

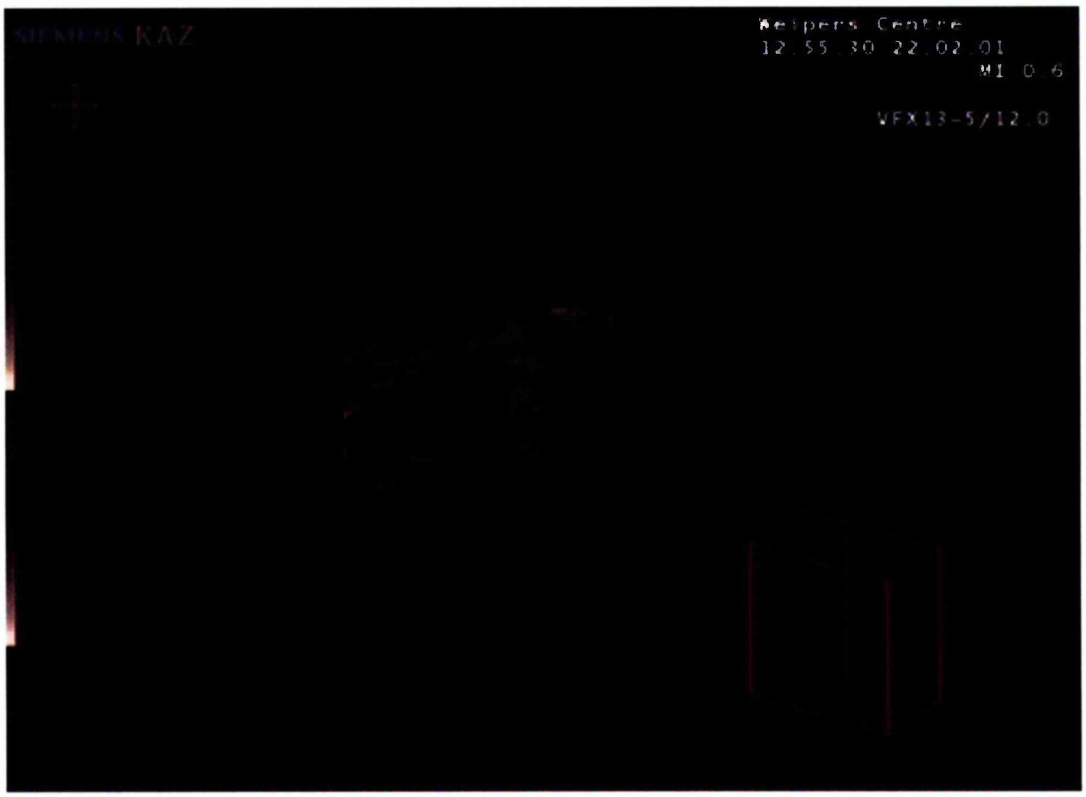

Fig. 4.17. The transverse plane taken at the point of interest in the reconstructed three dimensional volume sample of the m. biceps brachii and its tendon of origin as they lie on the proximal humerus of the left leg of a dog using Elegra with a 12 MHz linear transducer is indicated in the bottom right. The enlarged image is revealed in the centre of the picture with the hyperechoic tendon surrounded by the anechoic synovial sheath of the joint capsule.

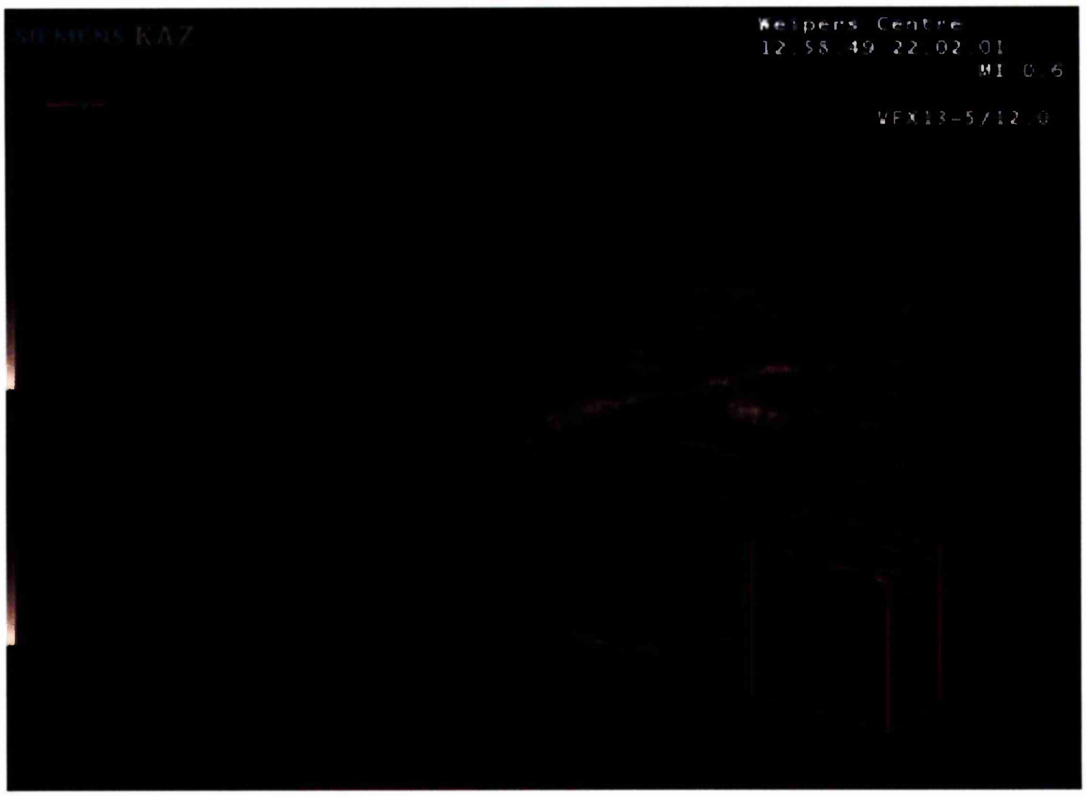

Fig. 4.18. An eccentric dorsal (coronal) plane taken at the point of interest in the reconstructed three dimensional volume sample of the m. biceps brachii and its tendon of origin as they lie on the proximal humerus of the left leg of a dog using Elegra with a 12 MHz linear transducer is indicated in the bottom right. The enlarged image is revealed in the centre of the picture with the hyperechoic tendon surrounded by the anechoic synovial sheath of the joint capsule with the involvement of the joint space and the humeral articular surface displayed.

Fig. 4.19. Short axis view of the left thoracic limb of a dog using Diasus with a 16 MHz linear transducer. The round hypoechoic m. teres minor is displayed on the centre of the picture lying beneath the hypoechoic acromial part of the m. deltoideus.

1) M. deltoideus-acromial part

2) M. teres minor

3) Joint space

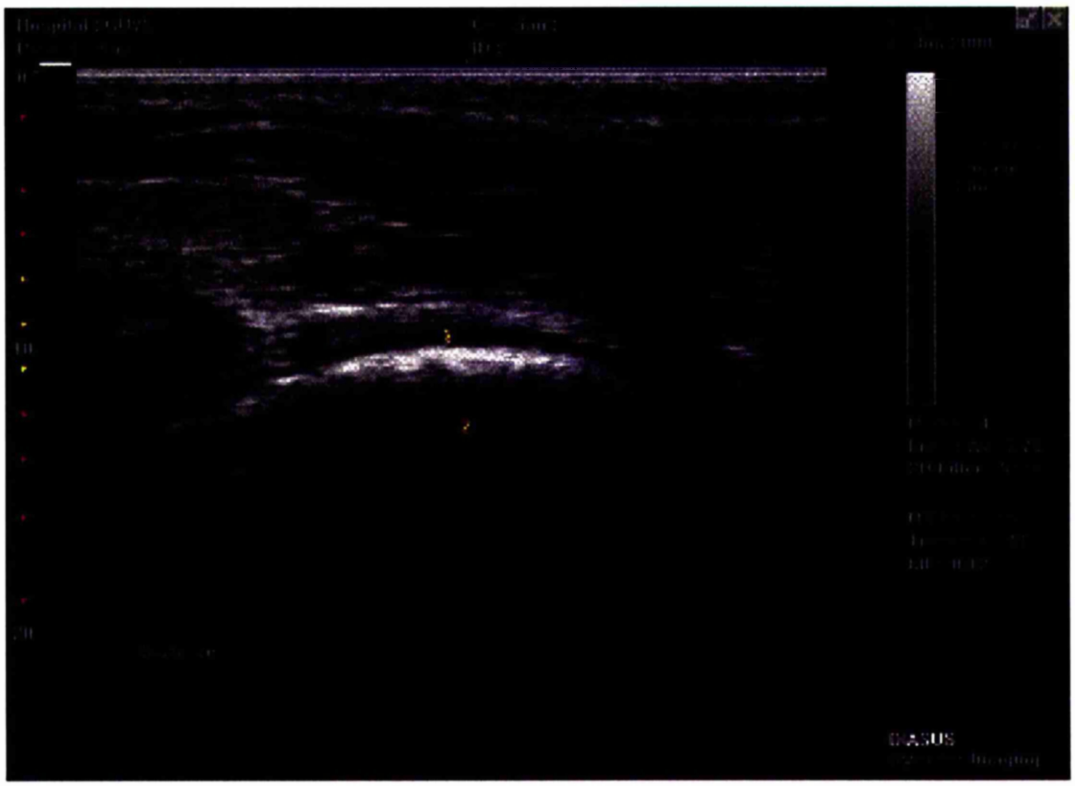

Fig. 4.20. Short axis view of the left thoracic limb of a dog using Diasus with a 16 MHz linear transducer. The round hyper reflective head of the humerus with an anechoic area of acoustic shadowing distal to it is displayed on the bottom of the picture lying beneath the anechoic shoulder joint space.

1) Joint space with articular cartilage

2) Head of the humerus

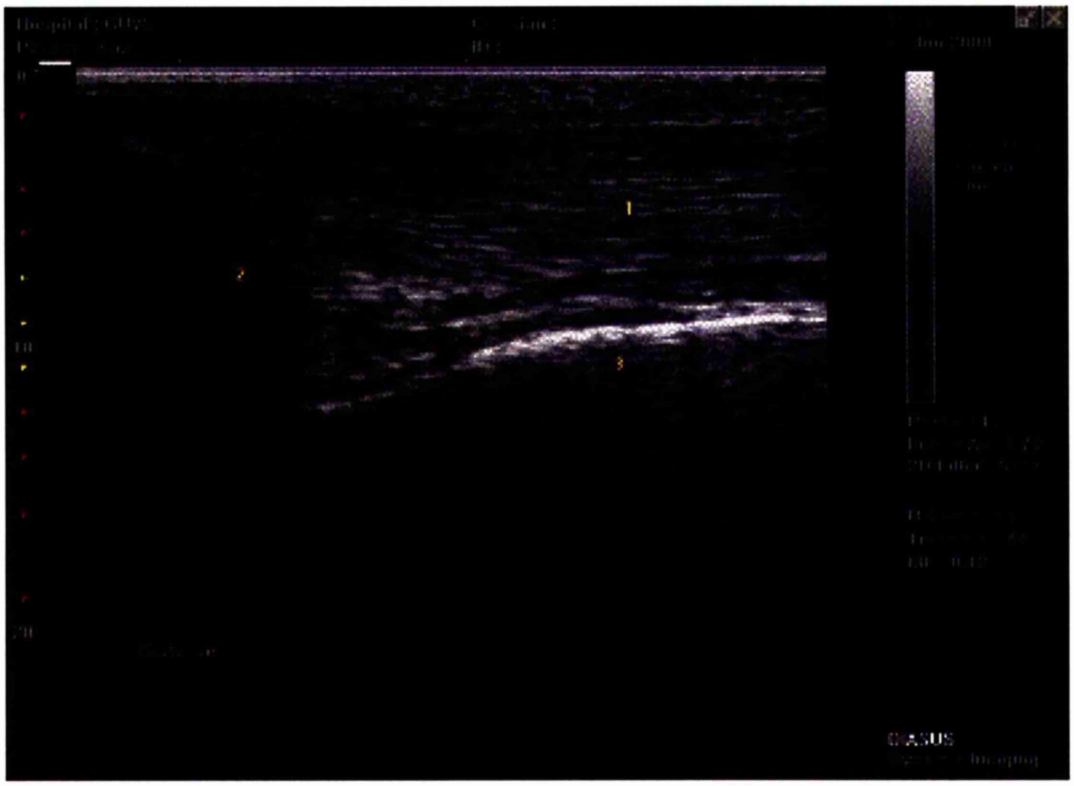

Fig. 4.21. Long axis view of the left pelvic limb of a dog using Diasus with a 16 MHz linear transducer. The hyperechoic distal part of the m. quadriceps femoris runs from right to left in the picture, merging into the patellar ligament. The round hyper reflective patella with an anechoic area of acoustic shadowing distal to it lies on the left of the picture.

1) M. quadriceps femoris

2) Patella

3) Femur

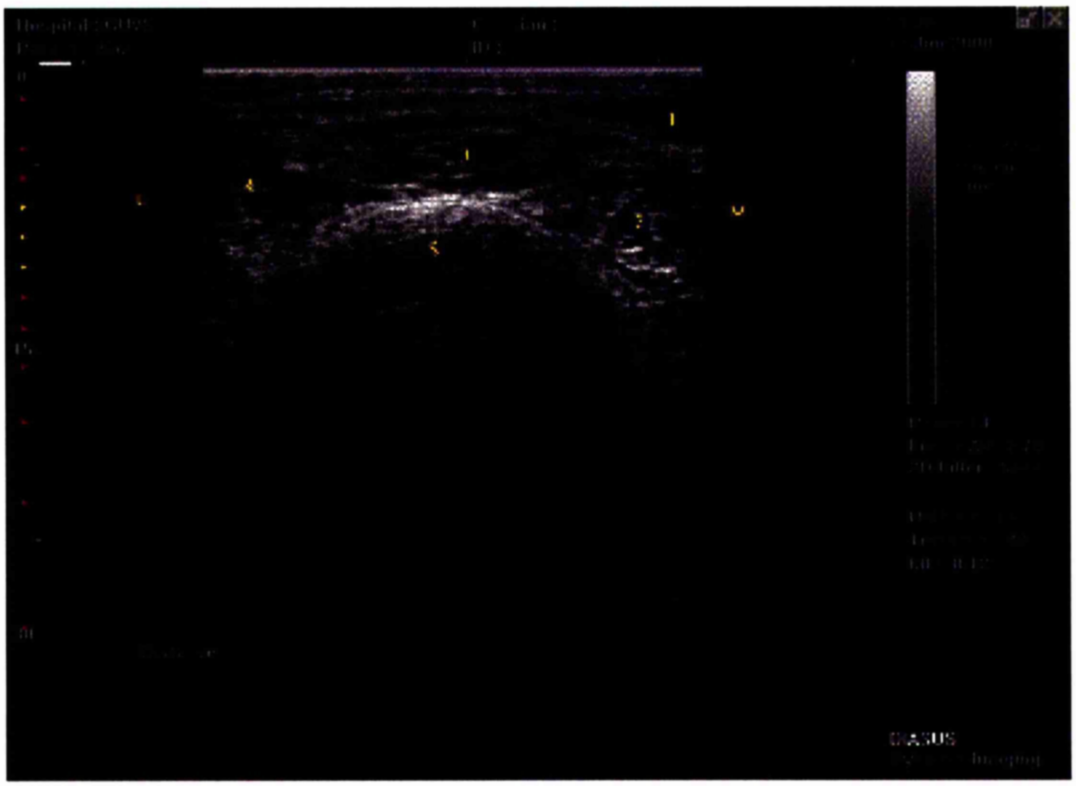

Fig. 4.22. Short axis view of the left pelvic limb of a dog using Diasus with a 16 MHz linear transducer. The different components of the m. quadriceps are imaged. From right to left, the mm. vastus intermedius, vastus medialis, rectus femoris and vastus lateralis are displayed at the top of the picture and superficial to the hyper reflective femur with an anechoic area of acoustic shadowing distal to it.

1) M. vastus intermedius

2) M. vastus medialis

3) M. rectus femoris

4) M. vastus lateralis

5) Femur

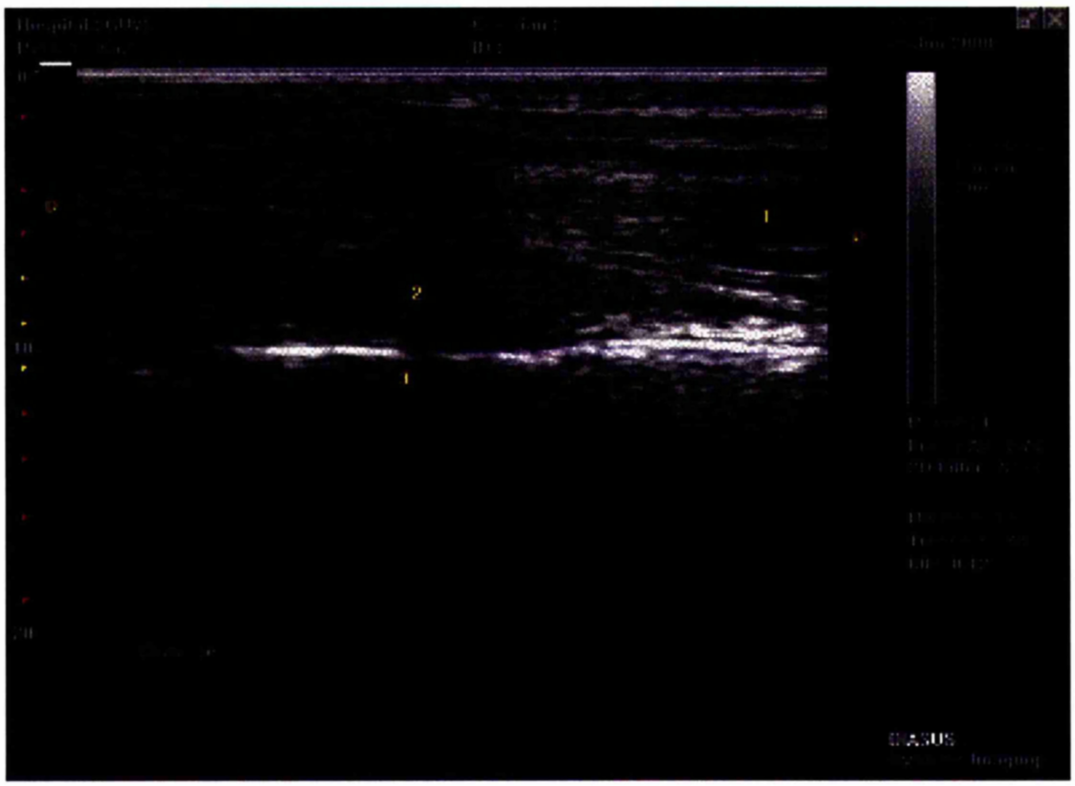

Fig. 4.23. Long axis view of the left pelvic limb of a dog using Diasus with a 16 MHz linear transducer. The hyperechoic distal part of the m. quadriceps femoris runs from right to left on the picture and the anechoic bursa lies beneath it.

1) M. quadriceps femoris

2) Bursa of the m.quadriceps femoris

3) Femur

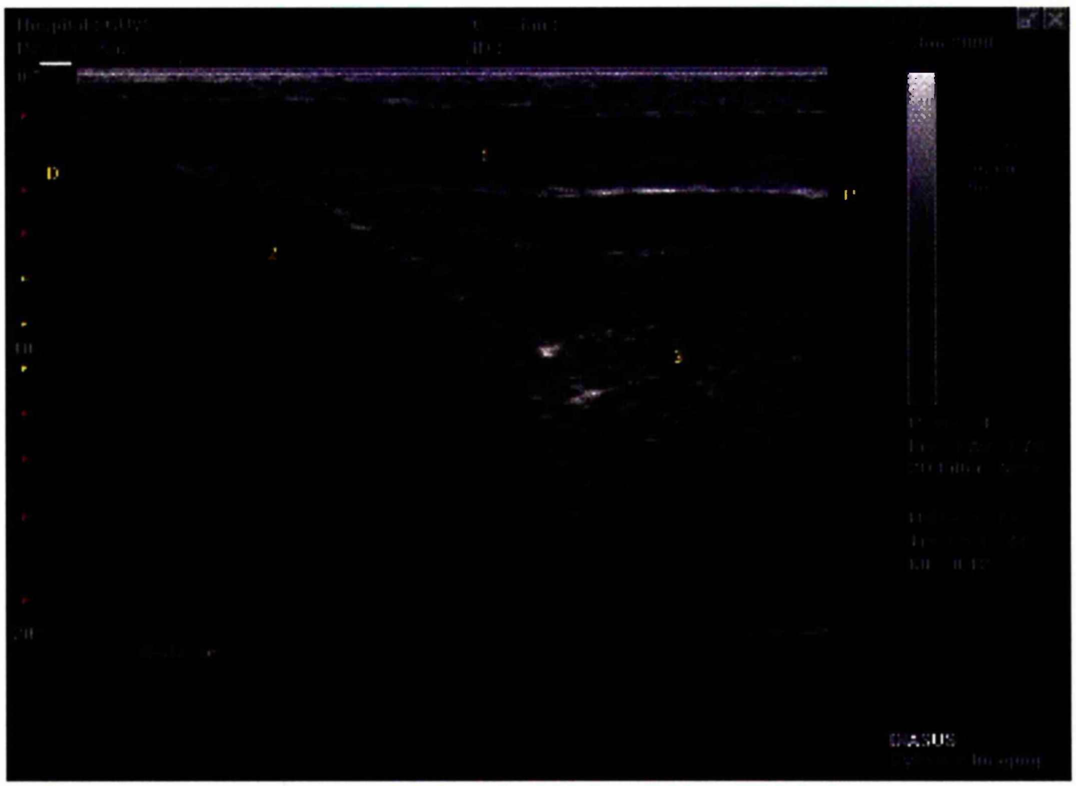

Fig. 4.24. Long axis view of the left pelvic limb of a dog using Diasus with a 16 MHz linear transducer. The moderately echoic skin is distinguished from the hypoechoic patellar ligament. The infrapatellar fat which has bright echoes in its parenchyma lies beneath the patellar ligament.

1) Patellar ligament

2) Tibial tuberosity

3) Infrapatellar fat

Fig. 4.25. Extended field of view image of the left stifle joint of a dog using Elegra with a 12 MHz linear transducer. The femoral condyles lie to the right, as does the hyperechoic patella which is in the near field. The hyperechoic tibial tuberosity lies in the left near field. The patellar ligament runs through the near field from right to left and is seen as a linear layered echoic structure. The echogenic fat pad is seen in the mid field and increases in echogenicity deeper in the joint space. Deep to the fat pad the hypoechoic cruciate ligament is imaged in the left running obliquely from its tibial insertion into the intercondylar space on the deep right.

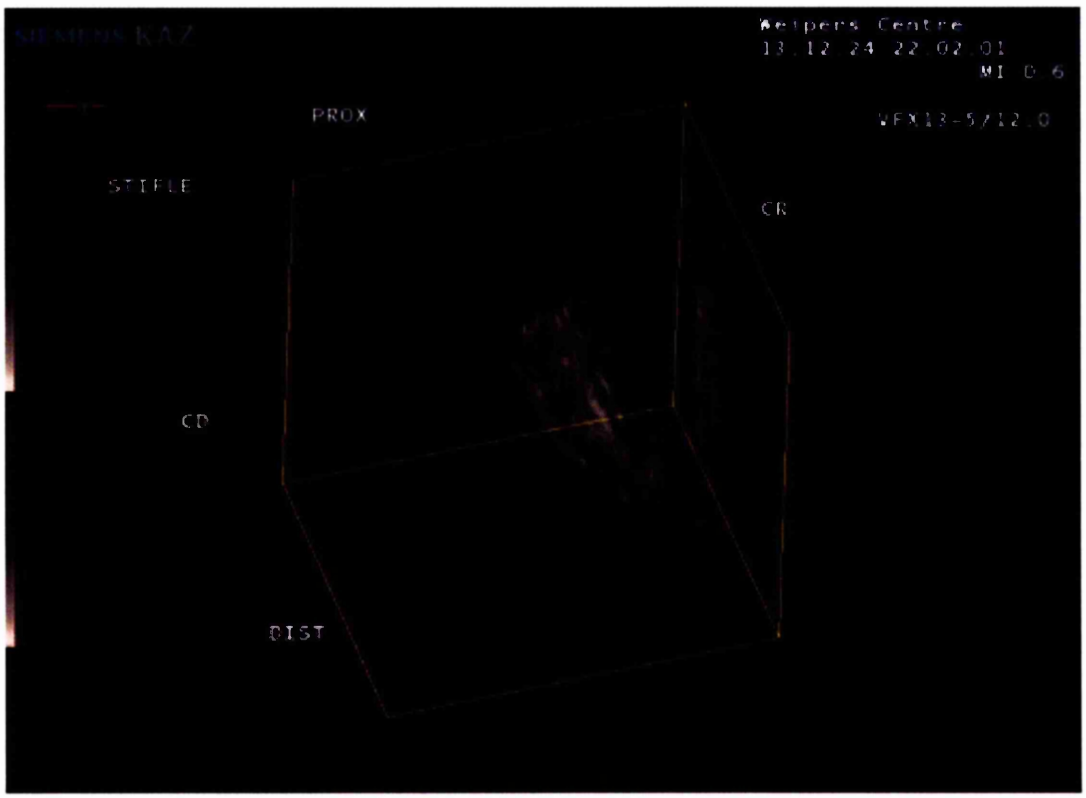

Fig. 4.26. A three-dimensional reconstructed volume sample of the left stifle of a dog scanned with Elegra and a 12 MHz linear transducer. The sample is viewed from the medial aspect and the patellar ligament lies to the right with the deeper structures, e.g. cranial cruciate ligament, to the extreme left. The sample has been rotated around a polar axis.

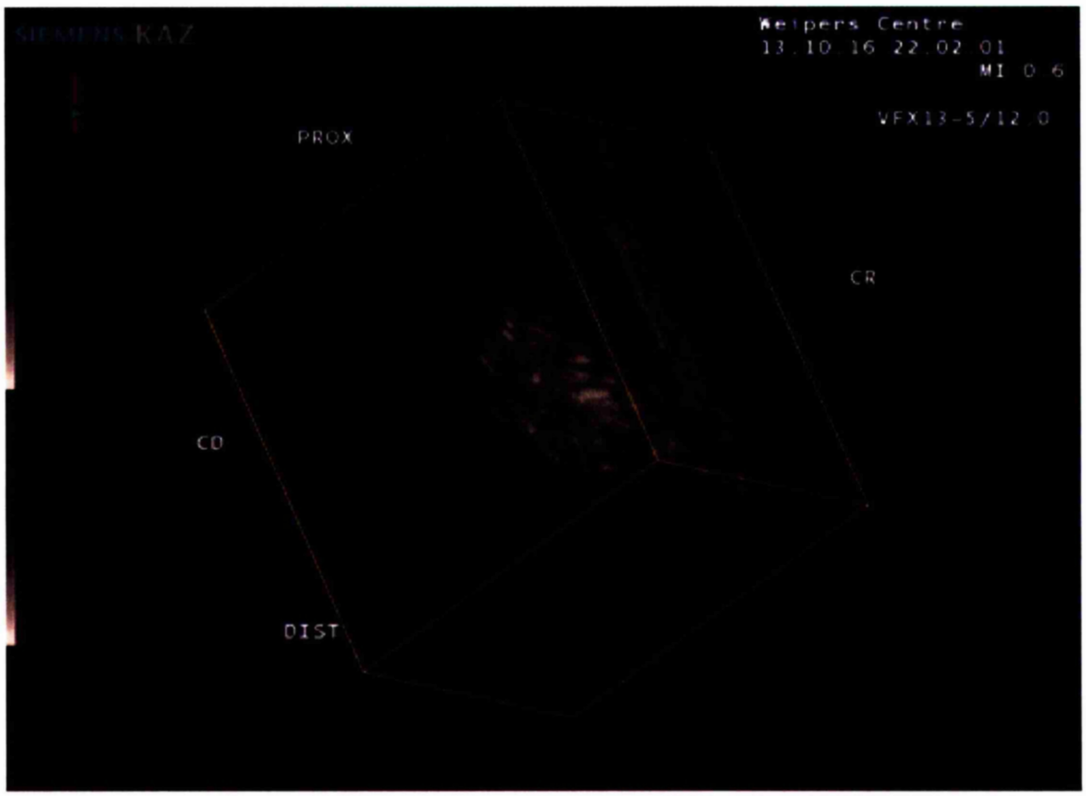

Fig 4.27. A three-dimensional reconstructed volume sample of the left stifle of a dog scanned with Elegra and a 12 MHz linear transducer. The sample is viewed from the medial aspect and the patellar ligament lies to the right with the deeper structures to the left, e.g. cranial cruciate ligament, which is hypoechoic compared to the hyperechoic fat pad. The sample has been rotated about an equatorial axis.

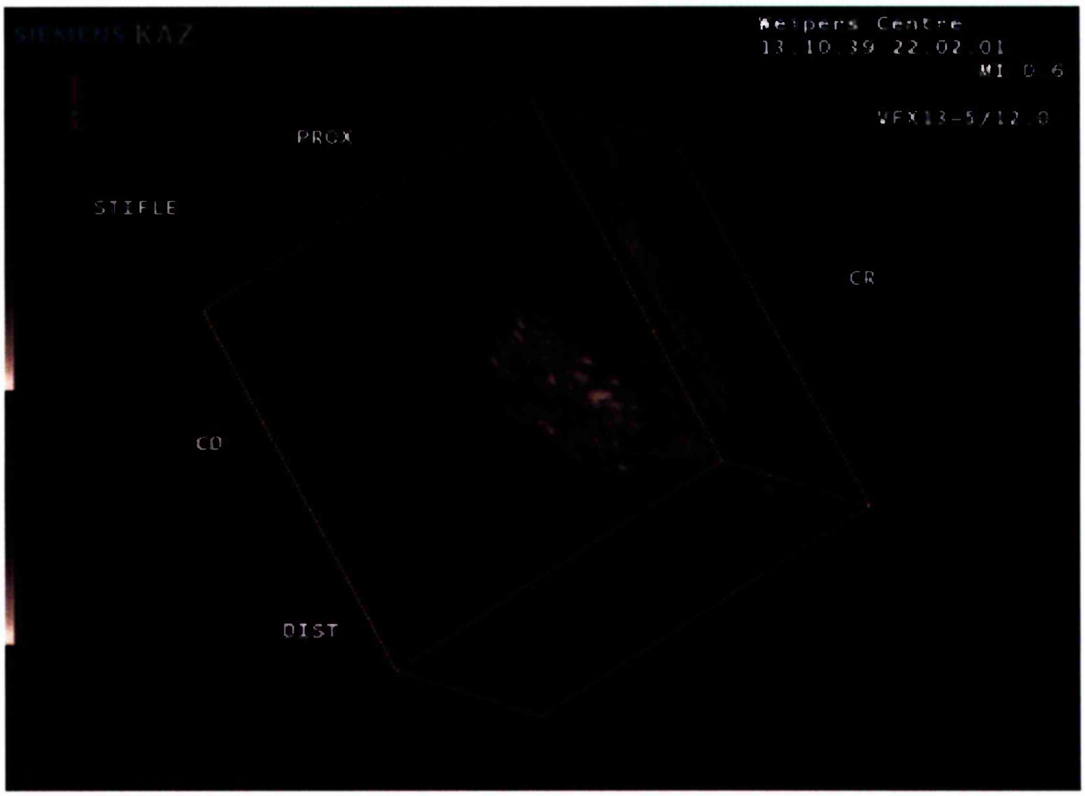

Fig. 4.28. A three-dimensional reconstructed volume sample of the left stifle of a dog scanned with Elegra and a 12 MHz linear transducer. The sample is viewed from the medial aspect and the patellar ligament lies to the right with the deeper structures to the left, e.g. cranial cruciate ligament, which is hypoechoic compared to the hyperechoic fat pad. The sample has been further rotated about an equatorial axis compared to Fig. 4.27.

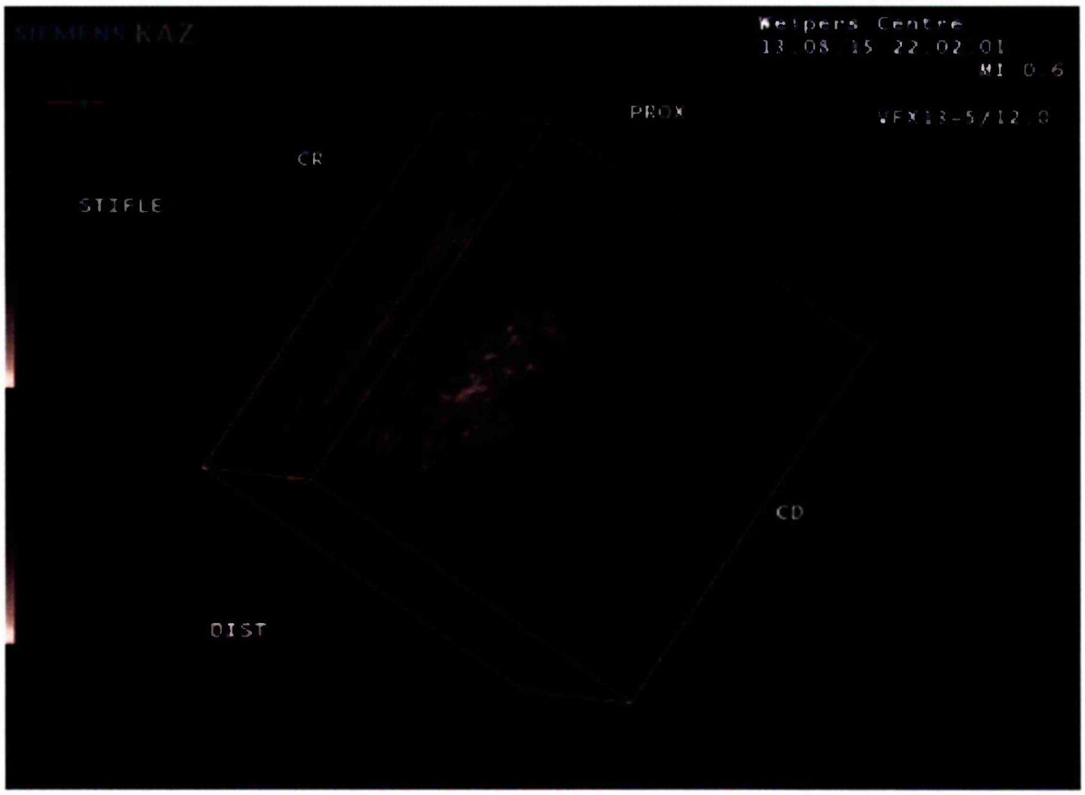

Fig. 4.29. A three-dimensional reconstructed volume sample of the left stifle of a dog scanned with Elegra and a 12 MHz linear transducer. The sample is viewed from the lateral aspect and the patellar ligament lies to the left with the deeper structures to the right, e. g. cranial cruciate ligament, which is more echoic than in figures of the medial aspect. This is due to the anistrophic effect.

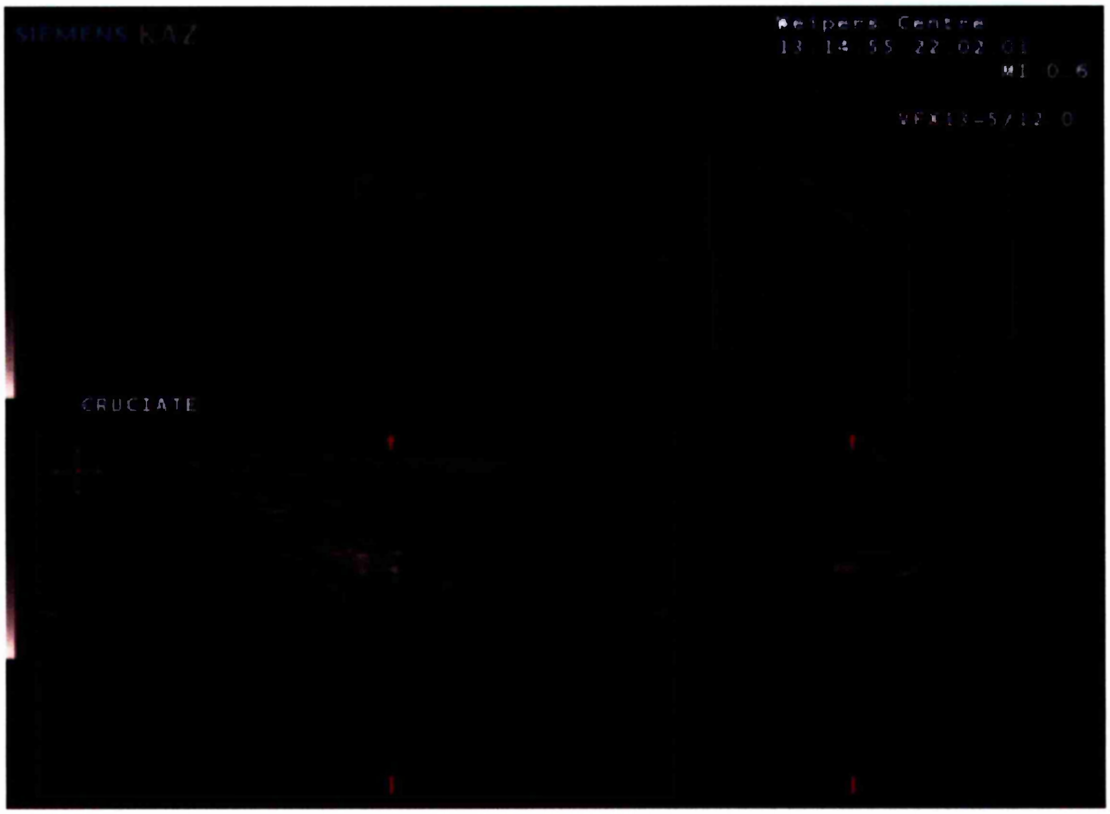

Fig. 4.30. A selected sagittal plane in a reconstructed three dimensional volume sample of the stifle joint of a left leg of a dog taken with Elegra using a 12 MHz linear transducer is displayed in the upper right. The arrow marks the point of interest in the viewed plane and the area of interest is displayed in three planes. The left upper is the dorsal (coronal) plane, the left lower is the sagittal or long axis plane and the right lower the transverse or short axis plane. The cross shaped marker is placed at the cranial cruciate ligament, which is hypoechoic lying deep to the hyperechoic fat pad. There is a line of acoustic shadowing running through the sample being evident on the dorsal and transverse planes.

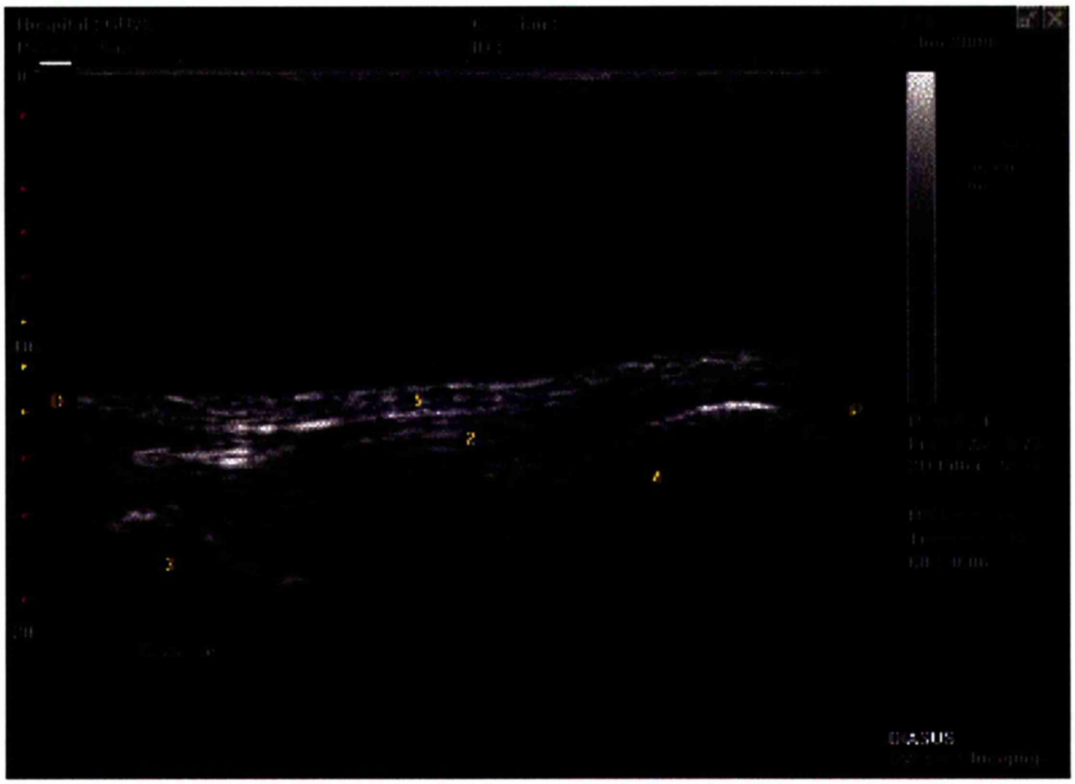

Fig. 4.31. Long axis view of the left pelvic limb of a dog using Diasus with a 16 MHz linear transducer. The tendon of origin of the m. extensor digitorum longus is clearly defined from the overlying skin and it lies between the hyper reflective tibia and femur with an anechoic area of acoustic shadowing distal to them. The anechoic area on the top of the picture corresponds to the stand-off pad.

1) Skin

2) Tendon of origin of the m. extensor digitorum longus

3) Tibia

4) Femur

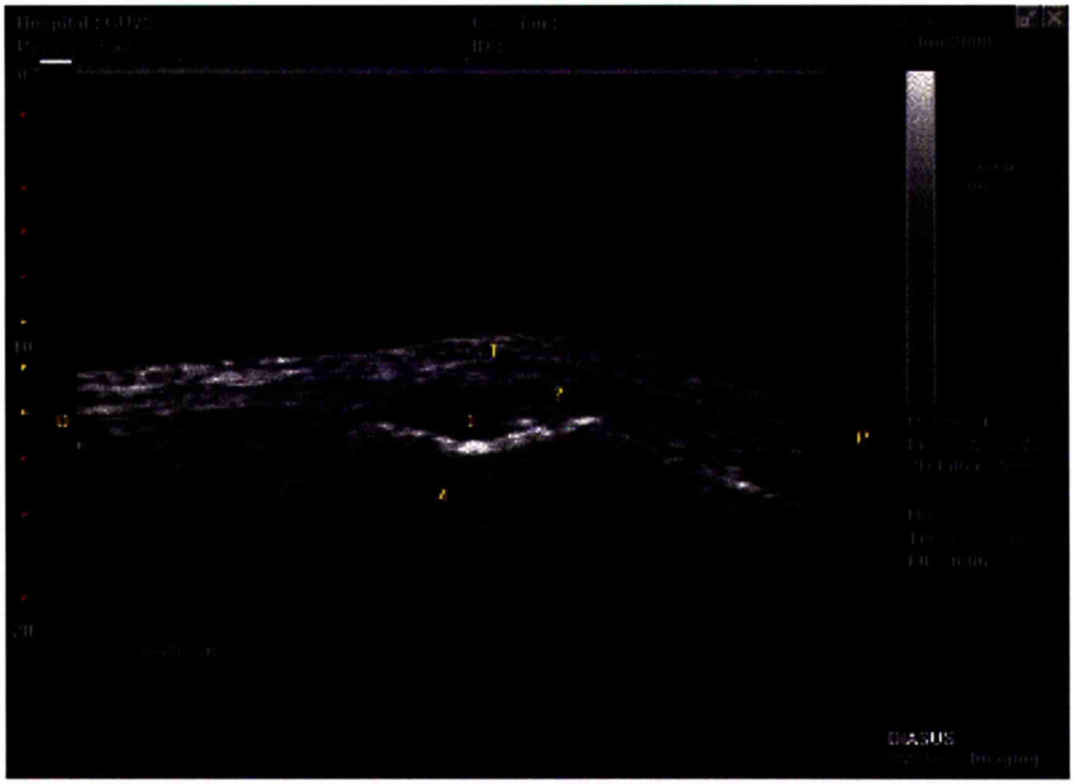

Fig. 4.32. Long axis view of the left pelvic limb of a dog using Diasus with a 16 MHz linear transducer. The tendon of origin of the m. extensor digitorum longus is clearly defined from the overlying skin and it lies over an anechoic area representing the synovial pouch of the meniscotibial portion of the stifle joint capsule. The hyper reflective femur with an anechoic area of acoustic shadowing distal to it lies at the bottom of the picture. The anechoic area on the top of the picture corresponds to the stand-off pad.

1) Skin

2) Tendon of origin of the m. extensor digitorum longus

3) Synovia

4) Femur

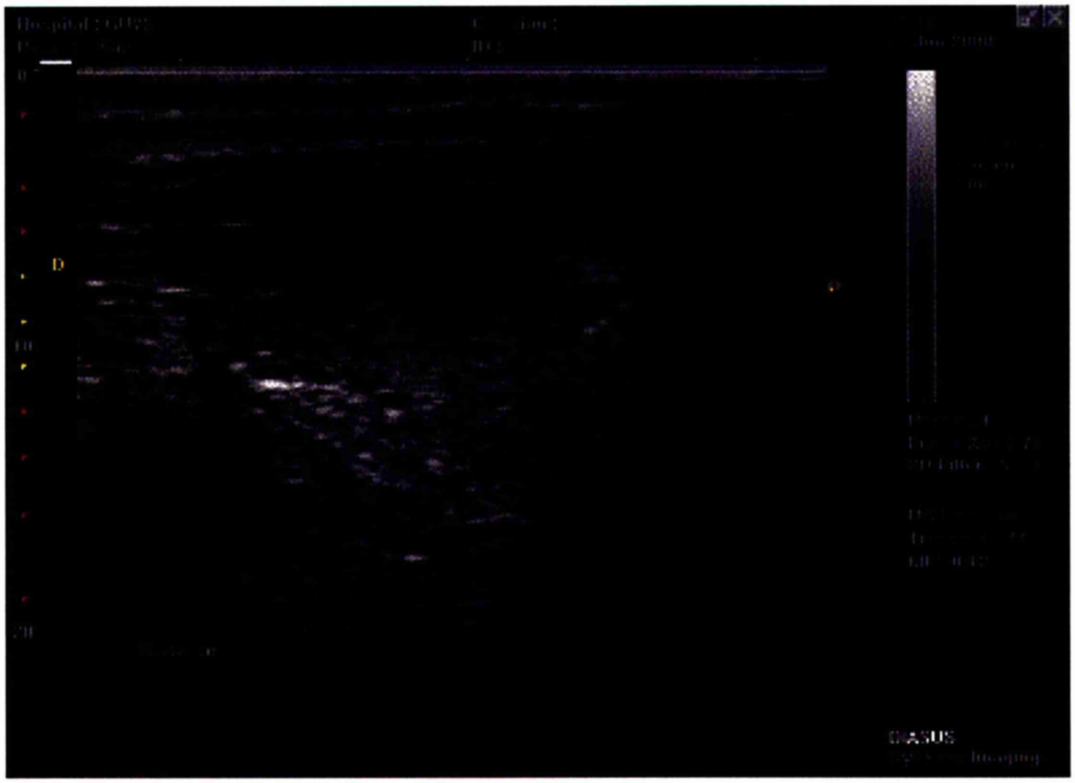

Fig. 4.33. Long axis view of the left pelvic limb of a dog using Diasus with a 16 MHz linear transducer. The femur and the patella lie to the right, the tibia to the left. The infrapatellar fat is clearly imaged becoming hyperechoic in its deeper position. Deep to these bright areas of the fat pad lie the cruciate ligaments which are crossing over each other, imaging as hypoechoic linear structures with more echogenic edges.

Fig. 4.34. Extended field of view image of the left stifle joint of a dog using Elegra with a 12 MHz linear transducer. The femoral condyles lie to the right, as does the hyperechoic patella which is in the near field. The hyperechoic tibial tuberosity lies in the left near field. The patellar ligament runs through the near field from right to left and is seen as a linear layered echoic structure. The echogenic fat pad is seen in the mid field and increases in echogenicity deeper in the joint space. Deep to the fat pad the hypoechoic cruciate ligament is imaged in the left running obliquely from its tibial insertion into the intercondylar space on the deep right.

Fig. 4.35. Long axis view of the left pelvic limb of a dog using Diasus with a 16 MHz linear transducer. The medial collateral ligament is fused with the overlying skin in the middle of the picture and the hyperechoic triangular meniscus lies beneath it between the hyper reflective tibia (on the left) and the femur (on the right). The anechoic area on the top of the picture corresponds to the stand-off pad.

1) Medial collateral ligament

2) Meniscus

3) Tibia

4) Femur

Fig. 4.36. Long axis view of the left pelvic limb of a dog using Diasus with a 16 MHz linear transducer. The hypoechoic lateral collateral ligament is distinguished from the overlying skin in the centre of the picture and the hyper reflective tibia with an anechoic area of acoustic shadowing distal to it is imaged on the left of the image. The structure lying deep to the ligament is the tendon of origin of the m. popliteus, which separates the ligament from the lateral meniscus.

1) Skin

2) Lateral collateral ligament

3) M. popliteus

4) Tibia

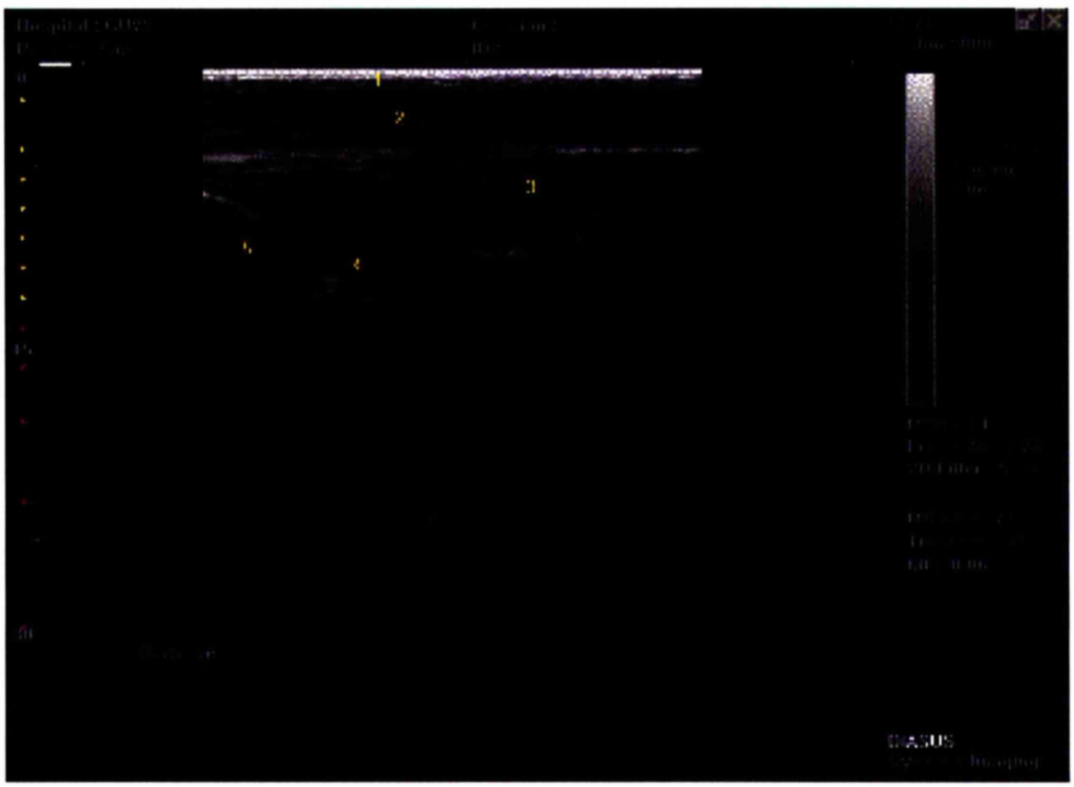

Fig.4.37. Long axis view of the left tarsal region of a dog using Diasus with a 16MHz linear transducer. The component layers of the common calcanean tendon are displayed from superficial to deep as the tendon of m. flexor digitorum superficialis and the tendon of m. gastrocnemius. The contribution from the mm. gracilis, semitendinosus and biceps femoris is not imaged in this plane. The hyper reflective image of the calcaneus lies to the left and the small anechoic round area to the right of it corresponds to the calcaneal bursa.

1) Skin 2) Tendon of m. flexor digitorum superficialis

3) Tendon of m. gastrocnemius 4) Bursa 5) Calcaneal tuberosity

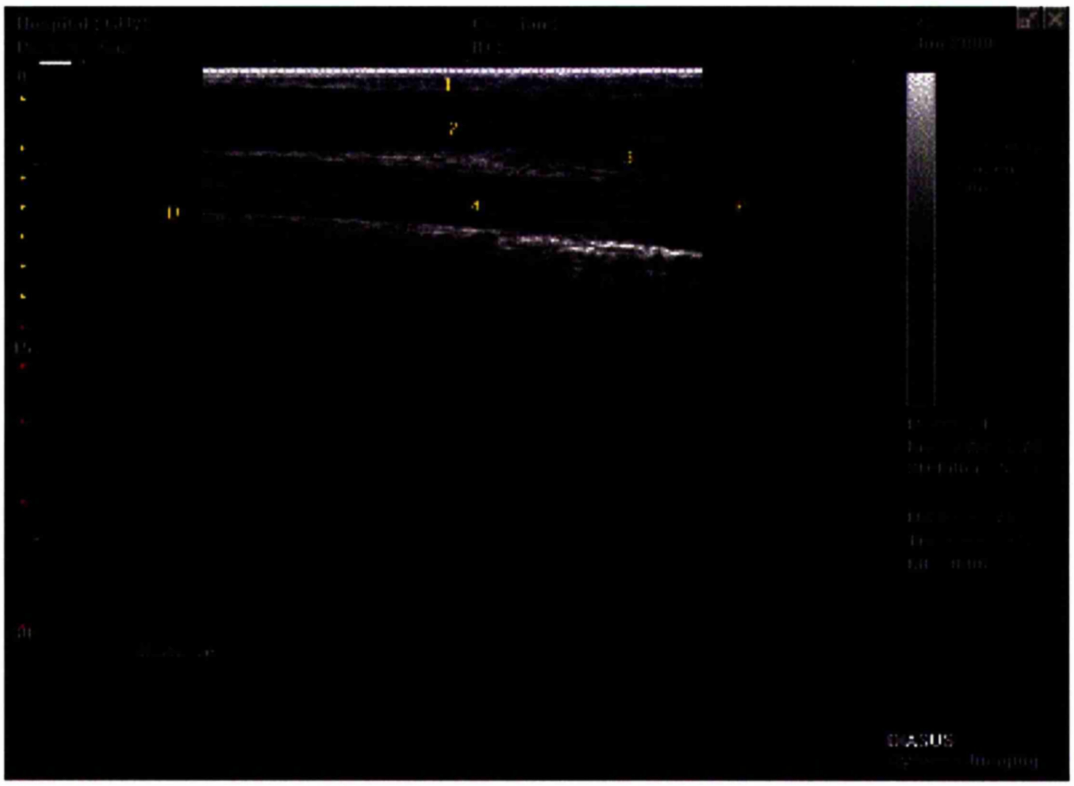

Fig. 4.38. Long axis view of the left tarsal region of a dog using Diasus with a 16MHz linear transducer. The component layers of the common calcanean tendon are displayed from superficial to deep as the tendon of m. flexor digitorum superficialis, the tendon of m. gastrocnemius lying to the right and deep to that the part formed by the tendons of mm. gracilis, semitendinosus and biceps femoris. The hyper reflective tibia lies deep to these structures.

1) Skin 2) Tendon of m. flexor digitorum superficialis

3) Tendon of m. gastrocnemius

4) Tendon formed by mm.gracilis, semitendinosus and biceps femoris.

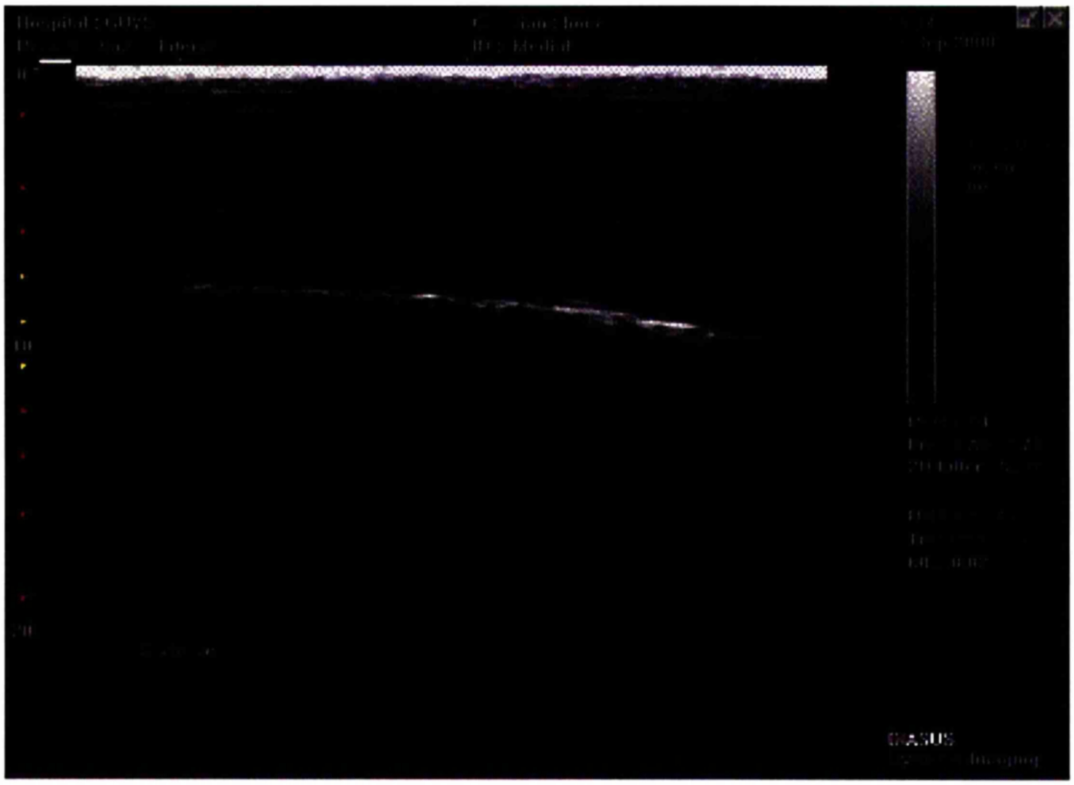

Fig. 4.39. Long axis view of the left pelvic limb of a dog using Diasus with a 22 MHz linear transducer. The different layers of the common calcaneal tendon are clearly distinguished from each other. The skin lies at the extreme top of the image and the tendon of the m. flexor digitorum superficialis lies beneath it. The portion corresponding to the tendon of the m. gastrocnemius lies deep to the above and to the right of the picture, whereas the deepest hyperechoic tendinous portion corresponds to the part of the tendon being formed by the tendons of the mm. gracilis, semitendinosus and biceps femoris. The hyper reflective area with an anechoic area of acoustic shadowing distal to it at the bottom of the image corresponds to the tibia.

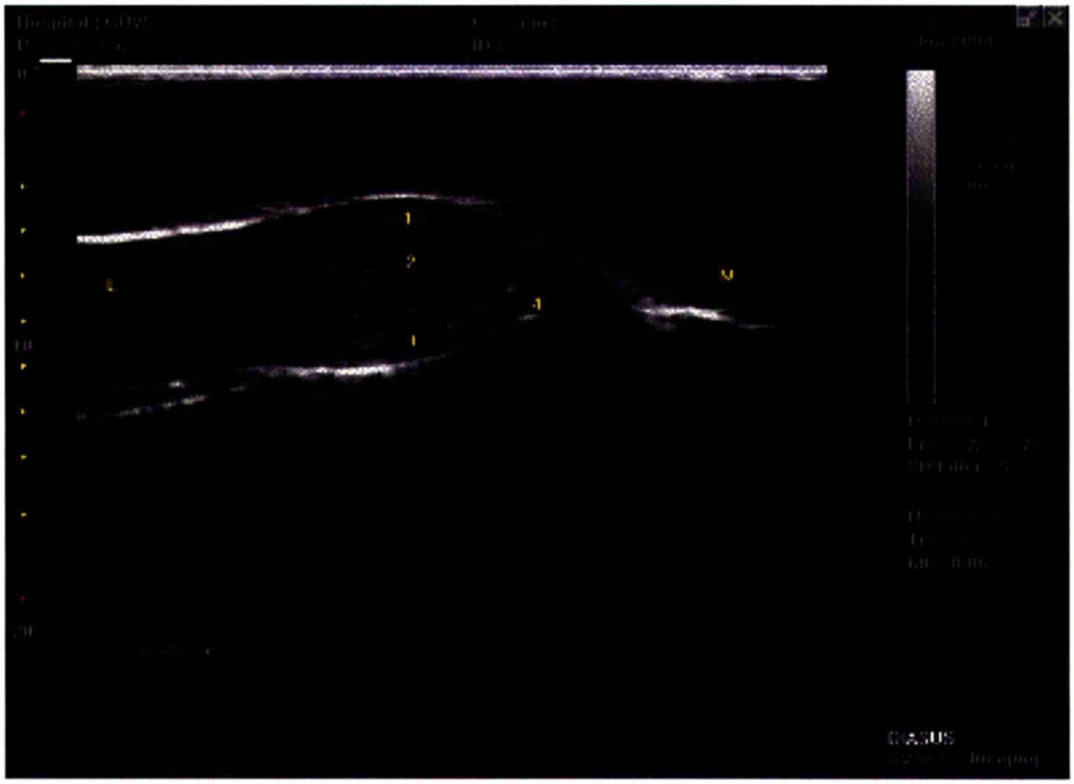

Fig. 4.40. Long axis view of the left tarsal region of a dog using Diasus with a 16MHz linear transducer. A stand-off pad lies most superficially. The component layers of the common calcanean tendon are displayed from superficial to deep as the tendon of m. flexor digitorum superficialis and the tendon of m. gastrocnemius. There is a small anechoic area at the right of the tendon representing a portion of the calcaneal bursa. The contribution from the mm. gracilis, semitendinosus and biceps femoris is not imaged in this plane. The hyper reflective calcaneus lies deep to these structures.

1) Skin 2) Tendon of m. flexor digitorum superficialis

3) Tendon of m. gastrocnemius 4) Bursa

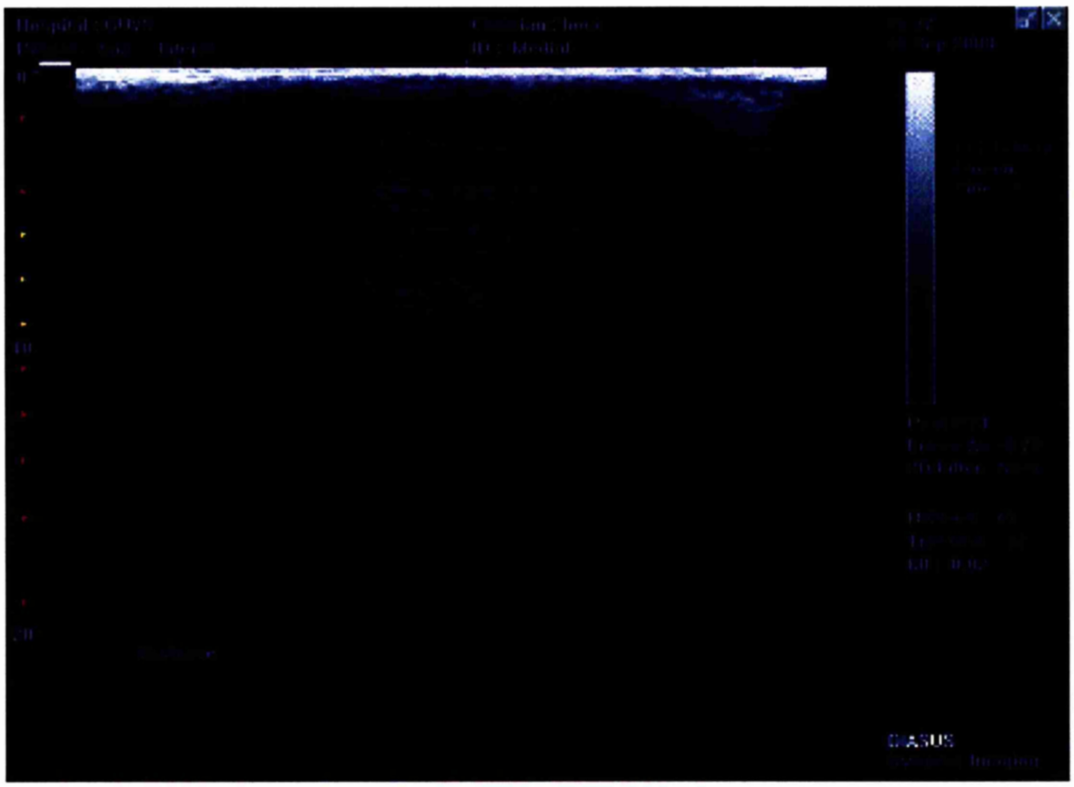

Fig. 4.41. Long axis view of the left pelvic limb of a dog using Diasus with a 22 MHz linear transducer. The different layers of the common calcaneal tendon are clearly distinguished. The skin lies at the extreme top of the image and the tendon of the m. flexor digitorum superficialis lies beneath it. The portion corresponding to the tendon of the m. gastrocnemius lies deep to the above and to the right of the picture, whereas the deepest hyperechoic tendinous portion corresponds to the part of the tendon being formed by the tendons of the mm. gracilis, semitendinosus and biceps femoris. The anechoic area running through the deepest layer of the tendon corresponds to the calcaneal bursa.

Fig. 4.42. Lateral radiograph of the left shoulder joint of the Border Collie, case 1. The scapula is displayed in the top right, the shoulder joint space in the centre and the humerus in the bottom of the picture. A mild subluxation of the joint is observed in the centre of the picture.

Fig. 4.43. Caudio - cranial radiograph of the left shoulder joint of the Border Collie case 1. The scapula is displayed in the top of the image, the shoulder joint space in the mid field and the humerus in the bottom field. A separate bone fragment on the medial aspect of the glenoid tubercle is imaged in the left of the picture.

Fig 4.44. Short axis view of the tendon of origin of the m. biceps brachii of the left shoulder joint of the Border Collie, case number 1 using Corevision and an 8 MHz linear transducer. The round hyperechoic tendon is imaged in the mid field in the hyper reflective intertubercular groove with an anechoic acoustic shadow distal to it in the right of the picture. The latter structure, though, appears disrupted and a round hyperechoic fragment is displayed towards the very right of the picture. The synovial sheath that surrounds the tendon appears distended and is filled with moderately hypoechoic fluid. Superficially and on the right of it the hypoechoic transverse ligament lies intact, whereas on the left a hypoechoic area is evident.

Fig.4.45. Short axis view of the tendon of origin of the m. biceps brachii of the left shoulder joint of the Border Collie, case number 1 using Corevision and an 8 MHz linear transducer. The round hyperechoic tendon is imaged in the mid field in the hyper reflective intertubercular groove with an anechoic acoustic shadow distal to it. The latter structure, though, appears disrupted in the centre of the picture. The synovial sheath that surrounds the tendon appears distended and is filled with moderately hypoechoic fluid. Superficially and on the right of it the hypoechoic transverse ligament lies intact, whereas on the left a hypoechoic area is evident.

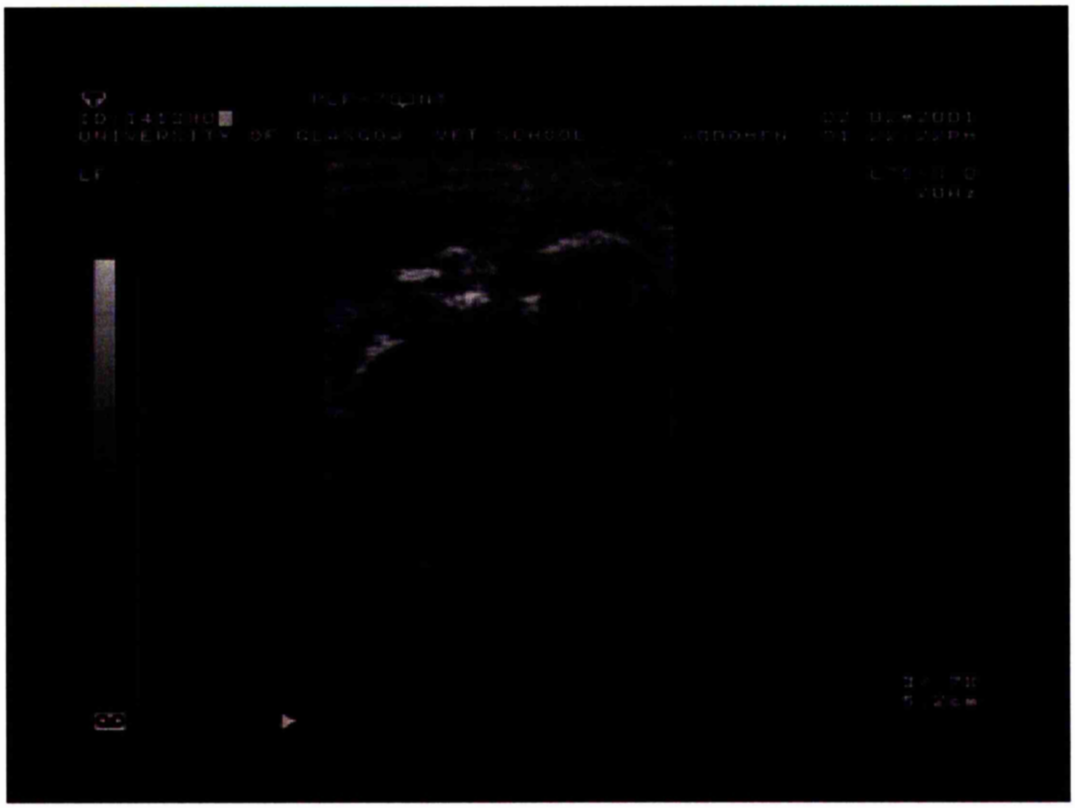

Fig. 4. 46. Short axis view of the intertubercular groove of the left shoulder joint of the Border Collie, case number 1 using Corevision and an 8 MHz linear transducer. The image is of the more medial region closer to the lesser tubercle of the humerus. The surface of the groove is disrupted and hyper reflective portions of bone lie around the area indicating a fracture site.

Fig. 4.47. Lateral radiograph of the right shoulder joint of the Weimaraner case 2. The scapula is displayed in the top right, the shoulder joint space in the centre and the humerus in the bottom of the picture. Patches of new bone are displayed at the level of the intertubercular groove in the mid field.

Fig. 4.48. Caudio - cranial radiograph of the right shoulder joint of the Weimaraner case 2. The scapula is displayed in the top of the image, the shoulder joint space in the mid field and the humerus in the bottom field. A smooth osteophyte is imaged on the medial humeral head in the right of the picture.

Fig. 4.49. An arthrogram of the right shoulder joint of the Weimaraner case 2. The scapula is displayed in the top right, the shoulder joint space in the centre and the humerus in the bottom of the picture. Contrast agent is evident in the shoulder joint space in the mid field, whereas to the left of it a narrowed contrast column is imaged in the bursa of the tendon of origin of the m. biceps brachii. Irregular filling defects are present throughout the joint space.

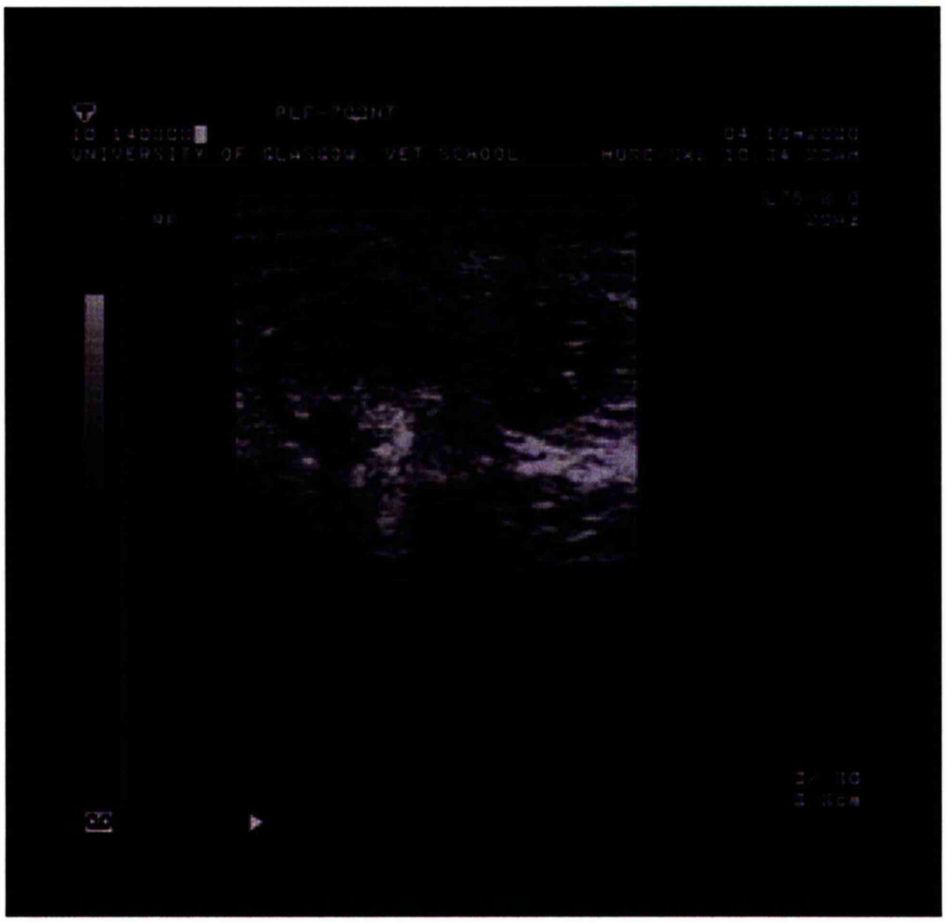

Fig. 4.50. Short axis image of the tendon of origin of the m. biceps brachii of the right forelimb of the Weimaraner, case 2 using Corevision with an 8 MHz linear transducer. The tendon is imaged to the left of the mid field of the picture. It appears hypoechoic and surrounded by echogenic fluid. The synovial sheath appears distended and hyperechoic. A small anechoic area appears on the lower left of the tendon. The hyper reflective area with anechoic acoustic shadowing distal to it at the bottom of the image corresponds to the intertubercular groove of the humerus.

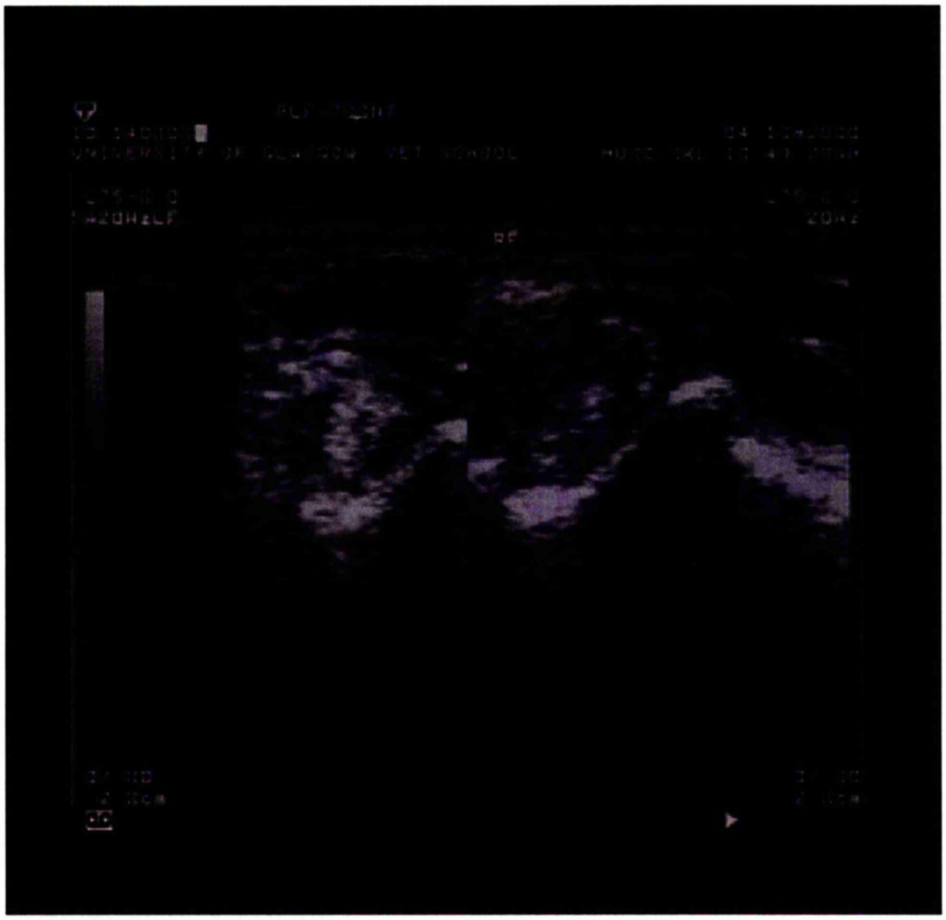

Fig. 4.51. Short axis image of the tendon of origin of the m. biceps brachii of both the right and the left forelimbs of the Weimaraner, case 2 using Corevision with an 8 MHz linear transducer. The tendon of the left leg appears to the left of the picture, the right to the right. The former appears echogenic in the mid field of that image with a small amount of hypoechoic fluid surrounding it. The latter is imaged to the left of the mid field of that image and appears hypoechoic and surrounded by echogenic fluid. The synovial sheath appears distended and thickened. The hyper reflective area with anechoic acoustic shadowing distal to it on the bottom of both images corresponds to the intertubercular groove of the humerus.

Fig. 4.52. Lateral radiograph of the left shoulder joint of the Greyhound case 3. The scapula is displayed in the top right, the shoulder joint space in the centre and the humerus in the centre and bottom of the picture. A reduction on opacity of the left proximal humerus with a mottled appearance and multiple punctate lucencies, as well as irregular new bone formation is evident throughout the bone surface. A separate area of mineralisation is located in the soft tissue on the left of the greater tubercle in the upper left of the picture.

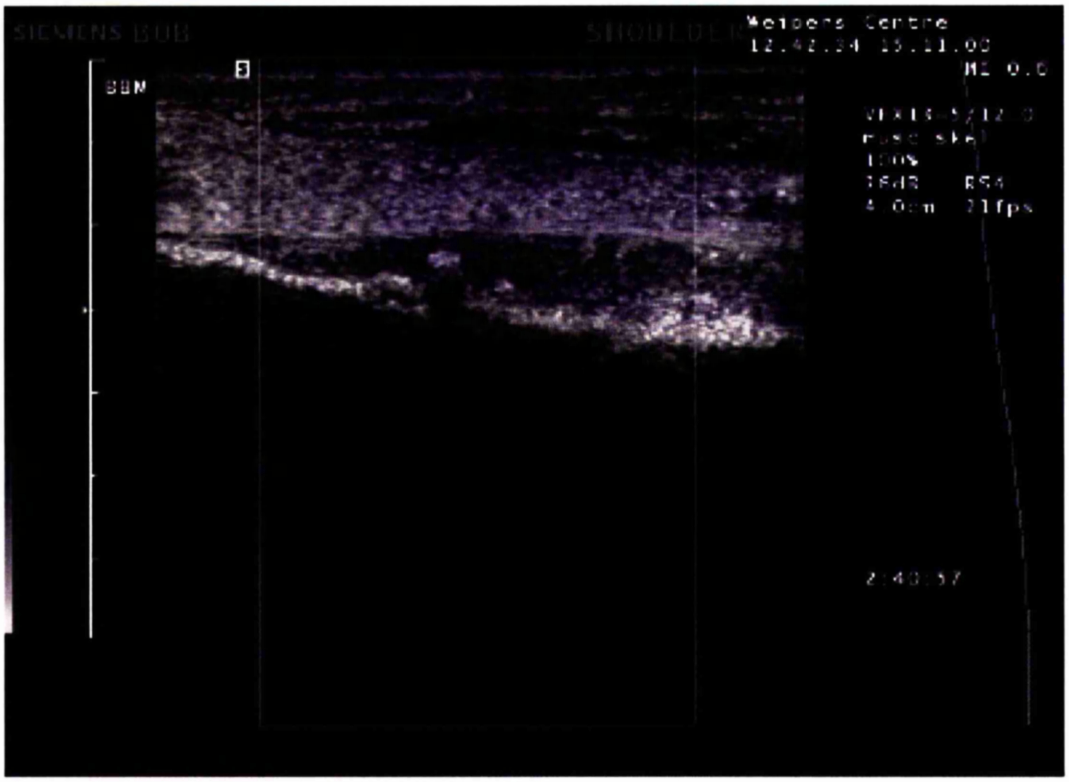

Fig. 4.53. Long axis image taken with Elegra using a 12 MHz linear transducer of the musculotendinous junction of the m. biceps brachii of the left shoulder region of the Greyhound case 3. The tendon of origin of the muscle is seen running from proximal (right) to distal (left) as a hyperechoic broad linear structure in mid field and deep to it the cortex of the humeral body appears roughened with bony growths protruding from the surface causing areas of acoustic shadowing.

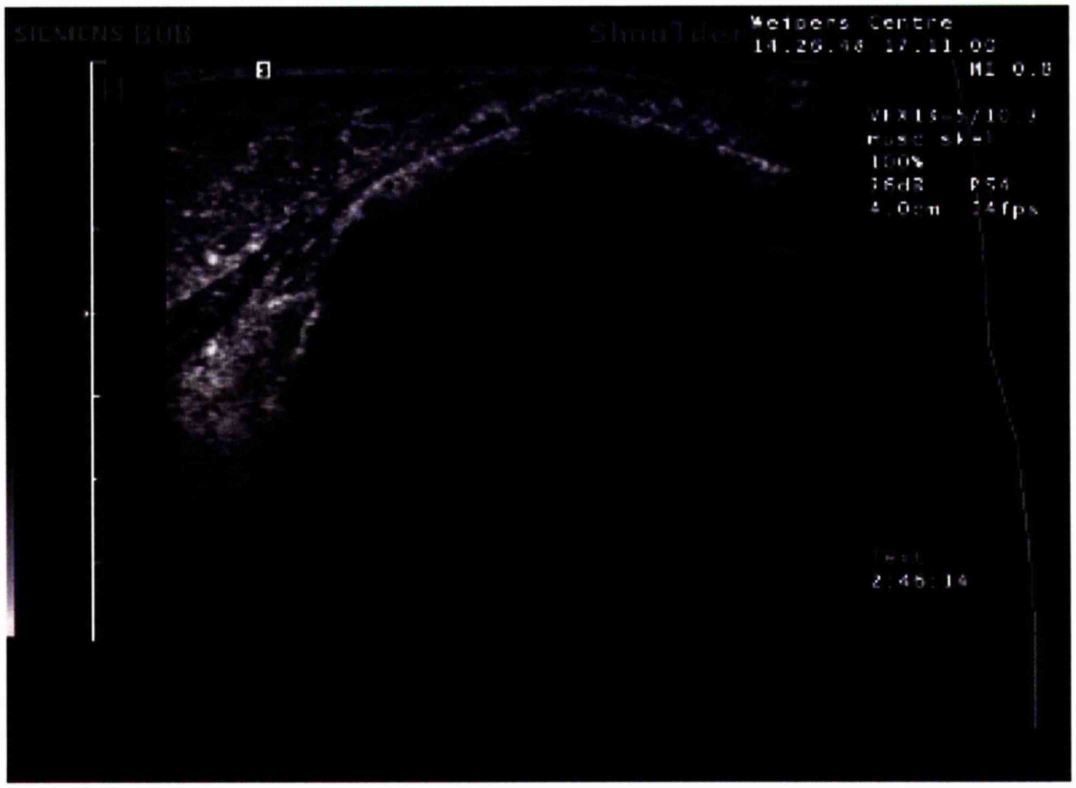

Fig. 4.54. Short axis image taken with Elegra using a 12 MHz linear transducer of the left proximal humeral region of the Greyhound, case number 3. The hyperechoic line of the bony cortex is disrupted with abnormal bone growth which is raised from the surface of the humeral body.

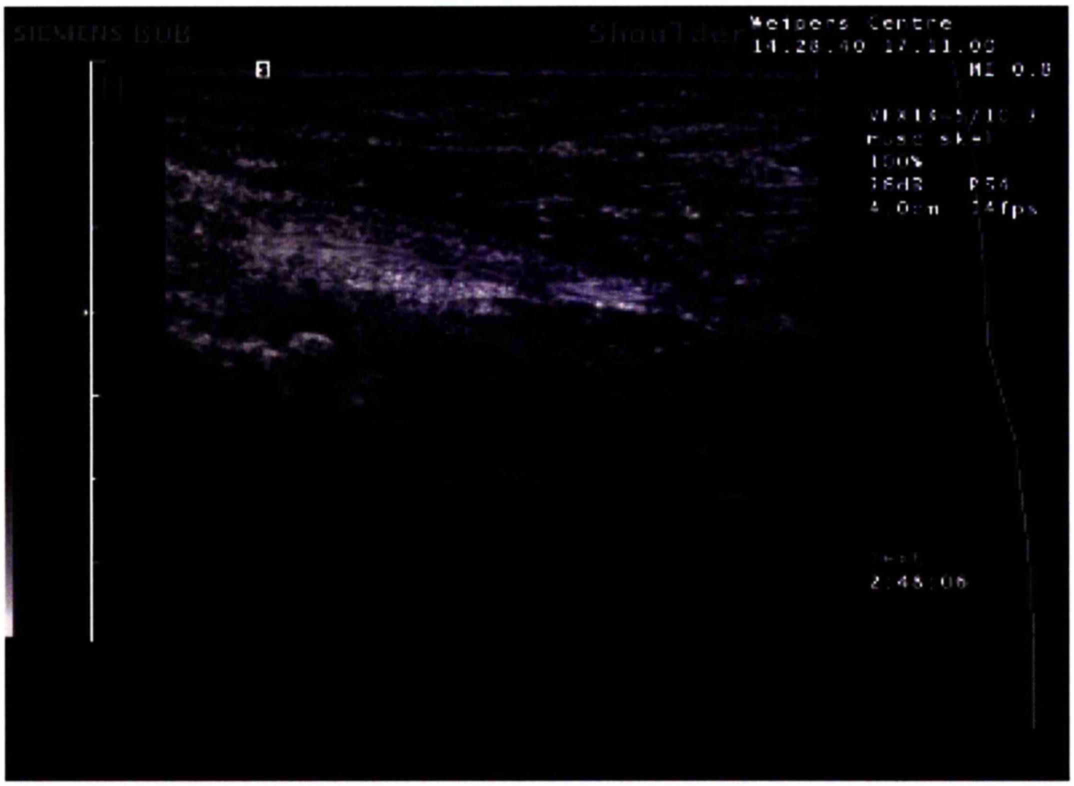

Fig. 4.55. Long axis image taken with Elegra using a 12 MHz linear transducer of the caudolateral aspect of the left shoulder region of the Greyhound case 3. The m. deltoideus is imaged lying superficial to the proximal humeral body. The bony cortex lies deep to the muscle and the hyperechoic surface is considerably disrupted with raised bony growth producing acoustic shadowing.

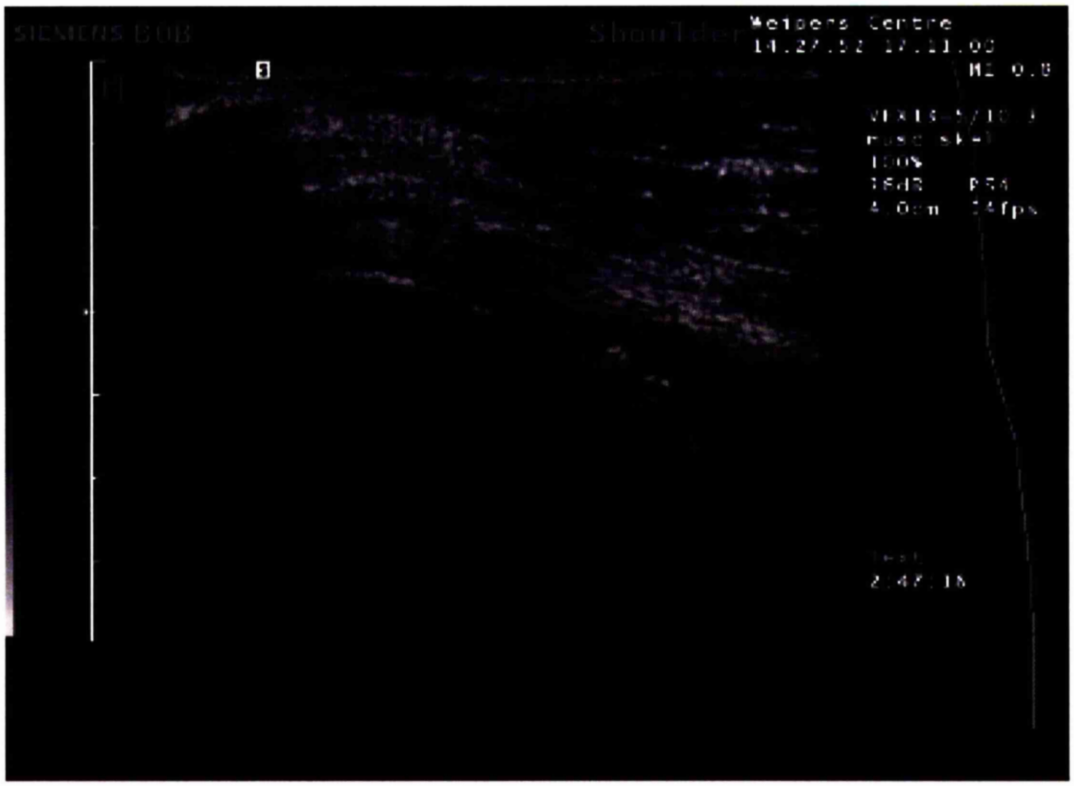

Fig. 4.56. Long axis image taken with Elegra using a 12 MHz linear transducer of the tendon of origin of the m. biceps brachii running from proximal (left) to distal (right) through the intertubercular groove of the left shoulder region of the Greyhound case 3. The hyperechoic tendon is running over the roughened surface of the groove which exhibits raised bony growth and disruption of the cortex.

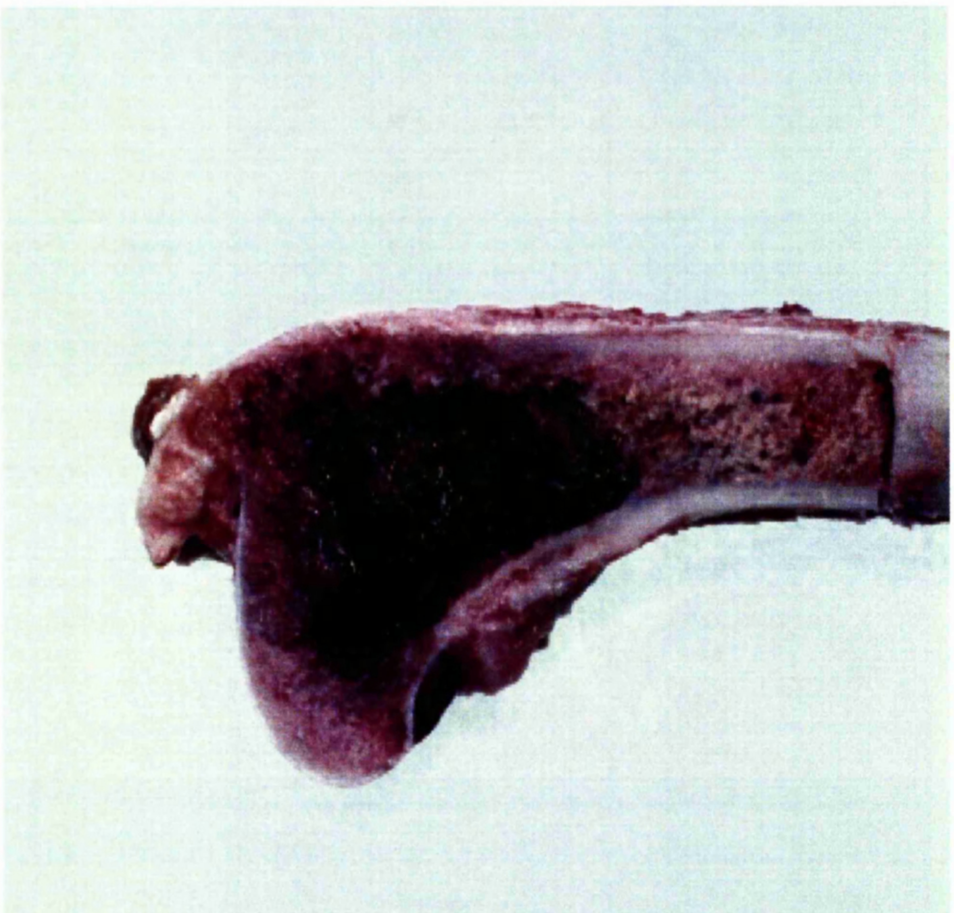

Fig. 4.57. Pathology specimen of the left humerus of the Greyhound, case number 3. The bone has been sectioned in a sagittal plane to reveal the infiltration of the bony cortex at the proximal extremity by tumour tissue. The surface of the bone is roughened and there is disruption of the normal contour of the intertubercular groove, which lies to the extreme left and the underlying cancerous bone.

Fig. 4.58. Lateral radiograph of the left shoulder joint of the Rottweiler case 4. The scapula is displayed in the top right, the shoulder joint space in the centre and the humerus in the bottom of the picture. A cluster of small, well-defined mineralised opacities is shown towards the left of the image forming a line overlying the cranial aspect of the greater tubercle of the humerus.

Fig. 4.59. Short axis view of the musculotendinous junction of the m. supraspinatus of the left shoulder joint of the Rottweiler case 4 using Corevision and an 8 MHz linear transducer. It is displayed on the centre of the picture and it has some hyperechoic areas that are suggestive of calcification. The hyper reflective line with anechoic acoustic shadowing distal to it that lies beneath the musculotendinous junction in the mid field corresponds to the humeral cortex and appears roughened with a raised surface.

Fig. 4.60. Lateral radiograph of the left shoulder joint of the Labrador case 5. The scapula is displayed in the top right, the shoulder joint space in the centre and the humerus in the bottom of the picture. All appear radiographically unremarkable.

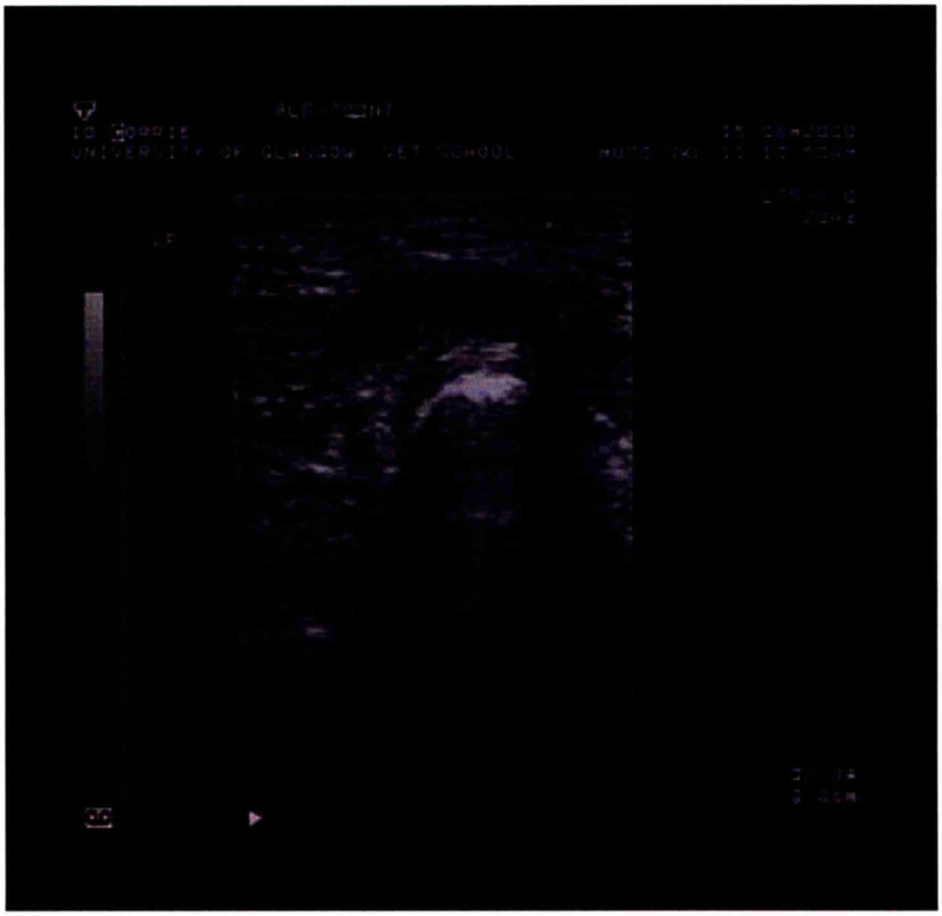

Fig. 4.61. Short axis image of the tendon of insertion of the m. infraspinatus of the left forelimb of the Labrador case number 5 using Corevision with an 8 MHz linear transducer. The tendon is imaged with mixed echogenicity in the mid field and contains hyperechoic foci that possibly correspond to mineralisation. The hyper reflective area with anechoic acoustic shadowing distal to it on the bottom of the image corresponds to the level of the shoulder joint space and greater tubercle of the humerus.

CHAPTER 5.

DISCUSSION AND CONCLUSIONS

5. DISCUSSION AND CONCLUSIONS

5.1. Discussion

Diagnostic ultrasonography for the study of abnormalities of the musculoskeletal system in small animals has been a relatively under utilised technique compared to its use with other body systems. The reports in the literature all highlight the problems presented by the need for the best possible resolution when dealing with small or physically slight structures, the anatomical confinement in obtaining sufficiently large acoustic windows for the transducer face and the problem of orientation of the images received and their placement into the total topography of the region under study. With the new breakthroughs occuring in transducer technology, image processing and the advent of extended field of view imaging with three dimensional capability it is hoped that these problems might be addressed to a greater or lesser extent. The purpose of the initial area of work in this thesis is to identify what has been achieved with ultrasound to date using conventional technology and to see if the problems identified with individual anatomical areas can be answered using transducers of higher frequency or extended field of view and three dimensional technology.

The cadaver work was an attempt to overcome the uncertainty of ultrasound imaging where it is difficult to verify that the image produced on the screen does in fact represent the anatomical structure and topographical field of interest. The use of the echocontrast agent as a marker has not to our knowledge been previously described and coupled with the more conventional anatomical technique of cross sectioning frozen material. This proved to be an invaluable technique during the process of selecting scanning planes for specific musculoskeletal structures. It is anticipated that this will be a useful training tool for future projects.
Once confidence had been built in identifying the structures around the joints under investigation, the ability to readily obtain an image and the quality of image

received were evaluated using the differing imaging modalities. Conclusions were then drawn as to the scanning unit and the technique of choice which was anticipated that would be most beneficial as a clinical tool for that area or structure. Corevision was considered for comparison to be our unit most closely representing the conventional ultrasonography used by previous authors (Kramer et al., 1997, Kramer et al., 1999, Long and Nyland, 1999), while Diasus and Sonoline Elegra with extended field of view and three dimensional capability were assessed as to whether they had additional benefit over the conventional technique.

5.2. Shoulder joint:

In the shoulder joint region the m. supraspinatus and its tendon of insertion were successfully imaged using Corevision both in long and short axis and the structural detail was in agreement with that described by Long and Nyland (1999). With Diasus the structural detail especially of the epimysial and perimysial layers and the tendinous insertion considerably exceeded that exhibited by Corevision and the images of Long and Nyland (1999), which was not unexpected as this was comparing a 16 MHz transducer with a 10 MHz used by these authors. The detail within the muscle belly with Corevision would be adequate for diagnostic assessment of gross muscular change, but it was considered that the use of Diasus at the musculotendinous junction and over the passage of the tendon at the distal scapula onto the greater tubercle would be necessary to detect subtle changes to the tendon. As this muscle is extensive and relatively massive in the Greyhound it was difficult to find and then consistently return to re-examine a specific area of the muscle using the two previous units.

The extended field of view technique of Elegra allowed a panoramic image to be acquired which permitted the specific area of interest to be located consistently and thus the individual frames of that spot could be re-examined in detail. This was easily accomplished over the muscle belly and most information was received with the length of the transducer face being driven in the long axis but when the transducer was moved distally into the field of the tendon, it was difficult to continue to drive the transducer in the same constant plane due to the curvature of the tendon and the bony prominences and so the ability to consistently produce an extended field of view image was impaired. With three dimensional acquisition the transducer face was driven with its length in short axis and so it was possible to collect a volume sample for the muscle belly but again the continuity was lost distally due to the bony prominences of the region. It would thus appear that the m. supraspinatus is readily imaged through its entirety using conventional transducers of 8-10 MHz, but that for fine detail especially of the tendon of insertion Diasus would be of great advantage. In cases of lesions within the muscle belly which could require regular monitoring for shape and size the added modality of extended field of view would be of assistance and a three dimensional volume would allow such a lesion to be interrogated in all planes to give further information of changes in shape and size.

In the same region but caudal to the spine of the scapula the m. infraspinatus was observed using Corevision and the findings of the structure were similar to those of Long and Nyland (1999), but the tendon of insertion of the muscle, although recognisable as an entity, lacked the fine tissue definition and as with the previously quoted authors the bursa lying deep to the tendon was not identified ultrasonographically. With Diasus the quality of image was greatly enhanced in the muscle belly itself both in long and short axis, but the imaging of the tendon was of such a high quality that the linear fibre pattern was evident as was the bursa which lay between the tendon and the caudal part of the greater tubercle of the humerus. This synovial structure was imaged for the first time using Diasus proving this to be of potential diagnostic advantage in shoulder lameness problems.

As with the m. supraspinatus, extended field of view imaging was of great assistance when an overall review of the muscle was required, but in this case the path taken by the tendon of insertion was straighter and passed over a smoother location on the tubercle so that the entire muscle and tendon could be captured in one sweep. The accessibility of the complete structure made it possible to acquire a three dimensional volume of the muscle with all the advantages of revisiting precise areas and examining in multiple planes.

Craniomedial and distal to the shoulder joint the m. biceps brachii was imaged over the proximal half of its belly and along its tendon of origin from the supraglenoid tubercle. The craniomedial position of the muscle and in particular its tendon of origin made transducer size and placement critical in producing satisfactory images. The replacement of the compact hyperechoic appearance of the tendon by the coarse hypoechoic fibres of the muscle as the transducer passed distally was as described by Long and Nyland (1999), as was the recorded appearance of the invagination into the intertubercular groove of the joint capsule to form its synovial sheath as well. By following the tendon in both long and short axis it was possible to comment on the integrity of the tendon and the status of the sheath but fine detail was scarce with the Corevision transducer. It took the resolving power of the 16 MHz Diasus transducer to give sufficient detail to install confidence in defining these structures, in as much as the collagenous bundles of the tendon were evident and the villous nature of the synovial sheath lining could be seen as well as its full extent both in width and length which exceeded the ability of Long and Nyland (1999) who were limited to only visualising it near to the musculotendinous junction.

The curvaceous nature of the path of the tendon and its confinement within the intertubercular groove made passage of the Elegra transducer in long axis difficult thus precluding successful acquisition of extended field of view images. However, as the length of the tendon was relatively short, much of the information could be seen on screen with a conventional image so that topographical detail was simplified. The transducer placement for three dimensional volume acquisition was with the transducer face at right angles to the long axis of the muscle and tendon and thus it was possible to acquire a three dimensional model of the muscle and tendon as it lay against the cortex of the humerus and it could be followed through the intertubercular groove to its insertion. This facilitated the sequential and multiplanar examination of the tendon relative to the surface of the groove and the surrounding synovial sheath. This has immense diagnostic potential for evaluating pathology of this relatively commonly affected region.

The m. teres minor and its tendon of insertion were imaged with Corevision lying proximolateral to the shoulder joint as described by Long and Nyland (1999), but even with Diasus orientation of the muscle was difficult as it lay obliquely across the joint and deep to the m. deltoideus. The course of the muscle was relatively short and so there was little to be gained by imaging it with extended field of view imaging or three dimensional modalities.

An ability to image the joint space and articular surfaces with accompanying synovial structures has been described by various authors, Kramer et al. (1997) with both a 7.5 or a 5 MHz transducer and Long and Nyland (1999) with a 10 MHz transducer. With Corevision the articular cartilage of the joint was imaged as an anechoic layer from a more caudo-lateral window and the synovial joint capsule could be seen but as with the image reproduced with the previously quoted authors, the definition of fine structure was somewhat lacking for making critical assessment of health status of the structures. It was not until Diasus with the 16 MHz transducer was used that the fine detail of the cartilage contour became evident and also the layering of the capsule was truly imaged. Access to the joint through transmission of sound was limited by the anatomy of the region and so Diasus proved to be much more successful in obtaining joint information compared to the images obtained with attempts at extended field of view and three dimensional modalities.

5.3. Stifle joint:

The region immediately proximal to the trochlear groove of the femur has been described by Kramer et al. (1999) and was similar to the findings with Corevision, where the heads of the m. quadriceps femoris were imaged as they inserted onto the rounded patella. The authors described as a point of interest the indentation of the joint capsule but did not separate it from the bursa of deep to the m.quadriceps femoris in the distal third of the femur nor the bursae lying deep to the tendons of the mm. vastus medialis and lateralis. With Diasus it was possible to image the bursa on the femur while imaging in long axis over the midline axial plane, while the two small bursae were evident on imaging to medial and lateral of the axial line. The bursae could be differentiated from the proximal excursion of the joint capsule as it extended proximal to the trochlear groove. The detail afforded by Diasus also allowed recognition of the integration of the various muscular heads to eventually form the patellar ligament; this is not being recorded by the other authors.

The patellar ligament has been well documented by Kramer et al. (1999) and Reed et al. (1995) and the findings were matched using Corevision but exceeded with Diasus as to the detail of the linear pattern of the fibres of the tendon or so called patellar ligament. The infrapatellar fat pad was imaged with Corevision with a similar lack of demarcation as quoted by Kramer et al. (1999), but with Diasus the fat pad was imaged in detail with defined margins and could be followed extensively throughout the joint. Due to the length of the patellar ligament it was not possible to appreciate its total length from the patellar origin to the tibial insertion on one single image frame. This coverage of the total length however was readily achieved using extended field of view, which gave useful topographical detail.

Imaging of the medial and lateral collateral ligaments presented a problem to both authors who had studied the region using a a 5/10 MHz and a 7.5 MHz transducer (Kramer et al., 1999) and a 7.5 mechanical sector transducer (Reed et al., 1995) and this was the case when Corevision was used, but with Diasus the collateral ligaments were revealed in high detail and the association with the m. popliteus laterally and the medial meniscus was evident. Because of the nature of the structures extended field of view had nothing further to add to this area.

The cruciate ligaments have been described as being imaged as hypoechoic features at depth in the joint space deep to the hyperechoic fat pad on a sagittal plane by Kramer et al. (1999) and Reed (1995). This was not achieved in this study using Corevision but with Diasus the cranial and caudal cruciate ligaments were displayed but with a greater degree of echogenicity than that described by the previous authors giving an impression of a linear fibrous nature to the ligaments as they traversed the joint space. It was not possible to image the caudal cruciate ligament at its tibial attachment.

The menisci were visualised with Corevision as homogeneous triangular structures with medium echogenicity in long axis which agreed with the findings of Kramer et al. (1999). Both the menisci were observed but only in their abaxial portions and not in their entirety, as their caudal extremities were not able to be observed, which agreed with the findings of Reed et al. (1995). While imaging the collateral ligaments and the menisci the joint capsule was revealed in detail with Diasus and could be followed extensively.

The tendon of origin of the m. extensor digitorum longus was not visualised in the study performed by Reed et al. (1995) with a 7.5 MHz mechanical sector transducer. In a later study of Kramer et al. (1999) the same structure was visualised but the distinction between the joint capsule (represented by a tendon sheath which forms an invagination of the joint capsule covering the tendon) was not achieved. The tendon of origin of the m. extensor digitorum longus was accurately imaged both in long and in short axis in this study despite its very superficial position. It was imaged both with Corevision and Diasus as a hyper reflective surface and its tendon sheath (the so called capsular synovial bursa) was able to be differentiated with the superior resolution of the Diasus scanner.

The imaging for definitive detail of individual structures within the stifle joint was best accomplished using Diasus with the 16 MHz transducer but, as the transducer was of such high frequency and the foot print was limited in size, it was not possible to establish the continuity of the whole joint ultrasonographically. This was where extended field of view imaging came into its own especially when the transducer was drawn through the long axis of the joint. Thus it was possible to establish the entire integrity of the patellar ligament and interpret the intracapsular contents e.g. infrapatellar fat and cruciate ligaments as to their spatial relationships. The joint also lent itself to the application of three dimensional imaging where the transducer travelled rocking in a short arc thus producing a wedge shaped volume sample of the joint space which could then be interrogated in multiple planes.

5.4. Tarsal Joint:

The tarsal joint was investigated ultrasonographically from the point of imaging the common calcaneal tendon to determine its component make up and its region of insertion at the tuber calcanei of the calcaneus. This tendinous structure is a complex mixture of the insertions of the m. flexor digitorum superficialis, the two heads of the m. gastrocnemius and mm. semitendinosus, biceps femoris and gracilis. The division of the tendon into three ultrasonographic layers with different points of insertion and two bursal pouches has not been previously described in detail nor has the topography of the contributing muscle bundles, but this was made possible in this case due to the high resolution produced by Diasus with both a 16 MHz and a 22 MHz transducer and the use of contrast agent in the cadaver work. As this muscular group and tendon is prone to rupture, a detailed evaluation layer by layer could be of benefit in monitoring breakdown and repair. The extended field of view imaging modality was of assistance in viewing the whole tendon in context, but topography did not really present a problem with Diasus due to the superficial and palpable position of the tendon which also permitted the use of the 22 MHz transducer for fine detail.

5.5. Measurements

A series of measurements were taken with the transducers of Corevision, Diasus and Elegra scanners with the aim of detecting if any degree of consistency could be achieved through the repeatability of measurements. This was considered to have the potential of offering significant help to the clinician, since by this way differences in the size of various anatomical structures could be interpreted and contribute to the diagnosis of different musculoskeletal abnormalities.

The results obtained by the use of conventional ultrasound, represented in this study by the use of the 8 MHz transducer of Corevision, showed that there cannot exist any consistency between individual sessions in the measurements concerning the structures of the same joint. The significant differences in the dimensions of the different organs suggested that any degree of muscle atrophy or hypertrophy or even ligament or tendon thickening or thinning for instance cannot be safely diagnosed by this means. The difficulty in reproducing the same angle between the structures and the transducer, in combination with the poor resolution that had an impact in accuracy of measurements, made the project ineffective.

It was expected that with the help of an ultra high frequency transducer with Diasus scanner, which would provide the sonographer with greater accuracy, the same anatomical landmarks could be found during each measurement, in order to establish accuracy. But this was not achieved, as the whole particular project depended much on the angle between the structures and the transducer. The problem encountered with Corevision was not overcome, even with higher resolution.

Extended field of view was proved capable of providing the sonographer with constant anatomical landmarks in order to take the measurements. The calling up of a selected frame on the screen when the landmark was spotted was able to provide the researchers with accurate measurements in repeated sessions. This modality was considered to be promising in order to estimate even slight differences in the dimensions of musculoskeletal structures, that may suggest any kind of abnormality.

Further research is required in order to assess whether three dimensional measurements are able to offer accuracy in measurements of musculoskeletal anatomical structures. The machine equipped with this facility was not provided with an appropriate measurement package for this kind of measurement and consequently, this study was not able to give answers to that.

5.6. Clinical cases

Ultrasonography has proved to be valuable in the diagnosis of various musculoskeletal disorders of the dog. It has been useful in the identification of lesions that are not visible with radiography. This has been confirmed in a case where mineralisation of the m. infraspinatus and dilation of the synovial sheath of the m. biceps brachii were detected by ultrasound and were not visible in radiographs.

Although arthroscopy was eventually performed in most of the dogs examined, since the ultrasonographic findings were not optimal, because the frequency of the available transducer was only 8 MHz, it is estimated that it could be avoided if an ultra high frequency transducer was used that could provide additional information. Consequently, ultrasound seems to have enabled the diagnosis of several conditions that previously would have to be detected by invasive methods.

Tenosynovitis constitutes a pathologic condition that cannot be detected by conventional radiographic means. Ultrasound has proved to be useful for its detection since synovial inflammation is characterised by thickening of the synovial sheath and production of excessive amounts of fluid. as was found in the dog with tenosynovitis in its right biceps brachii synovial sheath. Imaging with high resolution transducers has shown that fluid echogenicity can vary from totally anechoic to hyperechoic and with a flocculent appearance (Martinoli et al., 1999). Moreover, thickening of the joint capsule has been able to be observed with ultrasound in the dog mentioned above, whereas it has not been accomplished with conventional radiographic methods. Arthroscopy or arthrotomy usually confirm ultrasonographic findings, but their invasive character constitutes a disadvantage as far as the dog's suffering and the cost effect are concerned.

Calcifications of muscles and tendons can be detected with accuracy with ultrasound. Various focal hyperechoic regions representing calcification, creating acoustic shadows in the far field can be imaged, indicating the presence of calcified tissue (Long and Nyland, 1999). Furthermore, their exact anatomical location can be detected, in contrast with radiography which can only identify their presence, but not their exact position in a component of a joint. This became evident in three cases, where radiographs were able to testify the presence of mineralisations, but the anatomical structures affected were able to be defined by ultrasound.

A clinical case examined with ultrasound proved that hypoechoic lesions that lay close to or overlay various anatomical structures of a joint (the shoulder joint in this case) could be detected with ultrasound, in contrast with radiography which could not provide the clinician with details of that kind.

Ultrasound can also provide information concerning bones. Irregularities of the bone cortex can be readily observed on radiographs and many bone abnormalities can be diagnosed with radiography with accuracy. In the case of the dog which suffered from a malignant bone tumour radiography was required to provide a definitive diagnosis, but by using the experience obtained from scanning this case ultrasound could provide a diagnosis in future cases.

5.7. Conclusions

While interest in musculoskeletal ultrasound imaging in small animals has been increasing in recent years as the quality of scanners and transducers has improved, the advent of ultra high frequency transducers and the extensive increase in computer power in post processing images is leading to a renewed interest in imaging joint structures, ligaments, muscles and tendons. In this study the use of transducers ranging from 12 to 22 MHz greatly enhanced the detailed imaging of structures placed around the shoulder, stifle and tarsal joints in the dog. However the use of these transducers did not produce an improvement in the ability to consistently and repetitively measure the dimensions of these structures. This was due to the problems of variation in the operator's skill and interpretation plus the problem of angulation of the transducer and overcoming the topography of these regions. These problems could be off set by the use of extended field of view imaging, where it was possible to be more consistent in revisiting areas of interest and to be able to select specific image frames for measurement. Even so, in certain areas the anatomy of the region would not allow a panoramic image to be built up.

The most recent development of three dimensional reconstruction would appear to have a promising future in musculoskeletal imaging. The benefits of building up a large volume sample of an area allows a specific area of interest to be selected and then investigated in multiple planes and detail of the structure to be compared in three dimensions. Thus structures which run through an area of interest can be followed in context to their surrounding topography, which is extremely difficult to accomplish with conventional two dimensional imaging with high frequency transducers which have relatively small fields of view. Possibly the greatest advantage with three dimensional imaging is that once acquired the reconstructed volume sample can be stored electronically and revisited for subsequent detailed viewing of further areas of interest or the same area of interest for comparison and the plane of examination altered to suit the individual case. This ability is not available in conventional two dimensional scanning when only the individual slices of information in one dimension can be stored for further scrutiny. There is much more work to be accomplished in the field of three dimensional imaging with exciting discoveries for the future when imaging the musculoskeletal system of small animals.

BIBLIOGRAPHY.

LIST OF REFERENCES

Aisen A.M., McCune W.J., MacGuire A., Carson P.L., Silver T.M., Jafri S.Z., Martel W. (1984) Sonographic Evaluation of the Cartilage of the Knee. Radiology **153**, 781-784

Barr F. (1990) Diagnostic ultrasound in the dog and cat. Blackwell Scientific Publications, Oxford, pp 1-20

Barr F. (1995) Manual of Small Animal Diagnostic Imaging, Second edition. Edited by R. Lee, British Small Animal Veterinary Association, Gloucester, pp 157-167

Bartrum R.J., Crow H.C. (1977) Gray-scale Ultrasound: A Manual for Physicians and Technical Personnel. W.B. Saunders, Philadelphia.

Beggs I. (1998) Ultrasound of Soft Tissue Masses. BMUS Bulletin, **6** (4), 25-28

Beissert M., Jenett M., Kellner M., Wetzler T., Haerten R., Hahn D. (1998) SieScape imaging in radiological diagnosis. (German). Radiologe, **38**, 410-416

Bertolotto M., Perrone R., Martinoli C., Rollandi G.A., Patetta R., Derchi L.E. (1995) High Resolution Ultrasound Anatomy of Normal Achilles Tendon. The British Journal of Radiology, **68** (813), 986-991

Boyd J.S. (1995) Veterinary Ultrasonography. Edited by P.J. Goddard. CAB International, Cambridge, pp 233-255

Campani R., Bottinelli O., Calliada F., Coscia D. (1998) The latest in Ultrasound: three-dimensional imaging. Part II. European Journal of Radiology, **27** Suppl. 2, S183-S187

Cartee R.E. (1981) Diagnostic real-time ultrasonography of the liver of the dog and cat. Journal of the American Animal Hospital Association, **17**, 731-737

Cartee R.E., Selcer B.A., Patton C.S. (1980) Ultrasonographic diagnosis of renal disease in small animals. Journal of the American Veterinary Medical Association, **176** (5), 426-430

Cook J.L., Khan K.M., Kiss Z.S., Purdam C.R., Griffiths L. (2000) Prospective Imaging Study of Asymptomatic Patellar Tendinopathy in Elite Junior Basketball Players. Journal of Ultrasound in Medicine, **19**, 473-479

Craychee T.J. (1995) Veterinary Diagnostic Ultrasound. Edited by T.G. Nyland and J.S. Matoon, W.B.Saunders, Philadelphia, pp 265-304

Deane C. (2000) Extended Field of View and B-flow Ultrasound: Fashion or future? Ultrasound in Obstetrics and Gynecology, **15**, 96-97

Downey D.B., Fenster A., Williams J.C. (2000) Clinical Utility of Three-dimensional US. Radiographics, **20**, 559-571

Dyce K.M., Sack W.O., Wensing C.J.G. (1987) Textbook of Veterinary Anatomy. W.B. Saunders Company, Philadelphia, pp 1-28

Engelke A. (2000) An Atlas and Textbook of Diagnostic Ultrasonography of the Dog and Cat. Edited by R.E. Cartee, Manson Publishing Ltd, London, pp 355-360

Engelke A., Gassner G. (2000) An Atlas and Textbook of Diagnostic Ultrasonography of the Dog and Cat. Edited by R.E. Cartee, Manson Publishing Ltd, London, pp 329-336

Engelke A., Gassner G., Dohner C., Kresken J-G (2000) An Atlas and Textbook of Diagnostic Ultrasonography of the Dog and Cat. Edited by R.E. Cartee, Manson Publishing Ltd, London, pp 346-347

Erickson S.J. (1997) High-Resolution Imaging of the Musculoskeletal System. Radiology, **205**, 593-618

Evans D.H., McDIcken W.N. (2000) Doppler Ultrasound: Physics, Instrumentation and Signal processing. John Wiley and sons, West Sussex, pp 71-96

Evans H.E. (1993) Miller's Anatomy of the Dog, Third Edition. Edited by H.E.Evans. W.B.Saunders, Philadelphia.

Farin P.U., Jaroma H., Soimakallio S. (1995) Rotator Cuff Calcifications: Treatment with US-guided Technique. Radiology, **195**, 841-843

Farrell T., Leslie J., Chien P.F.W. (2000) Three Dimensional Ultrasound: Reliability and Validity of Volumetric Measurements and Potential Applications in Obstetrics and Gynaecology. BMUS Bulletin, **8** (4), 28-35.

Farrow C.S. (1996) Small Animal Ultrasound. Edited by R.W. Green. Lippincott-Raven Publishers, Philadelphia.

Fornage B.D., Atkinson E.N., Nock L.F., Jones P.H. (2000) US with Extended Field of View: Phantom-tested Accuracy of Distance Measurements. Radiology, **214**, 579-584

Fornage B.D., Rifkin M.D., Touche D.H., Segal P.M. (1984) Sonography of the Patellar Tendon: Preliminary Observations. American Journal of Roentgenology, **143**, 179-182

Fornage B.D., Schernberg F.L. (1986) Sonographic Diagnosis of Foreign Bodies of the Distal Extremities. American Journal of Roentgenology, **147**, 567-569

Forrester A.W. (1998) In: Ultrasound Examination of the Shoulder. BMUS Bulletin, **6** (4), 21-24

Friedrich J.M., Schnarkowski P., Rubenacker S., Wallner B. (1993) Ultrasonography of Capsular Morphology in Normal and Traumatic Ankle Joints. Journal of Clinical Ultrasound, **21**, 179-187

Gassner G. (2000) An Atlas and Textbook of Diagnostic Ultrasonography of the Dog and Cat. Edited by R.E. Cartee, Manson Publishing Ltd, London, pp 347

Gassner G., Engelke A. (2000) An Atlas and Textbook of Diagnostic Ultrasonography of the Dog and Cat. Edited by R.E. Cartee, Manson Publishing Ltd, London, pp 336-344

Gerwing M., Kramer M. (1995) Sonographical findings of muscle diseases in dogs and cats. Veterinary Radiology and Ultrasound, **36** (5), 437

Ghate S.V., Scott Soo M., Mengoni P.M. (1999) Extended Field-of-View Two-Dimensional Ultrasonography of the Breast: Improvement in Lesion Documentation. Journal of Ultrasound in Medicine, **18**, 597-601

Ginther O.J. (1995) Ultrasonic Imaging and Animal Reproduction: Fundamentals, Book 1. Equiservices Publishing, Cross Plains.

Goddard P.J. (1995) Veterinary Ultrasonography. Edited by P.J. Goddard. CAB International, Cambridge, pp 1-19

Goldstein A. (2000) Errors in Ultrasound Digital Image Distance Measurements. Ultrasound in Medicine and Biology, **26** (7), 1125-1132

Hamper U.M., Trapanotto V., Sheth S., DeJong M.R., Caskey C.I. (1994) Three-dimensional US: Preliminary Clinical Experience. Radiology, **191**, 397-401

Hankaga C. (1995) Canine Splenic disease: A Clinico-Pathological and Ultrasonographical Study. MVM Thesis, Glasgow University Veterinary School, pp 1-22

Hara Y., Nakamura M., Tamaki N (1999) A New Sonographic Technique for Assessing Carotid Artery Disease: Extended-Field-of-View Imaging. American Journal of Neuroradiology, **20** (2), 267-270

Helper L.C. (1970) Diagnosis of pregnancy in the bitch with an ultrasonic Doppler instrument. Journal of the American Veterinary Medical Association, **156** (1), 60-62

Hermanson J.W., Evans H.E. (1993) Miller's Anatomy of the Dog, Third edition. Edited by H.E. Evans. W.B.Saunders, Philadelphia, pp 258-384

Herrtage M.E. (1998) BSAVA Manual of Small Animal Cardiorespiratory Medicine and Surgery. Edited by V.L. Fuentes and S. Swift, BSAVA, Cheltenham, pp 79-90

Holmes J.H., Howry D.H. (1963) Ultrasonic Diagnosis of Abdominal Disease. American. Journal of Digestive. Diseases., **8**, 12-32

Jozsa L.G., Kannus P. (1997) Human tendons: Anatomy, Physiology and Pathology. Human Kinetics, Champaign, USA.

Junqueira L.C., Carneiro J., Kelley R.O. (1995) Basic Histology, Eighth edition. Appleton and Lange, Connecticut, pp 124-131

Kirberger R.M. (1995) Imaging artifacts in diagnostic ultrasound-A review. Veterinary Radiology and Ultrasound, **36** (4), 297-306

Koch S.A., Rubin L.F. (1969) Diagnostic ultrasonography of the dog eye. Journal of Small Animal Practice, **10** (6), 357-361

Konermann W., Wuisman P., Ellermann A., Gruber G. (2000) Ultrasonographically Guided Needle Biopsy of Benign and Malignant Soft Tissue and Bone Tumors. Journal of Ultrasound in Medicine, **19**, 465-471

Kramer M., Gerwing M., Hash V., Schimke E. (1997) Sonography of the musculoskeletal system in dogs and cats. Veterinary Radiology and Ultrasound, **38** (2), 139-149

Kramer M., Gerwing M., Tellhelm B. (1995) Sonographical and radiological diagnosis of the biceps muscle in dogs. Veterinary Radiology and Ultrasound, **36** (5), 437

Kramer M., Stengel H., Gerwing M., Schimke E., Sheppard C. (1999) Sonography of the canine stifle. Veterinary Radiology and Ultrasound, **40** (3), 282-293

Lamm A.M. (1970) Ultrasound diagnosis of pregnancy in the dog. Acta Radiologica, Suppl. 319, 293-294

Lee J.I., Song I.S., Jung Y.B., Kim Y.G., Wang C.H., Yu H., Kim Y.S., Kim K.S., Pope T.L. (1996) Medial Collateral Ligament Injuries of the Knee: Ultrasonographic Findings. Journal of Ultrasound in Medicine, **15**, 621-625

Lindahl I.L. (1966) Detection of Pregnancy in Sheep by Means of Ultrasound. Nature, **212**, 642-643

Long C.D., Nyland T.G. (1999) Ultrasonographic evaluation of the canine shoulder. Veterinary Radiology and Ultrasound, **40** (4), 372-379

Mc Donnell C.H., Brooke Jeffrey R., Bjorkengren A.G., Li K.C.P. (1992) Intraarticular Sonography for Imaging the Knee Menisci: Evaluation in Cadaveric Specimens. American Journal of Roentgenology, **159**, 573-574

Mack L.A., Nyberg D.A., Matsen F.R. (III), Kilcoyne R.F., Harvey D. (1988) Sonography of the Postoperative Shoulder. American Journal of Roentgenology, **150**, 1089-1093

Main J.P.M. (1995) Veterinary Ultrasonography. Edited by P.J. Goddard. CAB International, Cambridge, pp 207-232

Martinoli C., Blanchi S., Derchi L.E. (1999) Tendon and Nerve Sonography. Radiologic Clinics of North America, **37** (4), 691-711

Meire H.B., Farrant P. (1995) Basic Ultrasound. John Wiley and sons, West Sussex.

Nazarian L.N., Rawool N.M., Martin C.E., Schweitzer M.E. (1995) Synovial Fluid in the Hindfoot and Ankle: Detection of Amount and Distribution with US. Radiology, **197**, 275-278

Nyland T.G., Bernard W.V. (1982) Application of abdominal ultrasound. California Vet, **36**, 21-25

Nyland T.G., Mattoon J.S., Wisner E.R. (1995) Veterinary Diagnostic Ultrasound. Edited by Nyland T.G., Mattoon J.S., W.B. Saunders, Philadelphia, pp 3-18

Nyland T.G., Park R.D., Lattimer J.C., Lebel J.L., Miller C.W. (1981) Gray scale ultrasonography of the canine abdomen. Veterinary Radiology, **22**, 220-227

O' Brien R.T. (1998) Attenuation: The clinical utility of subjective sonographic assessment. Veterinary Radiology and Ultrasound, **39** (3), 224-225

O' Connor P.J. (1998) Ultrasound Guided Musculoskeletal Intervention. BMUS Bulletin, **6** (4), 34-38

O' Keefe D., Mamtora H. (1992) Ultrasound in Clinical Orthopaedics. The Journal of Bone and Joint Surgery, **74** (B), 488-494

Pedersen N.C., Morgan J.P., Vasseur P.B. (2000) Textbook of Veterinary Internal Medicine Vol. 2, Fifth edition. Edited by Stephen J. Ettinger and Edward C. Feldman, W.B. Saunders, Philadelphia, pp 1862-1886

Penninck D.G. (1995) Veterinary Diagnostic Ultrasound. Edited by Nyland T.G., Mattoon J.S., W.B. Saunders, Philadelphia. pp 19-29

Poulsen Nautrup C. (2000) An Atlas and Textbook of Diagnostic Ultrasonography of the Dog and Cat. Edited by R.E. Cartee, Manson Publishing Ltd, London.

Rantanen N.W. (1981) Ultrasound Appearance of Normal Lung Borders and Adjacent Viscera in the Horse. Veterinary Radiology, **22**, 217-219

Rantanen N.W., Torbreck R.L., Dumond S.S. (1982) Early Pregnancy Diagnosis in the Mare using Transrectal Ultrasound Scanning Techniques: a Preliminary Report. Journal of Equine Veterinary Science, **2**, 27-29

Reed A.L., Payne J.T., Constantinescu G.M. (1995) Ultrasonographic anatomy of the normal canine stifle. Veterinary Radiology and Ultrasound, **36** (4), 315-321

Riccabona M., Nelson T.R., Pretorius D.H., Davidson T.E. (1995) Distance and Volume Measurement Using Three-Dimensional Ultrasonography. Journal of Ultrasound in Medicine, **14**, 881-886

Rubens D.J., Fultz P.J., Gottlieb R.H., Rubin S.J. (1997) Effective Ultrasonographically Guided Intervention for Diagnosis of Musculoskeletal Lesions. Journal of Ultrasound in Medicine, **16**, 831-842

Rubin L.F., Koch S.A. (1968) Ocular Diagnostic Ultrasonography. Journal of the American Veterinary Medical Association, **153** (12), 1706-1716

Rupp S., Tempelhof S., Fritsch E. (1995) Ultrasound of the Achilles tendon after surgical repair: morphology and function. The British Journal of Radiology, **68** (809), 454-458

Sandriek K. (2000) Sonography teams up with MRI in shoulder. Sports Imaging, Supplement of Diagnostic Imaging Europe, **16** (6), 10-11

Shah Z.R., Crass J.R., Oravec D.C., Bellon E.M. (1992) Ultrasonographic detection of foreign bodies in soft tissue using turkey muscle as a model. Veterinary Radiology and Ultrasound, **33** (2), 94-100

Siems J.J., Breur G.J., Blevins, W.E., Cornell K.K. (1998) Use of two-dimensional real-time ultrasonography for diagnosing contracture and strain of the infraspinatus muscle in a dog. Journal of the American Veterinary Medical Association, **212** (1), 77-80

Taylor K.J.W. (1978) Atlas of Gray-Scale Ultrasonography. Edited by K.J.W. Taylor, Churchill Livingstone, Longman, New York, pp.1-14

Temple R.S., Stonker H.H., Howry D., Posakony C., Hanaleus M.H. (1956) Ultrasonic and Conductivity Methods for Estimating Fat Thickness in Live Cattle. Proceedings, Western Section, American Society of Animal Science, **7**, 477

Vaughan L.C. (1969) Gracilis Muscle Injury in Greyhounds. Journal of Small Animal Practice, **10**, 363-375

Vaughan L.C. (1979) Muscle and tendon injuries in dogs. Journal of Small Animal Practice, **20**, 711-736

Waitches G.M., Rockett M., Brage M., Sudakoff G. (1998) Ultrasonographic-Surgical Correlation of Ankle Tendon Tears. Journal of Ultrasound in Medicine, **17**, 249-256

Wakefield R. (1998) The Role of Musculoskeletal Ultrasound in Rheumatology. BMUS Bulletin,**6** (4), 18-20

Weismann C.F. (2000) Three-D expands horizons in daily clinical practice. Diagnostic Imaging Europe, **16** (4), 30-33

Weng L., Tirumalai A.P., Lowery C.M., Nock L.F., Gustafson D.E., Von Behren P.L., Kim J.H. (1997) US Extended Field of View Imaging Technology. Radiology, **203**, 877-880

Whittingham T.A. (1997) New and Future developments in Ultrasonic Imaging. The British Journal of Radiology, Special Issue, **70**, S119-S132

Winter F. (1998) Musculoskeletal Ultrasound Imaging Technique and Normal Tissue Characteristics. BMUS Bulletin, **6** (4), 8-10

Zanetti M, Hodler J. (2000) Imaging of Degenerative and Posttraumatic Disease in the Shoulder Joint with Ultrasound. European Journal of Radiology, **35** (2), 119-125